UPPER-TROPOSPHERIC PRECURSORS ASSOCIATED WITH SUBTROPICAL CYCLONE FORMATION IN THE NORTH ATLANTIC BASIN

by

Alicia M. Bentley

A Thesis

Submitted to the University at Albany, State University of New York

in Partial Fulfillment of

the Requirements for the Degree of

Master of Science

College of Arts & Sciences

Department of Atmospheric and Environmental Sciences

2014

ABSTRACT

Oceanic cyclones exhibiting properties of both tropical and extratropical systems have been categorized as subtropical cyclones (STCs) since the early 1950s. The opportunity to investigate the roles of baroclinic and diabatic processes during the evolution of STCs from a potential vorticity (PV) perspective motivates this study. This study investigates the roles of baroclinic and diabatic processes during the evolution of STCs by calculating three PV metrics from the National Centers for Environmental Prediction Climate Forecast System Reanalysis 0.5° gridded dataset. The three PV metrics quantify the relative contributions of lower-tropospheric baroclinic processes, midtropospheric diabatic heating, and upper-tropospheric dynamical processes during the evolution of individual cyclones. Quantification of these three contributions reveals the changing PV structure of an individual cyclone, indicates fluctuations in the dominant energy source of the cyclone, and aids in categorizing the cyclone.

A cyclone-relative composite analysis performed on subjectively constructed clusters of North Atlantic STCs identified from a 1979–2010 climatology is presented to document the structure, motion, and evolution of upper-tropospheric features linked to STC formation. The STCs included in the climatology are separated into five clusters representing the most common upper-tropospheric features linked to STC formation: PV Streamers, Cutoffs, Midlatitude Troughs, Subtropical Disturbances, and PV Debris. STCs forming in association with PV streamers and cutoffs have a well-defined midlatitude connection, developing near a region of upper-tropospheric PV injected into the subtropics during an upstream anticyclonic wave breaking (AWB) event. STCs

forming in association with midlatitude troughs also have a well-defined midlatitude connection, but are not associated with an upstream AWB event. In contrast, STCs forming in association with subtropical disturbances do not have a well-defined midlatitude connection, developing in the vicinity of low-amplitude upper-tropospheric disturbances progressing around the northern periphery of upper-tropospheric subtropical anticyclones. STCs forming in association with a disorganized region of upper-tropospheric PV deposited in the subtropics several days prior to STC formation (i.e., PV debris) have the least-evident midlatitude connection of the STCs identified in this study. Case studies and conceptual models are presented to illustrate the upper-tropospheric features linked to STC formation within each cluster.

ACKNOWLEDGEMENTS

Upon completing my M.S. thesis, which culminates three years of research, I would like to take a moment to thank my parents, sister, and extended family for their unwavering support of my graduate studies. Their encouragement and love have been my greatest sources of inspiration and I cannot imagine having accomplished such a feat without them. I am also indebted to my academic co-advisors, Drs. Dan Keyser and Lance Bosart. Their belief in my abilities was often greater than my own, motivating me to exceed my personal expectations. The mentorship that I have received from Dan and Lance has helped me become a better scientist and person, and I am incredibly grateful for being given the opportunity to work with them.

I also wish to thank the members of the Department of Atmospheric and Environmental Sciences at the University at Albany for their direct and indirect support of this thesis. Special thanks to Barbara Zampella, Sandra George, and Denise Church for their administrative support, as well as Kevin Tyle and David Knight for their technical assistance. I also wish to thank my fellow graduate students, past and present, for their programming assistance, advice, and camaraderie. Finally, I would like to express my sincere appreciation for the support I have received from Kyle MacRitchie, Kristen Corbosiero, and Larry Gloeckler throughout my graduate studies. Their unconditional friendship has meant more to me over the last three years than I can possibly put into words and is something that I will always cherish about my time at the University at Albany.

I would like to conclude by thanking my friends, teachers, and coaches from Averill Park, NY, whose inspirational words motivate me as much today as they did a decade ago. I would not be the person or scientist that I have become without those individuals, who I think of regularly and miss often.

This research was made possible by the generous support of the National Science Foundation (NSF) grant AGS-0935830.

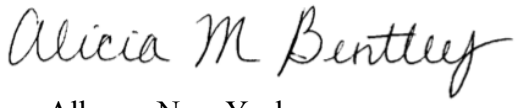

Albany, New York
July 2014

TABLE OF CONTENTS

LIST OF TABLES

LIST OF FIGURES

Fig 3.35. 500-hPa cyclonic relative vorticity (shaded, 10^{-5} s^{-1}), geopotential height (black solid contours, dam), temperature (red dashed contours, °C), ascent (blue contours, every 5×10^{-3} hPa s^{-1}), and winds (barbs, kts) for an STC forming in association with a PV streamer at 1800 UTC 21 August 1980 (t_0). Panels depict the aforementioned features at (a) t_0 – 120 h, (b) t_0 – 96 h, (c) t_0 – 72 h, (d) t_0 – 48 h, (e) t_0 – 24 h, and (f) t_0. The black cyclone symbol in each panel denotes the location of STC formation at t_0. Label "PV1" indicates the position of a region of relatively high upper-tropospheric PV. Label "C1" indicates the position of a surface cyclone.

Fig 3.36. Coupling index (shaded, K), 850-hPa geopotential height (black contours, dam), and 850–200-hPa wind shear (barbs, kts) for an STC forming in association with a PV streamer at 1800 UTC 21 August 1980 (t_0). Panels depict the aforementioned features at (a) t_0 – 120 h, (b) t_0 – 96 h, (c) t_0 – 72 h, (d) t_0 – 48 h, (e) t_0 – 24 h, and (f) t_0. The black cyclone symbol in each panel denotes the location of STC formation at t_0. Label "PV1" indicates the position of a region of relatively high upper-tropospheric PV. Label "C1" indicates the position of a surface cyclone.

Fig 3.37. As in Fig. 3.32, except for an STC forming in association with a cutoff at 0600 UTC 30 September 1980 (t_0). Label "PV2" indicates the position of a region of relatively high upper-tropospheric PV. Label "C2" indicates the position of a surface cyclone.

Fig 3.38. As in Fig. 3.33, except for an STC forming in association with a cutoff at 0600 UTC 30 September 1980 (t_0). Label "PV2" indicates the position of a region of relatively high upper-tropospheric PV. Label "C2" indicates the position of a surface cyclone.

Fig 3.39. As in Fig. 3.34, except for an STC forming in association with a cutoff at 0600 UTC 30 September 1980 (t_0). Label "PV2" indicates the position of a region of relatively high upper-tropospheric PV. Label "C2" indicates the position of a surface cyclone.

Fig 3.40. As in Fig. 3.35, except for an STC forming in association with a cutoff at 0600 UTC 30 September 1980 (t_0). Label "PV2" indicates the position of a region of relatively high upper-tropospheric PV. Label "C2" indicates the position of a surface cyclone.

Fig 3.41. As in Fig. 3.36, except for an STC forming in association with a cutoff at 0600 UTC 30 September 1980 (t_0). Label "PV2" indicates the position of a region of relatively high upper-tropospheric PV. Label "C2" indicates the position of a surface cyclone.

Fig 3.42. As in Fig. 3.32, except for an STC forming in association with a midlatitude trough at 0600 UTC 4 October 2005 (t_0). Labels "PV3a" and "PV3b" indicate the position of regions of relatively high upper-tropospheric PV. Labels "C3a" and "C3b" indicate the position of surface cyclones.

Fig 3.43. As in Fig. 3.33, except for an STC forming in association with a midlatitude trough at 0600 UTC 4 October 2005 (t_0). Labels "PV3a" and "PV3b" indicate the position of regions of relatively high upper-tropospheric PV. Labels "C3a" and "C3b" indicate the position of surface cyclones.

Fig 3.44. As in Fig. 3.34, except for an STC forming in association with a midlatitude trough at 0600 UTC 4 October 2005 (t_0). Labels "PV3a" and "PV3b" indicate the position of regions of relatively high upper-tropospheric PV. Labels "C3a" and "C3b" indicate the position of surface cyclones.

Fig 3.45. As in Fig. 3.35, except for an STC forming in association with a midlatitude trough at 0600 UTC 4 October 2005 (t_0). Labels "PV3a" and "PV3b" indicate the position of regions of relatively high upper-tropospheric PV. Labels "C3a" and "C3b" indicate the position of surface cyclones.

Fig 3.46. As in Fig. 3.36, except for an STC forming in association with a midlatitude trough at 0600 UTC 4 October 2005 (t_0). Labels "PV3a" and "PV3b" indicate the position of regions of relatively high upper-tropospheric PV. Labels "C3a" and "C3b" indicate the position of surface cyclones.

Fig 3.47. As in Fig. 3.32, except for an STC forming in association with a subtropical disturbance at 0000 UTC 5 June 1986 (t_0). Label "PV4" indicates the position of a region of relatively high upper-tropospheric PV.

Fig 3.48. As in Fig. 3.33, except for an STC forming in association with a subtropical disturbance at 0000 UTC 5 June 1986 (t_0). Label "PV4" indicates the position of a region of relatively high upper-tropospheric PV.

Fig 3.49. As in Fig. 3.34, except for an STC forming in association with a subtropical disturbance at 0000 UTC 5 June 1986 (t_0). Label "PV4" indicates the position of a region of relatively high upper-tropospheric PV.

Fig 3.50. As in Fig. 3.35, except for an STC forming in association with a subtropical disturbance at 0000 UTC 5 June 1986 (t_0). Label "PV4" indicates the position of a region of relatively high upper-tropospheric PV.

Fig 3.51. As in Fig. 3.36, except for an STC forming in association with a subtropical disturbance at 0000 UTC 5 June 1986 (t_0). Label "PV4" indicates the position of a region of relatively high upper-tropospheric PV.

Fig 3.52. As in Fig. 3.32, except for an STC forming in association with PV debris at 0000 UTC 24 August 2005 (t_0). Labels "PV5a" and "PV5b" indicate the position of regions of relatively high upper-tropospheric PV.

Fig 3.53. As in Fig. 3.33, except for an STC forming in association with PV debris at 0000 UTC 24 August 2005 (t_0). Labels "PV5a" and "PV5b" indicate the position of regions of relatively high upper-tropospheric PV.

Fig 3.54. As in Fig. 3.34, except for an STC forming in association with PV debris at 0000 UTC 24 August 2005 (t_0). Labels "PV5a" and "PV5b" indicate the position of regions of relatively high upper-tropospheric PV.

1. Introduction

1.1 Motivation

The National Hurricane Center (NHC) online glossary defines a subtropical cyclone (STC) as a "non-frontal low-pressure system that has characteristics of both tropical and extratropical cyclones**…**. Unlike tropical cyclones, subtropical cyclones derive a significant portion of their energy from baroclinic sources…often associated with an upper-level low or trough" (OFCM 2013). The NHC definition emphasizes the hybrid nature of STCs and suggests that both baroclinic and diabatic energy sources contribute to STC formation. The duality of baroclinic and diabatic energy sources contributing to STC formation causes STCs to be located somewhere between extratropical cyclones (ECs) and tropical cyclones (TCs) in an idealized cyclone energy source phase space, in which various combinations of baroclinic and diabatic energy sources are used to distinguish between cyclone types.

Despite the existence of an STC definition in the NHC online glossary, there is currently no objective set of characteristics used to define STCs (Evans and Guishard 2009). The lack of an objective set of characteristics used to define STCs presents an ongoing challenge to researchers and operational forecasters studying this phenomenon. In addition, the hybrid nature of STCs makes them likely candidates to become TCs via the tropical transition (TT) process (Davis and Bosart 2003, 2004). Noteworthy examples of STCs that became TCs via the TT process include Hurricane Grace (1991) (Pasch and Avila 1991), Hurricane Michael (2000) (Franklin et al. 2001), Hurricane Karen (2001) (Beven et al. 2003), and Tropical Storm (TS) Beryl (2012) (Beven 2012).

The tendency for STCs to form and rapidly undergo TT close to the east coast of the United States can create potential challenges for operational forecasters and emergency managers. One such cyclone, TS Beryl (May 2012), formed off the east coast of North Carolina as an STC, underwent TT, and made landfall as a TS near Jacksonville Beach, FL, in ~52 h (Beven 2012). Along with its rapid formation and TT, TS Beryl is also remembered for being the strongest TC to make landfall in the continental United States before the official start of the North Atlantic TC season.

In view of the appreciable contribution of STCs to the total number of cyclones included in the NHC Hurricane Database (HURDAT) (~12%) (Guishard et al. 2009), the lack of an objective set of characteristics used to define STCs motivates this research. The goal of this research is to formulate an objective identification technique for detecting STC formation by quantifying of the relative contributions of baroclinic and diabatic processes during the evolution of individual cyclones. This objective identification technique for detecting STC formation will be used to refine the NHC definition of STCs and to construct a North Atlantic STC climatology. Additionally, conceptual models of the most common upper-tropospheric features linked to STC formation will be constructed to inform operational forecasters and emergency managers of the potential pathways to STC formation, as well as to provide the research community with further insight into the TT process.

1.2 Literature Review

1.2.1 STC Formation

Oceanic cyclones exhibiting properties of both extratropical and tropical systems have been categorized as STCs since the early 1950s (e.g., Moore and Davis 1951; Simpson 1952). Moore and Davis (1951) and Simpson (1952) analyzed cold-core oceanic cyclones, initially collocated with regions of relatively cold upper-tropospheric air, that transitioned into warm-core oceanic cyclones above relatively warm sea surface temperatures (SSTs). Figure 1.1 shows the track of the transitioning STC discussed in Moore and Davis (1951) in relation to a region of relatively cold upper-tropospheric air in May 1951. Although the transitioning STC did not make landfall in the continental United States, the cyclone was noteworthy to operational forecasters for its unusual baroclinic development off the east coast of Florida, as well as its rapid intensification into a hurricane before the official start of the North Atlantic TC season.

Many questions concerning the dynamical and thermodynamic processes governing the baroclinic development of North Atlantic TCs remained unanswered until the advent of satellite observations and global gridded datasets. Bosart and Bartlo (1991) reexamined some of these questions in their study of the baroclinic development of Hurricane Diana off the east coast of Florida in September 1984. The lower-tropospheric disturbance that became Hurricane Diana developed slightly downshear of a region of relatively cold upper-tropospheric air accompanying the intrusion of a midlatitude potential vorticity (PV) streamer into the subtropics. Figure 1.2 shows the progression of the midlatitude PV streamer, represented in terms of 300-hPa relative vorticity, into the subtropics from 0000 UTC 3 September 1984 through 1200 UTC 7 September 1984. Diabatic heating, occurring in a region of upward motion and deep convection associated with positive PV advection by the thermal wind in the upper troposphere (Fig. 1.2), was

thought to have redistributed PV in the vertical by increasing lower-tropospheric PV and decreasing upper-tropospheric PV (Raymond 1992). This diabatic redistribution of PV in the vertical occurred simultaneously with a reduction in the relatively high vertical wind shear values that had been present over the developing cyclone. The work by Bosart and Bartlo (1991), along with subsequent work by Bracken and Bosart (2000) and Davis and Bosart (2001), not only demonstrated that TCs can develop in regions of appreciable vertical wind shear, but suggest that vertical wind shear may be necessary to focus the upward motion and deep convection needed for an EC to transition into a TC.

1.2.2 Tropical Transition

The apparent need for appreciable vertical wind shear values identified in Bosart and Bartlo (1991), Bracken and Bosart (2000), and Davis and Bosart (2001) differs substantially from the seminal findings of Gray (1968) and DeMaria et al. (2001), who suggest that weak vertical wind shear values are required for tropical cyclogenesis. Davis and Bosart (2003, 2004) reconciled these opposing ideas about vertical wind shear with the introduction of their TT paradigm.

In the initial stages of a TT event, advection of upper-tropospheric absolute vorticity by the thermal wind is associated with a region of upward motion that focuses deep convection and diabatic heating. Figure 1.3 illustrates this situation during the TT of Hurricane Humberto in September 2001, where absolute vorticity is represented in terms of PV on the 340 K isentropic surface and the direction of the thermal wind is represented in terms of the direction of the deep-layer shear. As stated in Davis and

Bosart (2003), "The location of deep convection prior to Humberto is directly downshear from the positive PV anomaly in the upper troposphere." The appreciable vertical wind shear values located over the developing cyclone are subsequently reduced by the diabatic redistribution of PV in the vertical and by divergent outflow in the upper troposphere (Fig. 1.4). The subsequent reduction in vertical wind shear values over the developing cyclone allowed Hurricane Humberto to continue to intensify via wind-induced surface heat exchange (Emanuel 1986, 1995). In this way, both baroclinic and diabatic processes contribute to the formation of TCs via the TT process. The same baroclinic and diabatic processes contribute to the formation of STCs, or cyclones with characteristics of both tropical and extratropical cyclones in the initial stages of the TT process. Subsequent studies by Hulme and Martin (2009a,b) continue to emphasize the importance of diabatic heating during the TT process and suggest that the TT process is comparable to the frontal occlusion process typical of ECs (e.g., Stoelinga et al. 2002; Posselt and Martin 2004).

1.2.3 Baroclinic Development in the North Atlantic Basin

Several studies examining the frequency of baroclinically influenced North Atlantic STC and TC development followed the publication of Davis and Bosart (2003, 2004). Evans and Guishard (2009) and Guishard et al. (2009) constructed a North Atlantic STC climatology (1957–2002), shown in Figure 1.5, using the 40-yr European Centre for Medium-Range Weather Forecasts (ECMWF) Re-Analysis (ERA-40) at 1.125° × 1.125° resolution (Uppala et al. 2005). The Guishard et al. (2009) criteria for STC identification are highly subjective, restricting STCs to cyclones in the 20°–40°N

latitude band that attained 925-hPa gale-force winds (>17 m s^{-1}) at some time during their life cycle and hybrid structure in the Hart (2003) cyclone phase space for ≥36 h during their life cycle. The Hart (2003) cyclone phase space criterion was included in the study to identify cyclones exhibiting hybrid structure consistent with the NHC STC definition (OFCM 2013). The Hart (2003) cyclone phase space places individual cyclones in a continuum of cyclone types by quantifying: 1) the vertical depth of the cyclone's interior temperature anomaly and 2) asymmetries in the cyclone's lower-tropospheric thickness field. Cyclones exhibiting "shallow" and "moderately deep" warm cores in the Hart (2003) cyclone phase space were considered to exhibit hybrid structure consistent with the NHC STC definition, regardless of the asymmetry of their horizontal thickness field.

In addition to the aforementioned STC identification criteria, Guishard et al. (2009) also rejected cyclones that were purely warm-core or cold-core for ≥24 h prior to obtaining hybrid structure in the Hart (2003) cyclone phase space. This STC identification criterion, as stated in Guishard et al. (2009), was designed to limit the climatology to STCs that developed suddenly in the North Atlantic basin, "surprising" operational forecasters.

McTaggart-Cowan et al. (2008) expanded upon the concept of the cyclone phase space developed by Hart (2003), utilizing a dynamically based classification scheme to describe baroclinically influenced TC development over the North Atlantic during 1948–2004 using the National Centers for Environmental Prediction–National Center for Atmospheric Research (NCEP–NCAR) reanalysis dataset at 2.5° × 2.5° resolution (Kalnay et al. 1996). TC developments included in their study were classified based on

two external forcings in the near-TC environment prior to TC formation: 1) quasigeostrophic (QG) forcing for ascent, determined by the average convergence of the 400–200-hPa Q vector within 6° of the cyclone center, and 2) lower-tropospheric baroclinicity, determined by asymmetries in the 1000–700-hPa thickness field within 10° of the cyclone center. The study found that only 40% of North Atlantic TCs formed in nonbaroclinic environments.

Subsequent work by McTaggart-Cowan et al. (2013) resulted in the construction of a global climatology of baroclinically influenced tropical cyclogenesis events from 1948 through 2010. This study, which used metrics representing the same external forcings in the near-TC environment as McTaggart-Cowan et al. (2008), found that 46% of North Atlantic TCs formed in association with an upper-tropospheric disturbance, represented by high values of 400–200-hPa Q-vector convergence. These results were consistent with the results of McTaggart-Cowan et al. (2008), who found that 47% of North Atlantic TCs from 1948 through 2004 formed in association with an upper-tropospheric disturbance.

McTaggart-Cowan et al. (2008, 2013) describe the near-TC environment prior to baroclinically influenced TC formation, but do not explicitly quantify the relative contributions of baroclinic and diabatic processes during the evolution of cyclones included in their studies. Prior work by Davis (2010) developed a methodology for quantifying the relative contributions of baroclinic and diabatic processes during the evolution of individual cyclones in order to identify STCs within idealized numerical simulations. The author believes that quantification of the relative contributions of baroclinic and diabatic processes during the evolution of individual cyclones could

provide the basis for formulating an objective identification technique for detecting STC formation in a reanalysis dataset, constructing a dynamically based STC climatology, and developing a better understanding of the dynamical and thermodynamic processes that govern STC formation.

1.3 Research Goals and Thesis Structure

This research expands upon the work of Davis (2010) by investigating the roles of baroclinic and diabatic processes during the evolution of individual cyclones in the NCEP Climate Forecast System Reanalysis (CFSR) 0.5° gridded dataset (Saha et al. 2010) from a PV perspective. An objective STC identification technique will be formulated and applied to baroclinically influenced tropical cyclogenesis events over the North Atlantic identified in McTaggart-Cowan et al. (2013) in order to construct a 1979–2010 STC climatology. A cyclone-relative composite analysis will also be performed on subjectively constructed clusters of North Atlantic STCs identified in the 1979–2010 climatology to document the structure, motion, and evolution of upper-tropospheric features linked to STC formation. The author hypothesizes that the 1979–2010 climatology will reveal a considerable amount of intraseasonal variability associated with the location and frequency of North Atlantic STC formation that is similar, but not identical, to the intraseasonal variability associated with the location and frequency of North Atlantic TCs. The author also hypothesizes that many STCs identified in the 1979–2010 climatology will form in association with a PV streamer injected into the subtropics by a precursor anticyclonic wave breaking (AWB) event (Fig. 1.6), as

suggested in the idealized numerical simulations of Davis (2010).

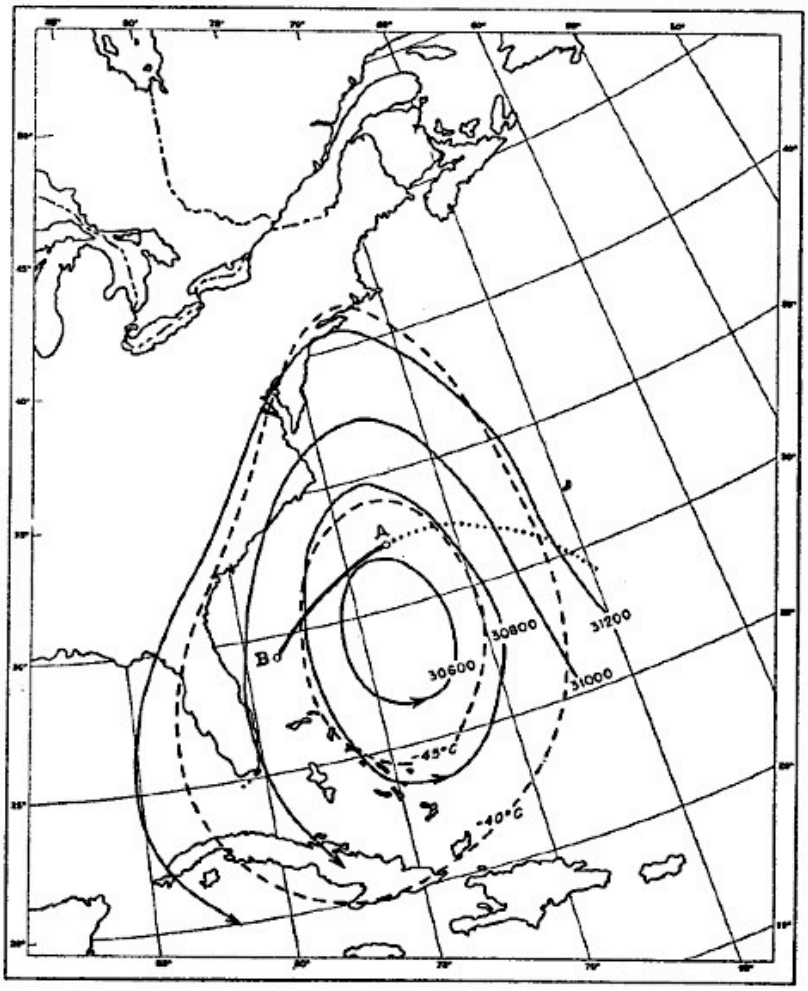

Fig. 1.1. Depiction of an STC forming in the presence of an upper-tropospheric disturbance in May 1951. Analysis shows 300-hPa geopotential height (solid contours, every 200 ft) and temperature (dashed contours, every 5°C) at 1500 UTC 16 May 1951. The track of the incipient surface vortex is denoted by the dotted line. Location "A" represents the position of the first closed circulation. The subsequent track of the closed circulation is denoted by the thick solid line. Location "B" represents the position where the cyclone reached hurricane intensity [Fig. 3 and adapted caption from Moore and Davis (1951)].

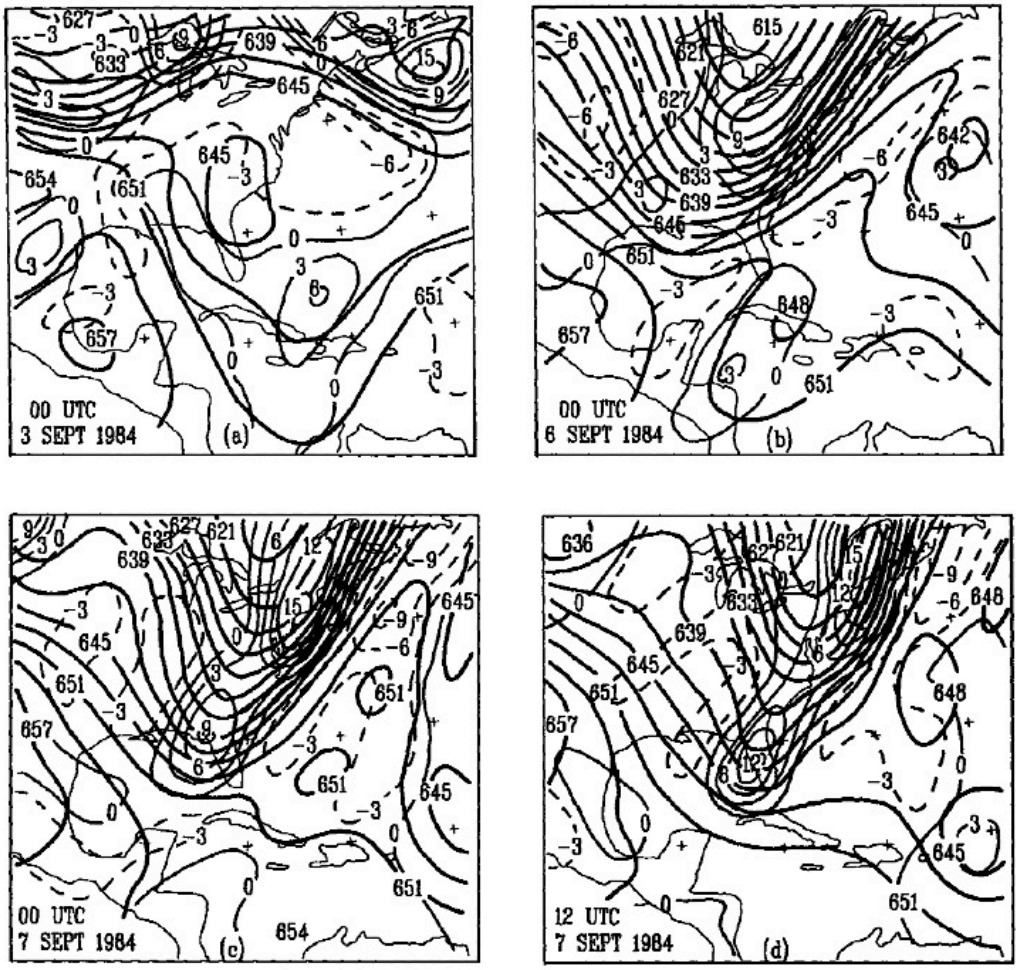

Fig. 1.2. Depiction of the upper-tropospheric features linked to the formation of Hurricane Diana off the east coast of Florida in September 1984. Analyses show 300-hPa relative vorticity [thin solid (dashed) contours represent positive (negative) values, every 3×10^{-5} s^{-1}] and 500–200-hPa thickness (thick solid contours, every 3 dam) at (a) 0000 UTC 3 September 1984, (b) 0000 UTC 6 September 1984, (c) 0000 UTC 7 September 1984, and (d) 1200 UTC 7 September 1984 [Fig. 14 and adapted caption from Bosart and Bartlo (1991)].

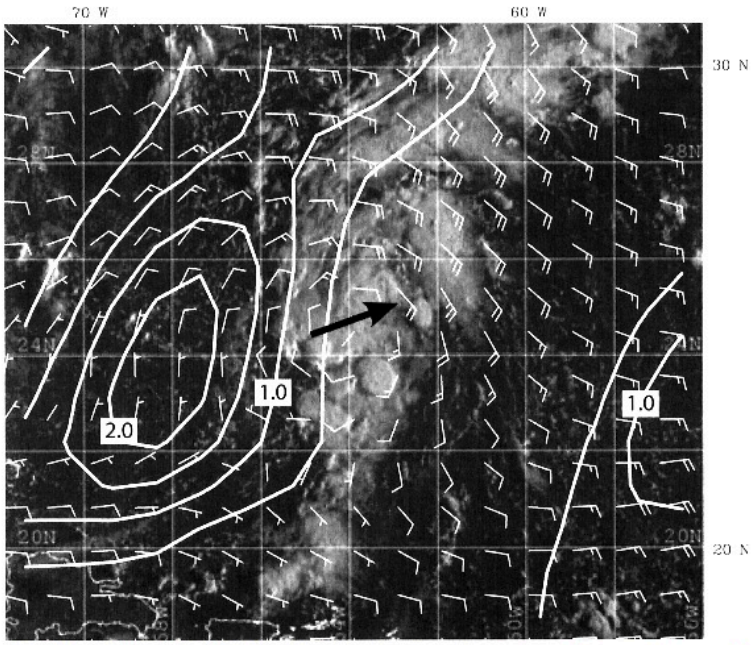

Fig. 1.3. Potential vorticity on the 340 K potential temperature surface (white contours, every 0.5 PVU) and 900-hPa winds (white barbs, m s^{-1}) from the National Centers for Environmental Prediction's Aviation model analysis valid at 1200 UTC 21 September 2001 overlaid on visible satellite imagery at the corresponding time. The heavy black arrow represents the deep-layer shear direction over the storm center (magnitude equals 5 m s^{-1}) [Fig. 2 and adapted caption from Davis and Bosart (2003)].

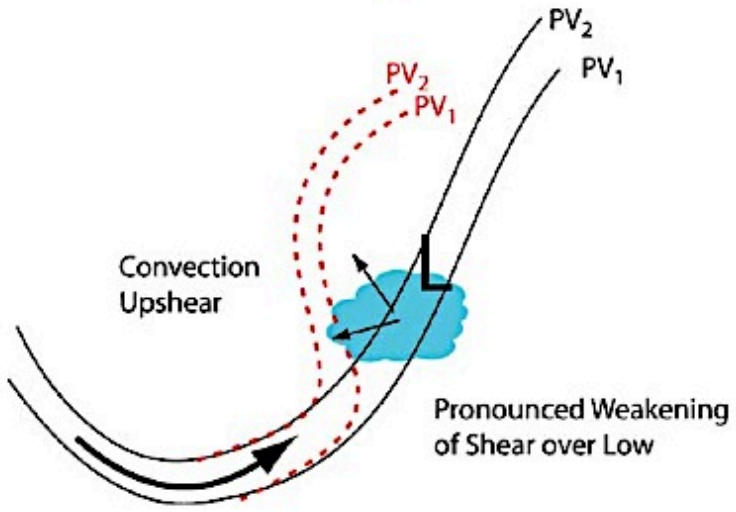

Fig. 1.4. Schematic showing the effect of convection (blue area) upshear of a surface low ("L"). Small arrows indicate divergent motion near the dynamic tropopause. Large arrow indicates flow within the upper-tropospheric jet. Solid lines are two initial potential vorticity contours ($PV_2 > PV_1$) and red dashed lines indicate the positions of the same contours after deep convection has developed [Fig. 3 and caption adapted from Davis and Bosart (2004)].

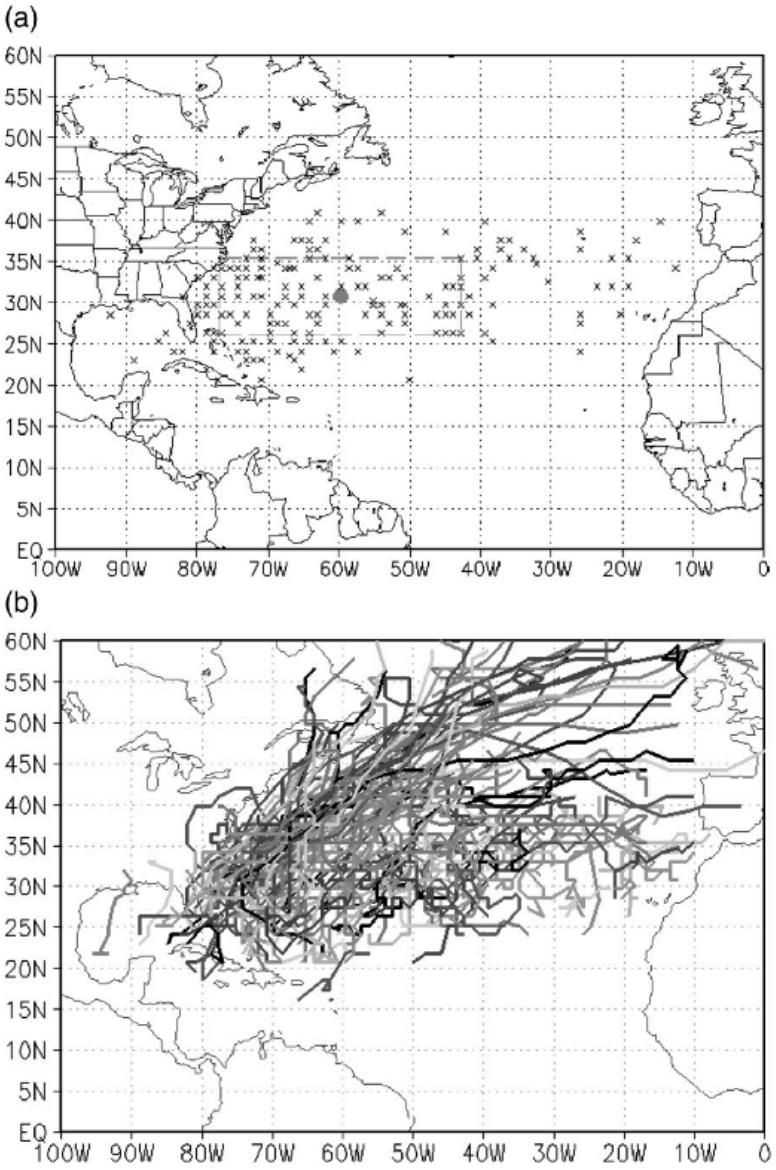

Fig. 1.5. Geographic distribution of North Atlantic STCs in the ERA-40: (a) genesis location (onset of gale-force winds) and (b) tracks. The gray dot in (a) indicates the average position of all 197 ERA-40 STCs at the onset of gale-force winds and the surrounding box (dashed line) encloses the area within one standard deviation from this mean location [Fig. 5 and adapted caption from Guishard et al. (2009)].

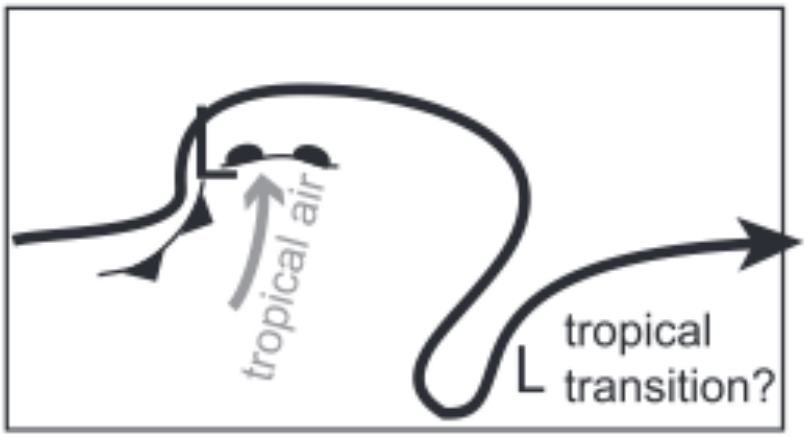

Fig. 1.6. Schematic representation of a possible pathway for STC formation. The subtropical jet (heavy solid line with arrow) is perturbed by a mature surface cyclone (large "L"), resulting in the injection of a PV streamer into the subtropics. The small "L" represents an incipient STC [Fig. 16 and caption adapted from Davis (2010)].

2. Data and Methodology

2.1 Candidate STCs

Baroclinically influenced tropical cyclogenesis cases identified in McTaggart-Cowan et al. (2013) that occurred over the North Atlantic from 1979 through 2010 were considered for potential STC identification (460 candidate STCs). The period from 1979 through 2010 was chosen to coincide with the period covered by the 0.5° CFSR dataset (Saha et al. 2010). North Atlantic cyclone tracks were obtained from the v03r03 edition of the International Best Track Archive for Climate Stewardship (IBTrACS) dataset (Knapp et al. 2010). In addition, North Atlantic cyclone tracks were extended backward 36 h from their first IBTrACS position using a reverse steering flow calculation described in detail in McTaggart-Cowan et al. (2008).

As previously discussed in section 1.2.3, McTaggart-Cowan et al. (2013) separated tropical cyclogenesis cases into one of five development pathways based on two external forcings in the near-TC environment prior to TC formation: 1) QG forcing for ascent (**Q**), determined by the average convergence of the 400–200-hPa Q vector within 6° of the cyclone center, and 2) lower-tropospheric baroclinicity (Th), determined by asymmetries in the 1000–700-hPa thickness field within 10° of the cyclone center. The five development pathways identified in McTaggart-Cowan et al. (2013) include: 1) Strong TT, 2) Weak TT, 3) Trough induced, 4) Low-level baroclinic, and 5) Nonbaroclinic events. The relative values of **Q** and Th associated with each development pathway, as well as a brief physical description of each development pathway, are given in Table 1. To ensure consistency with the NHC STC definition, only baroclinically

influenced tropical cyclogenesis cases occurring in the presence of an upper-tropospheric disturbance were considered for potential STC identification, restricting the development pathways considered to those with "high" values of QG forcing for ascent in Table 1: Strong TT, Weak TT, and Trough induced (222 candidate STCs out of 460 possible STCs).

2.2 Methodology

2.2.1 Adapted Davis (2010) Methodology

The Davis (2010) methodology for STC identification is based on the concept of Ertel PV and formulated in terms of two PV metrics that quantify the relative contributions of baroclinic processes and condensation heating during the evolution of individual cyclones. The Davis (2010) methodology distinguishes between cyclone types within an idealized numerical simulation based on the relative contributions of baroclinic processes and condensation heating during the evolution of individual cyclones and can be thought of as similar to the cyclone phase space diagrams developed by Hart (2003). The transition from identifying STCs within an idealized numerical simulation to the 0.5° CFSR dataset requires the adaptation of the original Davis (2010) methodology. All PV metrics considered in the present study are calculated in a 6° box centered over the surface cyclone. The first PV metric in the Davis (2010) methodology, PV1, represents lower-tropospheric baroclinic processes in terms of the near-surface potential temperature anomaly:

$$\mathrm{PV1} = g\eta G/\Delta p_1, \tag{1}$$

where

$$G = (G_x^2 + G_y^2)^{1/2},$$

$$G_x = \frac{1}{L_{xc}} \int_{-\frac{L_y}{2}}^{\frac{L_y}{2}} \theta' dy|_{x=\frac{L_x}{2}} - \frac{1}{L_{xc}} \int_{-\frac{L_y}{2}}^{\frac{L_y}{2}} \theta' dy|_{x=-\frac{L_x}{2}},$$

$$G_y = \frac{1}{L_y} \int_{-\frac{L_{xn}}{2}}^{\frac{L_{xn}}{2}} \theta' dx|_{y=\frac{L_y}{2}} - \frac{1}{L_y} \int_{-\frac{L_{xs}}{2}}^{\frac{L_{xs}}{2}} \theta' dx|_{y=-\frac{L_y}{2}},$$

η is the absolute vorticity, and θ' is the potential temperature anomaly calculated at an individual grid point from an 11-day centered mean. The potential temperature anomaly variations across the 6° box, G_x and G_y, are averaged between 925 hPa and 850 hPa prior to computing G. The horizontal scales, L_y and L_x, are the length of 6° of latitude and the longitudinal length of the box as a function of latitude, respectively. The horizontal scales, L_{xn}, L_{xc}, and L_{xs}, represent the lengths of the northern edge, center, and southern edge of the 6° box, respectively. The vertical scale, Δp_1, is equal to 425 hPa to match the vertical integration of the lower-tropospheric PV anomaly (see below).

The second PV metric in the Davis (2010) methodology, PV2, represents midtropospheric latent heat release in terms of the lower-tropospheric PV anomaly:

$$\text{PV2} = \frac{\int_{-\frac{L_x}{2}}^{\frac{L_x}{2}} dx \int_{-\frac{L_y}{2}}^{\frac{L_y}{2}} dy \int_{500\ hPa}^{925\ hPa} q' dp}{L_{xc} L_y \Delta p_2}, \quad (2)$$

where q' is the PV anomaly calculated at an individual grid point from an 11-day centered mean and Δp_2 is equal to 425 hPa.

For the purposes of this study, the author introduces an additional metric, PV3, representing upper-tropospheric dynamical processes in terms of the upper-tropospheric PV anomaly:

$$\mathrm{PV3} = \frac{\int_{-\frac{L_x}{2}}^{\frac{L_x}{2}} dx \int_{-\frac{L_y}{2}}^{\frac{L_y}{2}} dy \int_{200\ hPa}^{500\ hPa} q' dp}{L_{xc} L_y \Delta p_3}, \quad (3)$$

where Δp_3 is equal to 300 hPa. A schematic representation of the regions over which PV1, PV2, and PV3 are calculated is shown in Fig. 2.1.

The original Davis (2010) methodology used the ratio PV1/PV2 as a measure of the contribution of lower-tropospheric baroclinic processes relative to the contribution of condensation heating. With the introduction of PV3, the author introduces the ratio PV3/PV2 as a measure of the contribution of upper-tropospheric dynamical processes relative to the contribution of condensation heating. The values of PV1, PV2, PV3, and PV3/PV2 are smoothed using a 1–2–1 temporal filter prior to STC identification.

2.2.2 STC Identification

In order to determine the time and location of STC formation within the subset of baroclinically influenced tropical cyclogenesis cases specified in section 2.1, an objective identification technique for detecting STC formation was formulated, incorporating PV2 and PV3, and applied to the 0.5° CFSR dataset. STC formation was identified the first time ($t = t_0$) at which the following criteria were met:

1) There is a positive upper-tropospheric PV anomaly (representing an upper-tropospheric low or trough) and positive lower-tropospheric PV anomaly (e.g., representing a PV tower) over the cyclone center (i.e., PV3 > 0 and PV2 > 0 at $t = t_0$)

2) The upper-tropospheric PV anomaly begins to be eroded by midtropospheric latent heat release [i.e., d(PV3)/dt < 0 at $t = t_0 + 6$ h and $t_0 + 12$ h]

3) The ratio of the magnitude of the upper-tropospheric PV anomaly to the magnitude of the lower-tropospheric PV anomaly decreases [i.e., d(PV3/PV2)/dt < 0 at $t = t_0$ and $t_0 + 6$ h]

4) The cyclone has not been classified by NHC as a hurricane or tropical storm at $t = t_0$, or as a tropical depression for ≥ 12 h prior to $t = t_0$

The third criterion may be stated alternatively as d(PV3)/dt < (PV3/PV2)d(PV2)/dt at $t = t_0$ and $t_0 + 6$ h. This criterion and its simpler counterpart, d(PV3)/dt < d(PV2)/dt at $t = t_0$ and $t_0 + 6$ h, were tested and the same results were found for both (not shown). Based on this test, the simpler criterion, d(PV3)/dt < d(PV2)/dt at $t = t_0$ and $t_0 + 6$ h (i.e., the magnitude of the upper-tropospheric PV anomaly decreases faster than the magnitude of the lower-tropospheric PV anomaly), was adopted for interpreting graphical representations of STC formation.

An example of the application of the objective identification technique for detecting STC formation is shown in Fig. 2.2 for the case of STC Sean, which formed

over the western North Atlantic in November 2011. STC Sean was selected as an illustrative case of STC formation over the western North Atlantic in the presence of an upper-tropospheric disturbance. Figure 2.1 reveals the changing PV structure of STC Sean during its evolution. The objective identification technique for detecting STC formation indicates that Sean became an STC at 1200 UTC 7 November 2011, at the time when the upper-tropospheric PV anomaly began to be eroded by midtropospheric latent heat release (Fig. 2.2).

The objective identification technique for detecting STC formation applied to STC Sean was subsequently applied to the subset of baroclinically influenced tropical cyclogenesis cases specified in section 2.1 using the 0.5° CFSR dataset. The time and location of STC formation determined by the objective identification technique was used to construct a 1979–2010 climatology.

2.2.3 Clusters and Composite Analysis

In order to document the structure, motion, and evolution of the upper-tropospheric features linked to STC formation, a cyclone-relative composite analysis was performed on subjectively constructed clusters of STCs identified in the 1979–2010 climatology. STCs identified in the 1979–2010 climatology were separated into five clusters representing the most common upper-tropospheric features linked to STC formation: 1) PV Streamers, 2) Cutoffs, 3) Midlatitude Troughs, 4) Subtropical Disturbances, and 5) PV Debris. The characteristics of each of the five clusters will be discussed in detail in section 3.2. Cyclone-relative composites were constructed by

shifting STC events within each cluster to the average location of STC formation in that cluster and then averaging diagnostic fields across STC events for that cluster. Composites of derived diagnostic variables (e.g., coupling index, relative vorticity) were obtained by calculating the variable for each STC event and then averaging the variable across STC events within each cluster.

2.2.4 Case Studies

Illustrative STC events that typify each of the five clusters representing the most common upper-tropospheric features linked to STC formation were subjectively chosen as case studies based on the resemblance of their diagnostic fields to the corresponding composites. For consistency, the same diagnostic fields evaluated in the cyclone-relative composite analysis are considered for each case study.

Category (pathway)	Metric Value Q	Th	Brief description
Nonbaroclinic	Low	Low	No appreciable baroclinic influences
Low-level baroclinic	Low	High	Strong lower-level thermal gradients without an upper-level disturbance
Trough induced	High	Low	Upper-level disturbance without appreciable lower-level thermal gradients
Weak TT	High	Medium	Upper-level disturbance with moderate lower-level thermal gradients
Strong TT	High	High	Upper-level disturbance with strong lower-level thermal gradients

Table 1. Description of TC development pathways identified in McTaggart-Cowan et al. (2013). The name of each category (first column) will be used to describe the development pathway throughout the text [Table 2 and caption adapted from McTaggart-Cowan et al. (2013)].

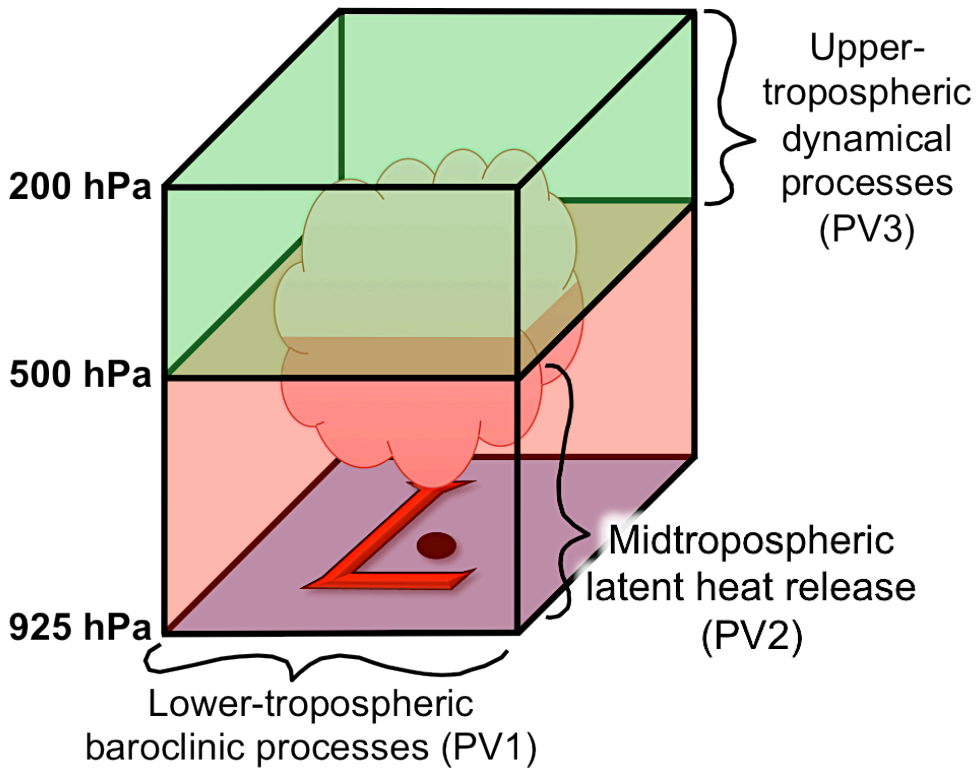

Fig 2.1. Schematic representation of the regions over which PV1, PV2, and PV3 are calculated. All calculations are performed within a 6° box centered over the surface cyclone (red "L"). The center of the surface cyclone is denoted by a purple dot. A region of latent heat release within the 6° box is denoted by a cloud.

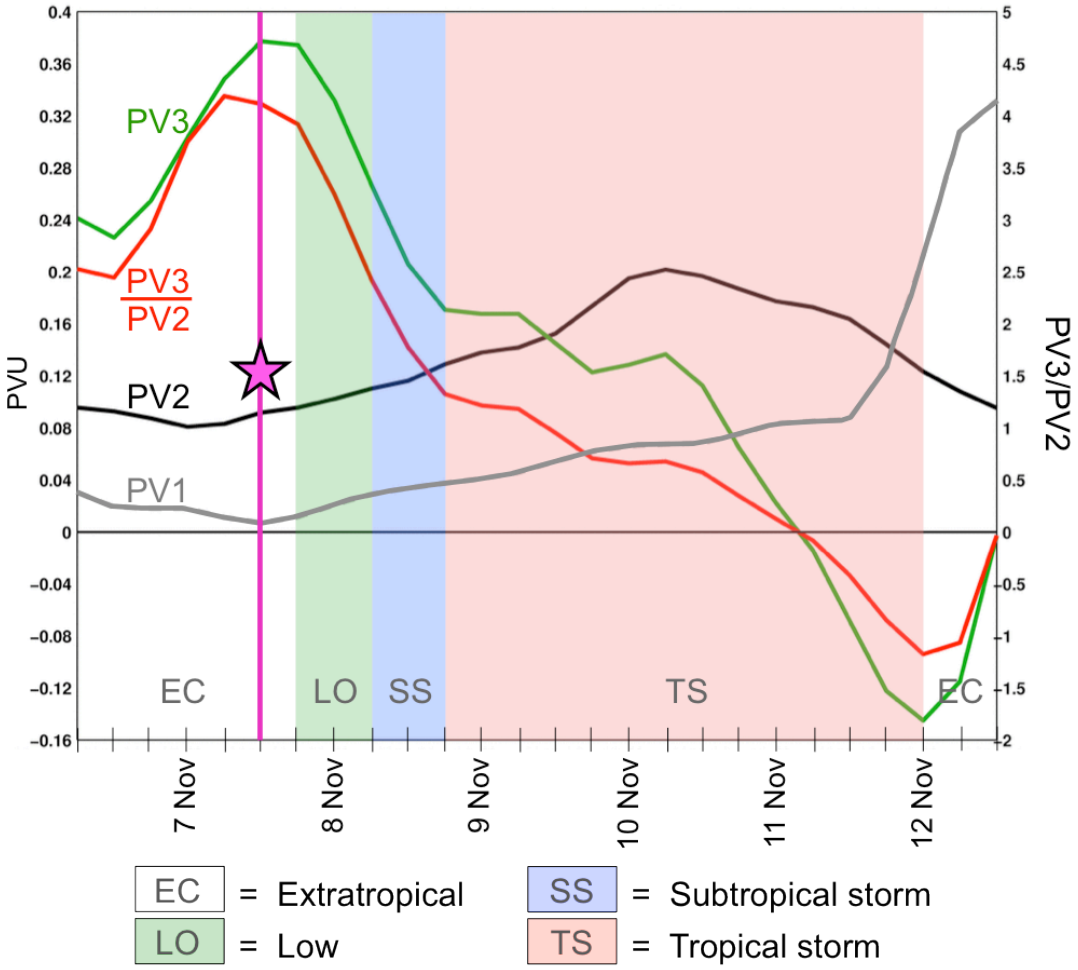

Fig. 2.2. Graphical representation of PV1, PV2, PV3, and PV3/PV2 during the evolution of STC Sean (2011). The white, green, blue, and pink regions of the graph denote the time periods when NHC classified Sean as an EC, low, subtropical storm, and tropical storm, respectively. The magenta line and star denote the time when the objective identification technique indicated STC formation had occurred.

3. Results

3.1 STC Climatology (1979–2010)

The objective identification technique for detecting STC formation, formulated in section 2.2.2, was applied to the subset of baroclinically influenced tropical cyclogenesis cases identified in McTaggart-Cowan et al. (2013) that occurred over the North Atlantic during 1979–2010 in the presence of an upper-tropospheric disturbance. Of the 222 candidate cyclones that met these requirements, 105 were identified as STCs (~3 STCs per year).

Figure 3.1 illustrates the intraseasonal variability associated with the location of STC formation in the North Atlantic basin. STC formation primarily occurs over the southern Gulf Stream and western Caribbean Sea during April–July, coinciding with the highest mean sea surface temperatures (SSTs) in the North Atlantic basin during that period (Fig. 3.2a). An intrusion of relatively cold upper-tropospheric air accompanying an upper-tropospheric disturbance moving over the southern Gulf Stream/western Caribbean Sea during April–July would steepen local lapse rates and facilitate the development of deep convection that serves as a catalyst for STC formation. STC formation becomes more frequent over the central and eastern North Atlantic during August–December (Fig. 3.1) as mean SSTs increase throughout the basin (Fig. 3.2b). The observed increase in mean SSTs during August–December causes the central and eastern North Atlantic to become favorable for the development of deep convection following an intrusion of relatively cold upper-tropospheric air accompanying an upper-tropospheric disturbance.

Intraseasonal variability is also associated with the frequency of STC formation in the North Atlantic basin. Figure 3.3 separates the 105 STCs identified in this study by the month during which they formed. STC formation occurs most frequently in September and October, with a secondary peak in June. A seasonal minimum in the frequency of STC formation is observed in July, likely associated with the lack of relatively cold upper-tropospheric air impinging upon the subtropics during that month (McTaggart-Cowan et al. 2008). This result is consistent with the results of Guishard et al. (2009), who found a seasonal minimum in the frequency of STC formation in July as well.

Figure 3.3 also indicates that STC formation can occur from April through December in the North Atlantic basin, outside the range of the official North Atlantic TC season (June–November). As previously discussed in section 1.1, the potential for STCs to form close to the east coast of the United States before the official start of the North Atlantic TC season (Fig. 3.1) creates ongoing challenges for operational forecasters and emergency managers.

3.2 STC Clusters

In order to document the structure, motion, and evolution of the upper-tropospheric features linked to STC formation, a cyclone-relative composite analysis was performed on subjectively constructed clusters of STCs identified in the 1979–2010 climatology. As mentioned in section 2.2.3, STCs included in the 1979–2010 climatology were separated into five clusters representing the most common upper-

tropospheric features linked to STC formation: 1) PV Streamers, 2) Cutoffs, 3) Midlatitude Troughs, 4) Subtropical Disturbances, and 5) PV Debris. The number of STCs included in each cluster, as well as the number of STCs with unclassifiable upper-tropospheric precursors, is shown in Fig. 3.4.

STCs forming in association with a PV streamer injected into the subtropics during the *initial stages* of an upstream anticyclonic wave breaking (AWB) event were included in the PV Streamer cluster (N = 8). In order to be included in this cluster, the PV streamer linked to STC formation must maintain a clear connection to the midlatitudes at the time of STC formation (t_0). A schematic representation of an STC forming in association with a PV streamer is shown in Fig. 3.5a.

STCs forming in association with a region of relatively high upper-tropospheric PV cut off in the subtropics during the *latter stages* of an upstream AWB event were included in the Cutoff cluster (N = 22). In order to be included in this cluster, the region of relatively high upper-tropospheric PV linked to STC formation must be entirely removed from the midlatitude flow at t_0. This region of relatively high upper-tropospheric PV typically fractures from the equatorward end of a PV streamer injected into the subtropics during the *initial stages* of an upstream AWB event. A schematic representation of an STC forming in association with a cutoff is shown in Fig. 3.5b.

STCs forming in association with a broad midlatitude trough that does *not* develop as a result of upstream AWB were included in the Midlatitude Trough cluster (N = 10). A schematic representation of an STC forming in association with a midlatitude trough is shown in Fig. 3.5c.

STCs forming in association with the progression of a small-scale PV filament around the northern edge of an upper-tropospheric subtropical anticyclone were included in the Subtropical Disturbance cluster (N = 22). The progressive PV filament associated with this cluster is considerably smaller in meridional extent than the upper-tropospheric disturbances associated with PV Streamers, Cutoffs, or Midlatitude Troughs. A schematic representation of an STC forming in association with a subtropical disturbance is shown in Fig. 3.5d.

STCs forming in association with a disorganized region of relatively high upper-tropospheric PV deposited in the subtropics several days prior to STC formation were included in the PV Debris cluster (N = 31). In order to be included in this cluster, a disorganized region of relatively high PV must be moving westward in the subtropics on the equatorward edge of a broad subtropical anticyclone at t_0. A schematic representation of an STC forming in association with PV debris is shown in Fig. 3.5e.

Figure 3.6 illustrates the spatial distribution of the five most common upper-tropospheric features linked to STC formation in the North Atlantic basin. STCs forming in association with PV streamers, cutoffs, and midlatitude troughs have the most pronounced midlatitude connection, primarily developing poleward of 20°N across the majority of the North Atlantic. STCs forming in association with subtropical disturbances primarily develop over the southern Gulf Stream, western Caribbean Sea, and eastern Gulf of Mexico, considerably closer to North America than many of the STCs forming in association with PV streamers, cutoffs, and midlatitude troughs. This longitudinal restriction is likely related to the position of an upper-tropospheric subtropical anticyclone over Central America during Northern Hemisphere (NH)

summer—a feature required for STC formation to be associated with a subtropical disturbance. STCs forming in association with PV debris have the least pronounced midlatitude connection, primarily developing equatorward of 30°N over the Gulf of Mexico, northern Caribbean Sea, and main development region (MDR).

3.3 Composite Analysis

3.3.1 PV Streamer Cluster Composite

As discussed in section 3.2, STCs forming in association with a PV streamer injected into the subtropics during the initial stages of an upstream AWB event were included in the PV Streamer cluster (N = 8). Time-lagged cyclone-relative composites of PV and winds on the 350 K isentropic surface reveal rapid ridge amplification, beginning at t_0 – 48 h, upstream of the location of STC formation at t_0 (Figs. 3.7d–f). A region of 600–400-hPa layer-averaged ascent $< -3 \times 10^{-3}$ hPa s^{-1} has developed to the west of the amplifying ridge over the Tennessee Valley, in the poleward exit region of a 25–30 m s^{-1} 200-hPa jet streak, on the eastern edge of a broad upper-tropospheric trough (Fig. 3.8d). Figure 3.8d also depicts 300–200-hPa layer-averaged irrotational wind vectors ≥ 2 m s^{-1} directed toward higher 200-hPa PV values over Arizona/Colorado at t_0 – 48 h. The orientation of the 300–200-hPa layer-averaged irrotational wind vectors (perpendicular to 200-hPa PV contours, directed toward higher 200-hPa PV values) suggests that negative PV advection by the 300–200-hPa layer-averaged irrotational wind is strengthening the 200-hPa PV gradient over the central United States and contributing to the amplification of the upper-tropospheric ridge over the Tennessee Valley at t_0 – 48 h (Fig. 3.8d).

Rapid ridge amplification, reinforced by persistent southerly flow in the warm sector of a 1010 hPa surface cyclone on the eastern edge of the broad upper-tropospheric trough (Fig. 3.9c), continues between $t_0 - 48$ h and $t_0 - 24$ h (Figs. 3.9d,e) and results in the formation and deepening of an upper-tropospheric trough over the western North Atlantic (Figs. 3.7d,e). A broad region of 600–400-hPa layer-averaged ascent intensifies on the southwestern edge of the deepening upper-tropospheric trough at $t_0 - 24$ h (Fig. 3.8e). This broad region of 600–400-hPa layer-averaged ascent is associated with: (1) the equatorward entrance region of a 20–25 m s^{-1} upper-tropospheric jet streak (Fig. 3.9e), (2) positive differential vorticity advection by the thermal wind (Fig. 3.10e), and (3) relatively low values of the coupling index (Fig. 3.11e). Values of 600–400-hPa layer-averaged ascent $< -3 \times 10^{-3}$ hPa s^{-1} occur concurrently with the highest precipitable water (PW) values in the western North Atlantic basin (45–55 mm), creating a favorable environment the development of deep convection (Fig. 3.8e). The development of deep convection is suggested by the starburst pattern in the 300–200-hPa layer-averaged irrotational wind field, with vectors ≥ 5 m s^{-1} emanating from the broad region of 600–400-hPa layer-averaged ascent on the southwestern edge of the deepening upper-tropospheric trough over the western North Atlantic (Fig. 3.8e).

Persistent upstream ridge amplification over the eastern United States causes the deepening upper-tropospheric trough over the western North Atlantic to stretch and thin into the PV streamer linked to STC formation at t_0 (Figs. 3.7e,f). Values of 600–400-hPa layer-averaged ascent on the southeastern edge of the PV streamer, ~300 km to the east of the location of STC formation, change from $< -3 \times 10^{-3}$ hPa s^{-1} to $< -4 \times 10^{-3}$ hPa s^{-1} between $t_0 - 24$ h and t_0 (Figs. 3.8e,f). This increase in the magnitude of 600–400-hPa

layer-averaged ascent is associated with: (1) a weakly coupled jet streak configuration at 200 hPa (Fig. 3.8f), (2) an increase in the implied differential vorticity advection by the thermal wind (Fig. 3.10f), and (3) a decrease in the value of the coupling index near the location of STC formation (Fig. 3.11f).

Values of midtropospheric ascent $< -4 \times 10^{-3}$ hPa s^{-1} coinciding with 45–55 mm PW values suggest the continued presence of deep convection near the location of STC formation at t_0 (Fig. 3.8f). The deep convection implied by the starburst pattern in the 300–200-hPa layer-averaged irrotational wind field at t_0 (Fig. 3.8f) is hypothesized to result in the redistribution of PV in the vertical and an increase in lower-tropospheric PV over the location of STC formation between $t_0 - 24$ h and t_0. This increase in lower-tropospheric PV between $t_0 - 24$ h and t_0 is manifested as an increase in 925–850-hPa layer-averaged cyclonic relative vorticity (Figs. 3.7e,f) and a reduction in mean sea level pressure (MSLP) (Figs. 3.9e,f) over the newly formed STC. A $\sim 4 \times 10^{-5}$ s^{-1} increase in 500-hPa cyclonic relative vorticity over the location of STC formation between $t_0 - 24$ h and t_0 also suggests that the cyclonic circulation associated with the newly formed STC extends into the midtroposphere (Figs. 3.10e,f).

3.3.2 Cutoff Cluster Composite

STCs forming in association with a region of relatively high upper-tropospheric PV cut off in the subtropics during the latter stages of an upstream AWB event were included in the Cutoff cluster (N = 22). Many of the upper-tropospheric features linked to STC formation in the PV Streamer cluster composites between $t_0 - 48$ h and t_0 are also

observed in the Cutoff cluster composites between t_0 – 96 h and t_0 – 48 h, including: (1) rapid ridge amplification over the eastern United States (Figs. 3.12b–d) in the warm sector of a deepening surface cyclone (Figs. 3.14b–d), (2) the formation and deepening of an upper-tropospheric trough over the western North Atlantic (Figs. 3.13b,c), and (3) the stretching and thinning of the upper-tropospheric trough over the western North Atlantic into a PV streamer (Figs. 3.13c,d).

The Cutoff cluster composites begin to diverge from the PV Streamer cluster composites at t_0 – 24 h. Persistent ridge amplification over the eastern United States results in AWB over the Canadian Maritimes between t_0 – 24 h and t_0 (Figs. 3.13e,f). Negative PV advection by the 300–200-hPa layer-averaged irrotational wind tightens the 200-hPa PV gradient upstream of the amplifying ridge *and* downstream of the PV streamer between t_0 – 24 h and t_0, causing a region of relatively high upper-tropospheric PV to be cut off in the subtropics (Figs. 3.13e,f). Relatively cold upper-tropospheric air, represented in terms of lower 200-hPa geopotential heights in Fig. 3.12f, accompanies this region of relatively high upper-tropospheric PV into the subtropics and reduces the coupling index over the location of STC formation (Fig. 3.16f).

Values of midtropospheric ascent $< -2 \times 10^{-3}$ hPa s^{-1} coinciding with 40–45 mm PW values suggest the presence of deep convection near the location of STC formation at t_0 (Fig. 3.13f). As discussed in section 3.3.1, the presence of deep convection near the location of STC formation is hypothesized to result in the redistribution of PV in the vertical and an increase in lower-tropospheric PV over the location of STC formation between t_0 – 24 h and t_0. This increase in lower-tropospheric PV between t_0 – 24 h and t_0 is manifested as an increase in 925–850-hPa layer-averaged cyclonic relative vorticity

(Figs. 3.12e,f) and a reduction in MSLP (Figs. 3.14e,f) over the newly developed STC. A ~4 × 10^{-5} s^{-1} increase in 500-hPa cyclonic relative vorticity over the location of STC formation between t_0 – 24 h and t_0 also suggests that the cyclonic circulation associated with the newly formed STC extends into the midtroposphere (Figs. 3.15e,f).

3.3.3 Midlatitude Trough Cluster Composite

STCs forming in association with a broad midlatitude trough that does *not* develop as a result of upstream AWB were included in the Midlatitude Trough cluster (N = 10). Unlike STCs included in the PV Streamer and Cutoff clusters, STCs included in the Midlatitude Trough cluster form in a region preconditioned for the development of deep convection by a precursor disturbance in the upper troposphere. Time-lagged cyclone-relative composites of PV and winds on the 350 K isentropic surface highlight this precursor disturbance at t_0 – 96 h, manifested as a low-amplitude midlatitude trough over the western North Atlantic (Fig. 3.17b). The low-amplitude midlatitude trough progresses eastward between t_0 – 96 h and t_0 – 72 h and deposits a region of relatively high upper-tropospheric PV (4–5 PVU) in the subtropics, ~600 km upstream of the location of STC formation at t_0 (Fig. 3.17c). This region of relatively high upper-tropospheric PV is also associated with a reduction in the value of the coupling index between t_0 – 96 h and t_0 – 72 h (Fig. 3.21c).

Relatively high upper-tropospheric PV values persist over the following 24 h ~600 km upstream of the location of STC formation at t_0 (Fig. 3.17d). Weak southerly flow in the midtroposphere (Figs. 3.20c,d) advects 45–50 mm PW values poleward

between t_0 – 72 h and t_0 – 48 h, over the location of STC formation at t_0 (Fig. 3.18c,d). Discrete regions of 500-hPa ascent $< -1 \times 10^{-3}$ hPa s^{-1} occur concurrently with 45–50 mm PW values at t_0 – 48 h (Fig. 3.19d), suggesting the presence of deep convection.

The broad midlatitude trough linked to STC formation at t_0 has begun to develop in response to rapid ridge amplification over the eastern United States at t_0 – 24 h (Fig. 3.17e). Much like in the PV Streamer and Cutoff cluster composites, the upstream ridge amplification responsible for downstream trough development over the western North Atlantic is associated with negative PV advection in the upper troposphere (Fig. 3.18e) occurring in the warm sector of a surface cyclone (Fig. 3.19e).

Continued ridge amplification over the eastern United States between t_0 – 24 h and t_0 causes the broad midlatitude trough over the western North Atlantic to deepen and approach the location of STC formation at t_0 (Figs. 3.17e,f). This broad midlatitude trough is responsible for organizing deep convection over the location of STC formation at t_0, represented by ≥ 3 m s^{-1} 300–200-hPa layer-averaged irrotational winds emanating from the broad region of $< -3 \times 10^{-3}$ hPa s^{-1} 600–400-hPa layer-averaged ascent (Fig. 3.18f). As discussed in sections 3.3.1 and 3.3.2, the presence of deep convection near the location of STC formation is hypothesized to result in the redistribution of PV in the vertical and an increase in lower-tropospheric PV between t_0 – 24 h and t_0. This increase in lower-tropospheric PV between t_0 – 24 h and t_0 is manifested as an increase in 925–850-hPa layer-averaged cyclonic relative vorticity (Figs. 3.17e,f) and a reduction in MSLP (Figs. 3.19e,f) over the newly developed STC. A $\sim 6 \times 10^{-5}$ s^{-1} increase in 500-hPa cyclonic relative vorticity over the location of STC formation between t_0 – 24 h and

t_0 also suggests that the cyclonic circulation associated with the newly formed STC extends into the midtroposphere (Figs. 3.20e,f).

3.3.4 Subtropical Disturbance Cluster Composite

STCs forming in association with the progression of a small-scale PV filament around the northern edge of a subtropical anticyclone were included in the Subtropical Disturbance cluster (N = 22). As discussed in section 3.2, the progressive PV filament associated with the Subtropical Disturbance cluster is considerably smaller in meridional extent than the upper-tropospheric disturbances associated with PV Streamers, Cutoffs, or Midlatitude Troughs. This difference in meridional extent causes the cyclone-relative composites associated with Subtropical Disturbances to be less discriminating than those associated with PV Streamers, Cutoffs, or Midlatitude Troughs (Figs. 3.22–3.26).

While the progression of a small-scale PV filament around the northern edge of a subtropical anticyclone is detectable in each composite member at or before $t_0 - 72$ h, varying phase speeds of the small-scale PV filament cause it to be undetectable in the composite mean until $t_0 - 48$ h (Fig. 3.22d). Time-lagged cyclone-relative composites of PV and winds on the 350 K isentropic surface reveal the small-scale PV filament, a region of relatively high upper-tropospheric PV (2–3 PVU) on the northern edge of a subtropical anticyclone, ~1300 km to the northwest of the location of STC formation at t_0 (Fig. 3.22d). The small-scale PV filament is advected around the northern edge of the subtropical anticyclone over the following 24 h by ~35 kt northwesterly winds on the 350 K isentropic surface (Figs. 3.22d,e). The southeastward progression of the small-scale

PV filament lowers 200-hPa geopotential heights over southern Florida between t_0 – 48 h and t_0 – 24 h (Figs. 3.22d,e) and reduces the value of the coupling index in the surrounding region (Figs. 3.26d,e). The southeastward progression of the small-scale PV filament coincides with the development of $< -1.0 \times 10^{-3}$ hPa s^{-1} 600–400-hPa layer-averaged ascent ~500 km to the east of Florida (Fig. 3.23e). This region of 600–400-hPa layer-averaged ascent also coincides with 50–55 mm PW values (Fig. 3.23e), producing a favorable environment for the development of deep convection.

The continued southeastward progression of the small-scale PV filament between t_0 – 24 h and t_0 is associated with the enhancement of 600–400-hPa layer-averaged ascent ($< -3.0 \times 10^{-3}$ hPa s^{-1}) and 300–200-hPa layer-averaged irrotational winds (> 2 m s^{-1}) over the location of STC formation (Fig. 3.23f). The enhancement of 600–400-hPa layer-averaged ascent and 300–200-hPa layer-averaged irrotational winds suggests that deep convection is occurring over the location of STC formation at t_0 (Fig. 3.23f). As discussed in sections 3.3.1–3.3.3, the presence of deep convection near the location of STC formation is hypothesized to result in the redistribution of PV in the vertical and an increase in lower-tropospheric PV between t_0 – 24 h and t_0. This increase in lower-tropospheric PV between t_0 – 24 h and t_0 is manifested as an increase in 925–850-hPa layer-averaged cyclonic relative vorticity (Figs. 3.22e,f) and a reduction in MSLP (Figs. 3.24e,f) over the newly developed STC. A ~4×10^{-5} s^{-1} increase in 500-hPa cyclonic relative vorticity over the location of STC formation between t_0 – 24 h and t_0 also suggests that the cyclonic circulation associated with the newly formed STC extends into the midtroposphere (Figs. 3.25e,f).

3.3.5 PV Debris Cluster Composite

STCs forming in association with a disorganized region of relatively high upper-tropospheric PV deposited in the subtropics several days prior to STC formation were included in the PV Debris cluster (N = 31). Much like Subtropical Disturbances, the disorganized nature of PV Debris results in less discriminating cyclone-relative composites than those associated with PV Streamers, Cutoffs, or Midlatitude Troughs (Figs. 3.27–3.31).

While a region of relatively high upper-tropospheric PV moving westward on the equatorward edge of a broad subtropical anticyclone is detectable in each composite member at or before t_0 – 72 h, the disorganized nature of PV debris causes the aforementioned feature to be undetectable in the composite mean until t_0 – 48 h (Fig. 3.27d). Time-lagged cyclone-relative composites of PV and winds on the 350 K isentropic surface reveal a region of PV debris, represented as a region of relatively high upper-tropospheric PV (1.5–2 PVU), ~1000 km to the northeast of the location of STC formation at t_0, beginning to progress to the southwest in response to 5–10 kt northeasterly winds at t_0 – 48 h (Fig. 3.27d). A separate region of relatively high PW values (50–55 mm), centered ~1000 km to the southeast of the location of STC formation at t_0, begins to progress to the west-northwest at t_0 – 48 h (Fig. 3.28d) in response to east-southeasterly flow at and below 500 hPa (Fig. 3.30d).

The continued progression of this disorganized region of PV debris to the southwest between t_0 – 48 h and t_0 – 24 h (Figs. 3.27d,e) coincides with a decrease in the value of the coupling index over Hispaniola (Figs. 3.31d,e). The development of 600–

400-hPa layer-averaged ascent values $< -2 \times 10^{-3}$ hPa s^{-1} and 300–200-hPa layer-averaged irrotational winds > 2 m s^{-1} over Hispaniola at t_0 – 24 h suggests the presence of deep convection over the region (Fig. 3.28e).

The disorganized region of PV debris has progressed to the northwest of the location of STC formation by t_0 (Fig. 3.27f). PW values over the location of STC formation have increased to 55–60 mm by t_0, collocated with a region of deep convection represented by relatively high values of 600–400-hPa layer-averaged ascent ($\sim -1 \times 10^{-3}$ hPa s^{-1}) and 300–200-hPa layer-averaged irrotational winds (> 2 m s^{-1}) (Fig. 3.28f). As discussed in sections 3.3.1–3.3.4, the presence of deep convection near the location of STC formation is hypothesized to result in the redistribution of PV in the vertical and an increase in lower-tropospheric PV between t_0 – 24 h and t_0. This increase in lower-tropospheric PV between t_0 – 24 h and t_0 is represented in terms of an increase in 925–850-hPa layer-averaged cyclonic relative vorticity (Figs. 3.27e,f) and a reduction in MSLP (Figs. 3.29e,f) over the newly developed STC. A $\sim 4 \times 10^{-5}$ s^{-1} increase in 500-hPa cyclonic relative vorticity over the location of STC formation between t_0 – 24 h and t_0 also suggests that the cyclonic circulation associated with the newly formed STC extends into the midtroposphere (Figs. 3.30e,f).

3.4 Case Studies

3.4.1 PV Streamer Case Study

An STC forming in association with a PV streamer was identified ~700 km east of North Carolina at 1800 UTC 21 August 1980 (t_0) (Figs. 3.32f–3.36f). As discussed in

the PV Streamer cluster composites in section 3.3.1, the amplification of an upper-tropospheric trough leads to the formation of a PV streamer over the North Atlantic at t_0. A region of relatively high upper-tropospheric PV (≥ 10 PVU) on the 350 K isentropic surface (PV1), associated with the formation of a PV streamer over the North Atlantic at t_0, is located over southern Idaho/northern Utah at t_0 – 120 h (Fig. 3.32a). PV1 progresses northeastward toward southern Quebec between t_0 – 120 h and t_0 – 48 h on the northern edge of a broad subtropical anticyclone centered over the southeastern United States (Figs. 3.32a–d).

As discussed in the PV Streamer cluster composites in section 3.3.1, rapid ridge amplification begins upstream of the location of STC formation at t_0 – 48 h (Fig. 3.32d) in the warm sector of a developing surface cyclone (Fig. 3.34d). A ~1004-hPa surface cyclone (C1) has developed over the central Great Plains at t_0 – 48 h (Fig. 3.34d), on the eastern flank of a neutrally tilted upper-tropospheric trough (Fig. 3.32d). The neutrally tilted upper-tropospheric trough becomes negatively tilted between t_0 – 48 h and t_0 – 24 h (Figs. 3.32d,e), coinciding with a 4-hPa drop in the central pressure of C1 (Figs. 3.34d,e). A region of 600–400-hPa layer-averaged ascent $< -15 \times 10^{-3}$ hPa s^{-1} has developed over C1 at t_0 – 24 h (Fig. 3.33e) associated with: (1) the poleward exit (equatorward entrance) region of a 30–40 m s^{-1} (40–50 m s^{-1}) upper-tropospheric jet streak (Fig. 3.34e), (2) positive differential vorticity advection by the thermal wind (Fig. 3.35e), and (3) relatively low values of the coupling index (Fig. 3.36e). Diabatically driven outflow over C1, suggested by the starburst pattern in the 300–200-hPa layer-averaged irrotational wind field, contributes to strengthening of the 200-hPa PV gradient over the central Great Plains between t_0 – 48 h and t_0 – 24 h (Figs. 3.33d,e). Negative PV advection by the

300–200-hPa layer-averaged irrotational wind also contributes to rapid ridge amplification over the Great Lakes and enhances northwesterly flow over southern Quebec between t_0 – 48 h and t_0 – 24 h (Figs. 3.33d,e).

Enhanced northwesterly flow over southern Quebec between t_0 – 48 h and t_0 – 24 h causes PV1 to progress equatorward over the northeastern United States and results in the formation and amplification of an upper-tropospheric trough over the western North Atlantic by t_0 – 24 h (Figs. 3.32d,e). Persistent upstream ridge amplification and enhanced northerly flow over the northeastern United States during the following 24 h causes this upper-tropospheric trough to stretch and thin into the PV streamer linked to STC formation at t_0 (Fig. 3.32f). The deep convection implied by the starburst pattern in the 300–200-hPa layer-averaged irrotational wind field over the location of STC formation (Fig. 3.33f) is hypothesized to result in the redistribution of PV in the vertical and an increase in lower-tropospheric PV over the location of STC formation between t_0 – 24 h and t_0. This increase in lower-tropospheric PV between t_0 – 24 h and t_0 is manifested as an increase in 925–850-hPa layer-averaged cyclonic relative vorticity (Figs. 3.32e,f) and a reduction in MSLP (Figs. 3.34e,f) over the newly formed STC.

3.4.2 Cutoff Case Study

An STC forming in association with a cutoff was identified ~1000 km southwest of Portugal at 0600 UTC 30 September 1980 (t_0) (Figs. 3.37f–3.41f). As discussed in the Cutoff cluster composites in section 3.3.2, a precursor AWB event in the midlatitudes leads to the formation of a cutoff over the North Atlantic between t_0 – 24 h and t_0. A

region of relatively high upper-tropospheric PV (≥ 10 PVU) on the 350 K isentropic surface (PV2), associated with the formation of a cutoff over the North Atlantic between t_0 – 24 h and t_0, is located over northern Labrador at t_0 – 120 h (Fig. 3.37a). PV2 progresses southeastward toward the central North Atlantic between t_0 – 120 h and t_0 – 96 h on the southern edge of a broad upper-tropospheric trough (Figs. 3.37a,b).

Many of the upper-tropospheric features linked to STC formation in the PV Streamer case study between t_0 – 48 h and t_0 are also observed in the Cutoff case study between t_0 – 96 h and t_0 – 48 h, including: (1) rapid ridge amplification upstream of the location of STC formation (Figs. 3.37b–d) in the warm sector of a surface cyclone (C2) (Figs. 3.39b–d), (2) the equatorward progression of an upper-tropospheric disturbance (PV2), contributing to the formation and amplification of an upper-tropospheric trough downstream of the amplifying ridge (Figs. 3.37b,c), and (3) the stretching and thinning of the upper-tropospheric trough downstream of the amplifying ridge into a PV streamer (Figs. 3.37c,d). The Cutoff case study begins to diverge from the PV Streamer case study at t_0 – 24 h. Persistent ridge amplification over the central North Atlantic results in AWB over western Europe that cuts off PV2 in the subtropics between t_0 – 24 h and t_0 (Figs. 3.37e,f). Relatively cold upper-tropospheric air, manifested as lower 200-hPa geopotential heights in Figs. 3.37e,f, accompanies PV2 into the subtropics and decreases the value of the coupling index over the location of STC formation between t_0 – 24 h and t_0 (Figs. 3.41e,f).

A relatively small region of 500-hPa ascent $< -5 \times 10^{-3}$ hPa s^{-1} persists over the location of STC formation between t_0 – 24 h and t_0 (Figs. 3.40e,f), suggesting the development of deep convection. The deep convection suggested by persistent 500-hPa

ascent over the location of STC formation between t_0 – 24 h and t_0 (Figs. 3.40e,f) is hypothesized to result in the redistribution of PV in the vertical and an increase in lower-tropospheric PV over the location of STC formation between t_0 – 24 h and t_0. This increase in lower-tropospheric PV between at t_0 – 24 h and t_0 is manifested as an increase in 925–850-hPa layer-averaged cyclonic relative vorticity (Figs. 3.37e,f) and a reduction in MSLP (Figs. 3.39e,f) over the newly formed STC.

3.4.3 Midlatitude Trough Case Study

An STC forming in association with a midlatitude trough was identified ~500 km southwest of the Azores at 0600 UTC 4 October 2005 (t_0) (Figs. 3.42f–3.46f). As discussed in the Midlatitude Trough cluster composites in section 3.3.3, a precursor disturbance in the upper troposphere preconditions the region surrounding the location of STC formation for the development of deep convection prior to t_0.

A deepening cyclone over eastern North America (C3a) is associated with rapid ridge amplification and AWB over the central North Atlantic between t_0 – 120 h and t_0 – 72 h (Figs. 3.42a–c). AWB over the central North Atlantic results in the cutting off of a region of relatively high upper-tropospheric PV (PV3a) in the midlatitudes at t_0 – 72 h, ~800 km to the northwest of the location of STC formation at t_0 (Fig. 3.42c). PV3a persists upstream of the location of STC formation and elongates meridionally during the following 24 h (Figs. 3.42c,d). Southerly flow at 500-hPa, downstream of PV3a (Figs. 3.45d,e), aids in the movement of 35–40 mm PW values over the location of STC formation between t_0 – 48 h and t_0 – 24 h (Figs. 3.43d,e). The movement of 35–40 mm

PW values over the location of STC formation between t_0 – 48 h and t_0 – 24 h helps to precondition the region for the development of deep convection.

A broad midlatitude trough (PV3b) begins to develop over the central North Atlantic between t_0 – 48 h and t_0 – 24 h in response to rapid ridge amplification over central North America (Figs. 3.42d,e) in the warm sector of a deepening surface cyclone (C3b) (Figs. 3.44d,e). Persistent ridge amplification over central North America enhances northwesterly flow over the Labrador Sea between t_0 – 24 h and t_0, causing the broad midlatitude trough over the western North Atlantic to deepen and approach the location of STC formation (Figs. 3.42e,f). Two regions of 600–400-hPa layer-averaged ascent $< -10 \times 10^{-3}$ hPa s^{-1} coincide with 40–45 mm PW values near the location of STC formation at t_0 (Fig. 3.43f) following a ~5 K decrease in the value of the coupling index between t_0 – 24 h and t_0 (Figs. 3.46e,f). The deep convection suggested by relatively weak divergent outflow in the 300–200-hPa layer-averaged irrotational wind field over the location of STC formation (Fig. 3.43f) is hypothesized to result in the redistribution of PV in the vertical and an increase in lower-tropospheric PV over the location of STC formation between t_0 – 24 h and t_0. This increase in lower-tropospheric PV between t_0 – 24 h and t_0 is manifested as an increase in 925–850-hPa layer-averaged cyclonic relative vorticity (Figs. 3.42e,f) and a reduction in MSLP (Figs. 3.44e,f) over the newly formed STC.

3.4.4 Subtropical Disturbance Case Study

An STC forming in association with a subtropical disturbance was identified ~400 km east of Florida at 0000 UTC 5 June 1986 (t_0) (Figs. 3.47f–3.51f). As discussed in the Subtropical Disturbance cluster composites in section 3.3.4, the progression of a small-scale PV filament around the northern edge of a subtropical anticyclone is associated with STC formation at t_0. The small-scale PV filament associated with STC formation at t_0, manifested as a region of relatively high PV (≥ 4 PVU) on the 350 K isentropic surface (PV4), is located on the equatorward edge of a cutoff cyclone in the eastern North Pacific at t_0 – 120 h (Fig. 3.47a). PV4 breaks away from the cutoff cyclone in the eastern North Pacific between t_0 – 120 h and t_0 – 96 h and progresses eastward around the northern edge of an upper-tropospheric subtropical anticyclone until t_0 – 48 h (Figs. 3.47b–d). The eastward progression of PV4 around the northern edge of the upper-tropospheric subtropical anticyclone (Figs. 3.47b–d) also coincides with the eastward progression of a 30–40 m s^{-1} subtropical jet streak across the southern United States (Figs. 3.48b–d).

PV4 progresses southeastward across central Florida between t_0 – 48 h and t_0 – 24 h in response to ~25 m s^{-1} winds on the 350 K isentropic surface (Figs. 3.47d,e). Relatively cold upper-tropospheric air, manifested as lower 200-hPa geopotential heights in Figs. 3.47d,e, accompanies PV4 into the subtropics and reduces the value of the coupling index over the location of STC formation between t_0 – 48 h and t_0 – 24 h (Figs. 3.51d,e). Southerly flow at 500-hPa, downstream of PV4 (Figs. 3.50d,e), aids in the poleward movement of 55–60 mm PW values poleward toward the location of STC formation between t_0 – 48 h and t_0 – 24 h (Figs. 3.48d,e), creating a favorable environment for the development of deep convection.

Values of 600–400-hPa layer-averaged ascent $< -10 \times 10^{-3}$ hPa s^{-1} coincide with 55–60 mm PW values to the east of Florida by t_0 (Fig. 3.48f). The deep convection suggested by divergent outflow ≥ 5 m s^{-1} in the 300–200-hPa layer-averaged irrotational wind field near the location of STC formation (Fig. 3.48f) is hypothesized to result in the redistribution of PV in the vertical and an increase in lower-tropospheric PV over the location of STC formation between $t_0 - 24$ h and t_0. This increase in lower-tropospheric PV between $t_0 - 24$ h and t_0 is manifested as an increase in 925–850-hPa layer-averaged cyclonic relative vorticity (Figs. 3.47e,f) and a reduction in MSLP (Figs. 3.49e,f) over the newly formed STC.

3.4.5 PV Debris Case Study

An STC forming in association with PV debris was identified over the southern Bahamas at 0000 UTC 24 August 2005 (t_0) (Figs. 3.52f–3.56f). A disorganized region of PV debris, represented by two regions of relatively high PV (≥ 2 PVU) on the 350 K isentropic surface (PV5a and PV5b), is located on the southeastern edge of a broad subtropical anticyclone at $t_0 - 120$ h, ~800 km to the east-southeast of the location of STC formation at t_0 (Fig. 3.52a). PV5a and PV5b begin to stretch and thin between $t_0 - 120$ h and $t_0 - 96$ h in response to confluent flow to the north of Puerto Rico on the 350 K isentropic surface (Figs. 3.52a,b). Persistent northeasterly winds on the southeastern edge of the broad upper-tropospheric subtropical anticyclone advect relatively high upper-tropospheric PV values (≥ 2 PVU) associated with PV5a over the location of STC formation between $t_0 - 72$ h and $t_0 - 48$ h (Figs. 3.52c,d). Relatively high upper-

tropospheric PV values (≥ 1 PVU) associated with PV5b are subsequently advected over the location of STC formation between t_0 – 24 h and t_0 (Figs. 3.52e,f).

The southwestward movement of relatively high upper-tropospheric PV values associated with PV5a and PV5b coincides with the southwestward movement of relatively low values of the coupling index over the location of STC formation between t_0 – 72 h and t_0 (Figs. 3.56c–f), suggesting an increased potential for the development of deep convection over the southern Bahamas. Persistent ~5 m s^{-1} easterly winds at 500-hPa between t_0 – 72 h and t_0 – 24 h (Figs. 3.55c–e) aid in the movement of 55–60 mm PW values toward the location of STC formation (Figs. 3.53c–e). The development of deep convection is suggested near the location of STC formation by relatively weak (~5 m s^{-1}) 300–200-hPa layer-averaged irrotational winds emanating from a region of $< -5 \times 10^{-3}$ hPa s^{-1} of 600–400-hPa layer-averaged ascent at t_0 (Fig. 3.53f). The deep convection suggested by the 300–200-hPa layer-averaged irrotational wind field is hypothesized to result in the redistribution of PV in the vertical and an increase in lower-tropospheric PV over the location of STC formation t_0 – 24 h and t_0. This increase in lower-tropospheric PV between t_0 – 24 h and t_0 is manifested as an increase in 925–850-hPa layer-averaged cyclonic relative vorticity (Figs. 3.52e,f) and a reduction in MSLP (Figs. 3.54e,f) over the newly formed STC.

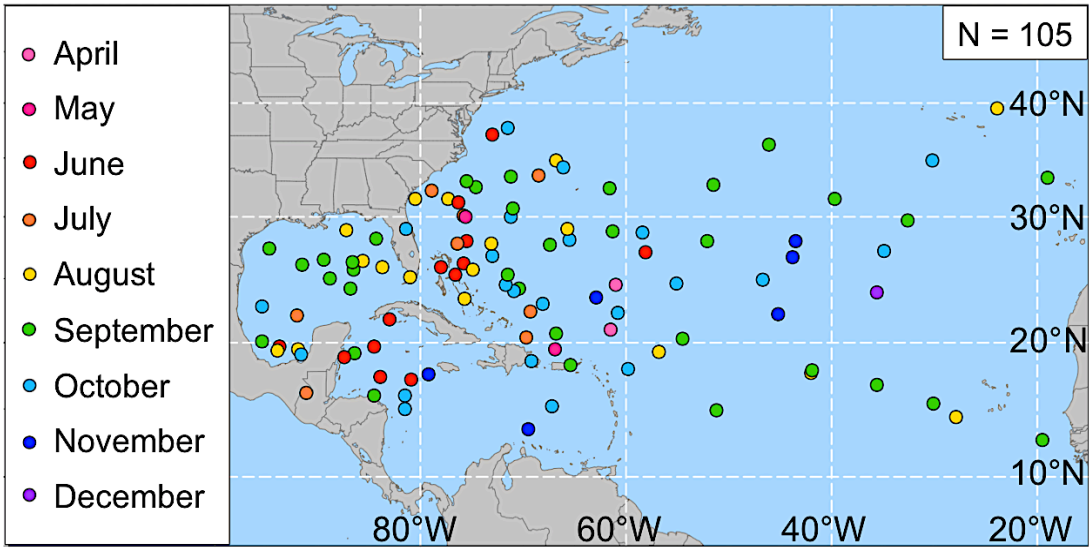

Fig 3.1. Locations of STC formation in the North Atlantic basin (1979–2010). The color of each dot represents the month STC formation occurred, according to the legend.

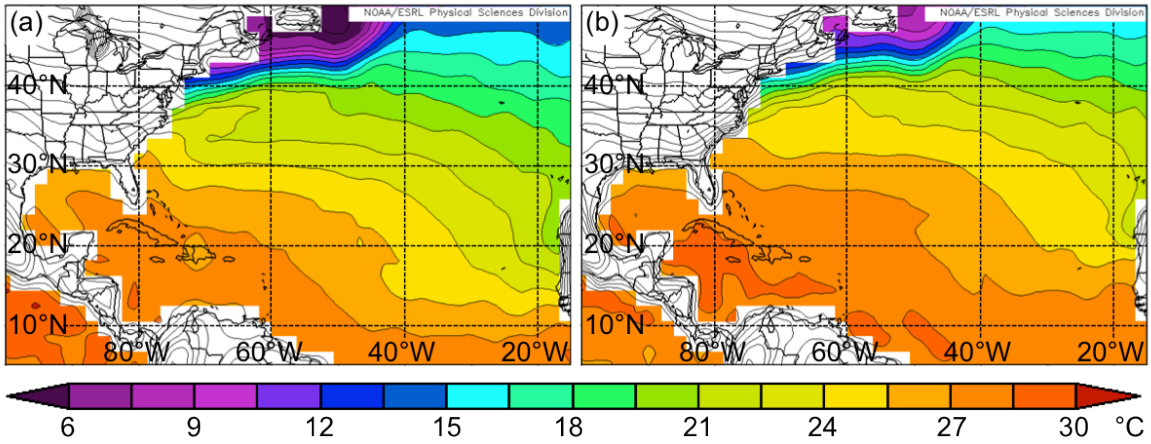

Fig 3.2. Mean surface skin temperature (contoured, °C) and SST (shaded, °C) during (a) April–July and (b) August–December (1979–2010) from the 2.5° NCEP-NCAR reanalysis dataset. Figure adapted from imagery provided by the NOAA/ESRL Physical Sciences Division, available online at http://www.esrl.noaa.gov/psd/.

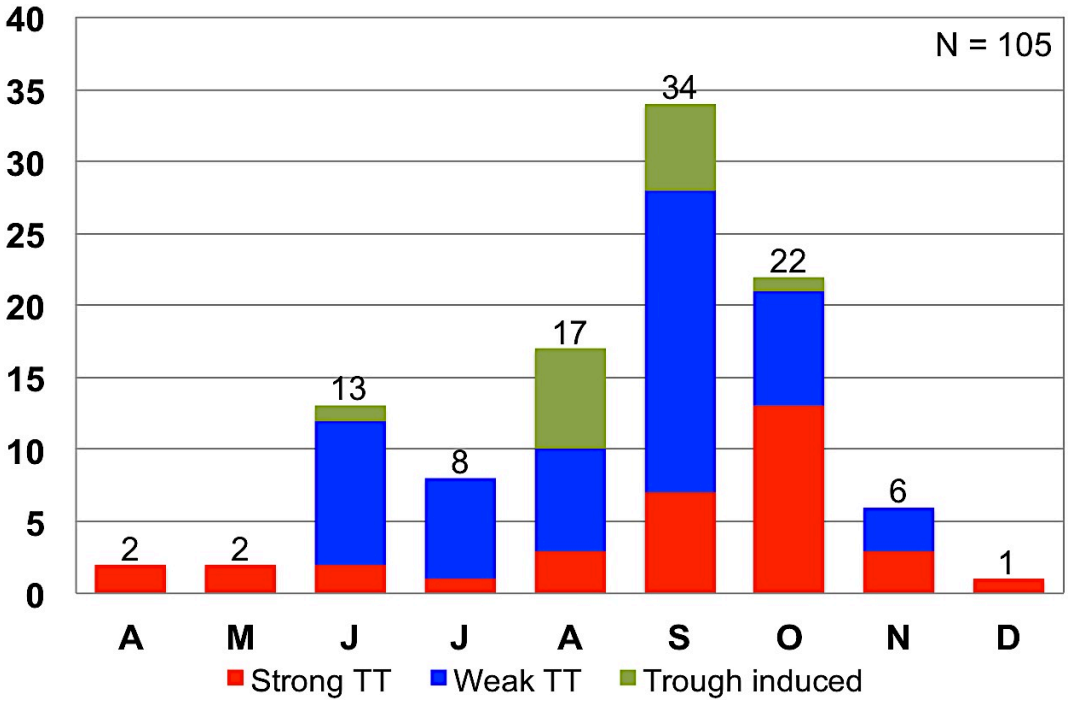

Fig 3.3. Frequency of STC formation in the North Atlantic basin (1979–2010) separated by month (April–December). Red, blue, and green regions represent the number of STCs classified as Strong TT, Weak TT, and Trough induced events, respectively, in McTaggart-Cowan et al. (2013).

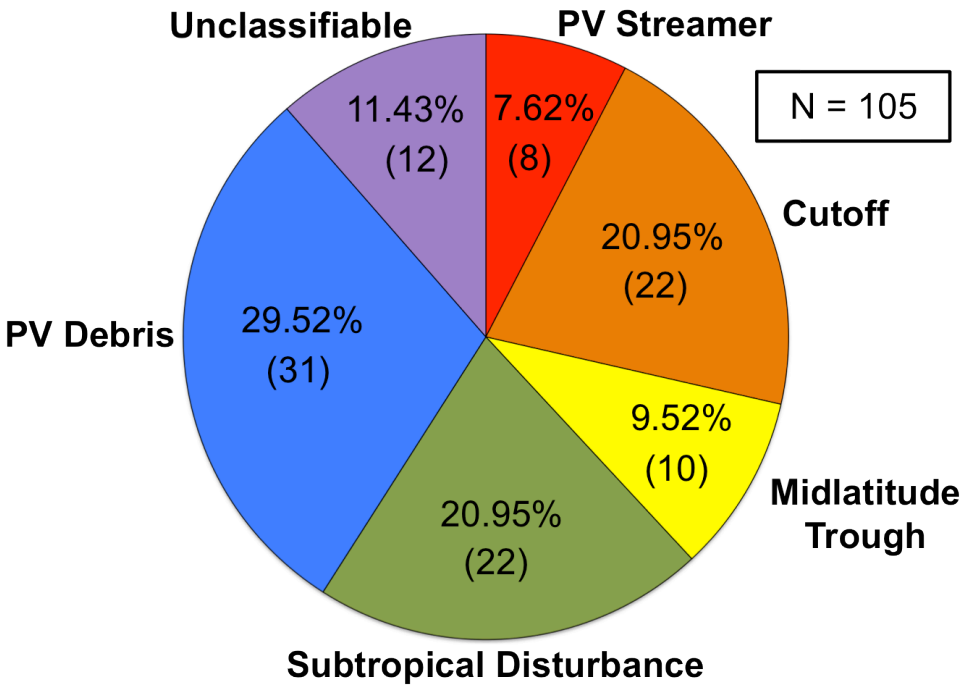

Fig. 3.4. Distribution of 105 cases of STC formation by cluster.

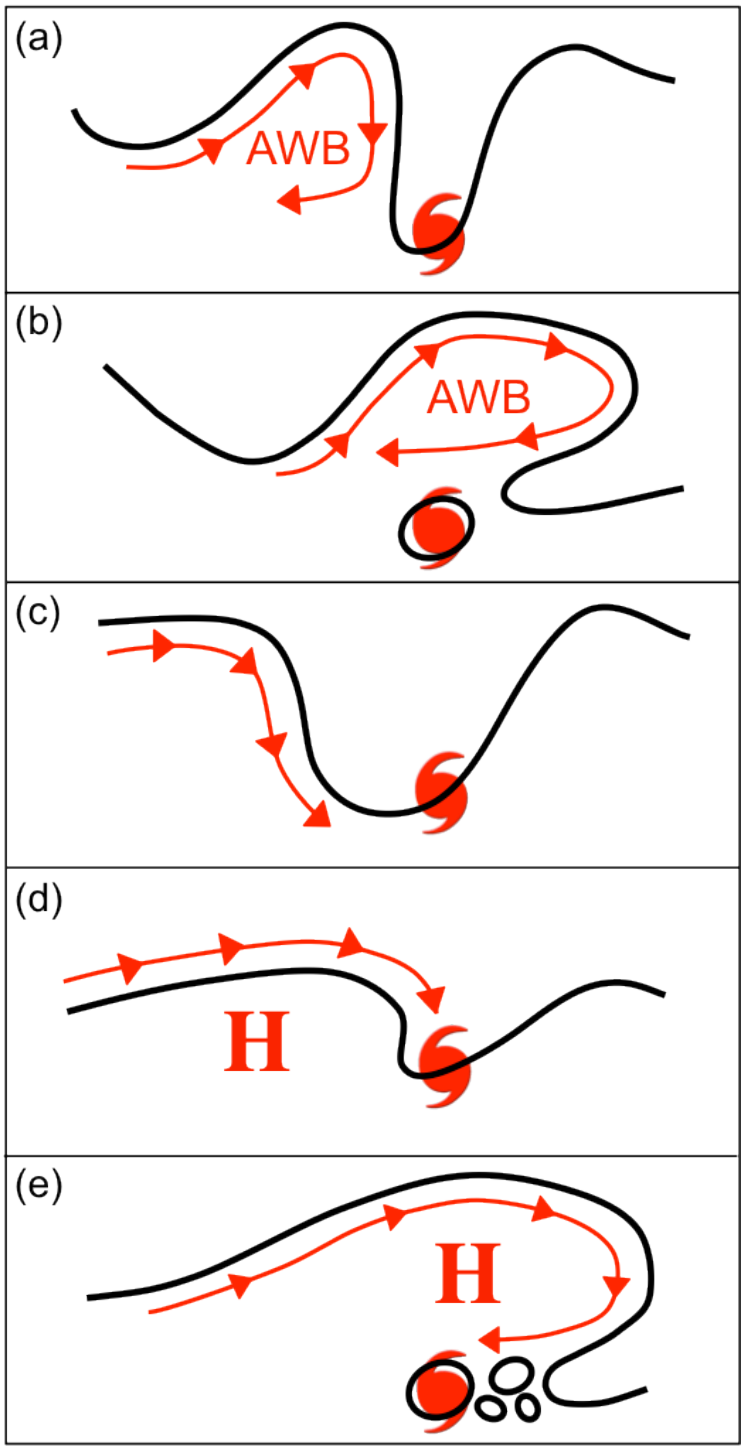

Fig. 3.5. Schematic representation of an STC forming in association with: (a) a PV streamer, (b) a cutoff, (c) a midlatitude trough, (d) a subtropical disturbance, and (e) PV debris. Black lines represent an arbitrary PV value on an idealized 350 K isentropic surface. Red arrows indicate the motion of the flow on the idealized 350 K isentropic surface. "AWB" denotes a region where anticyclonic wave breaking in occurring, while "H" denotes the location of an upper-tropospheric subtropical anticyclone.

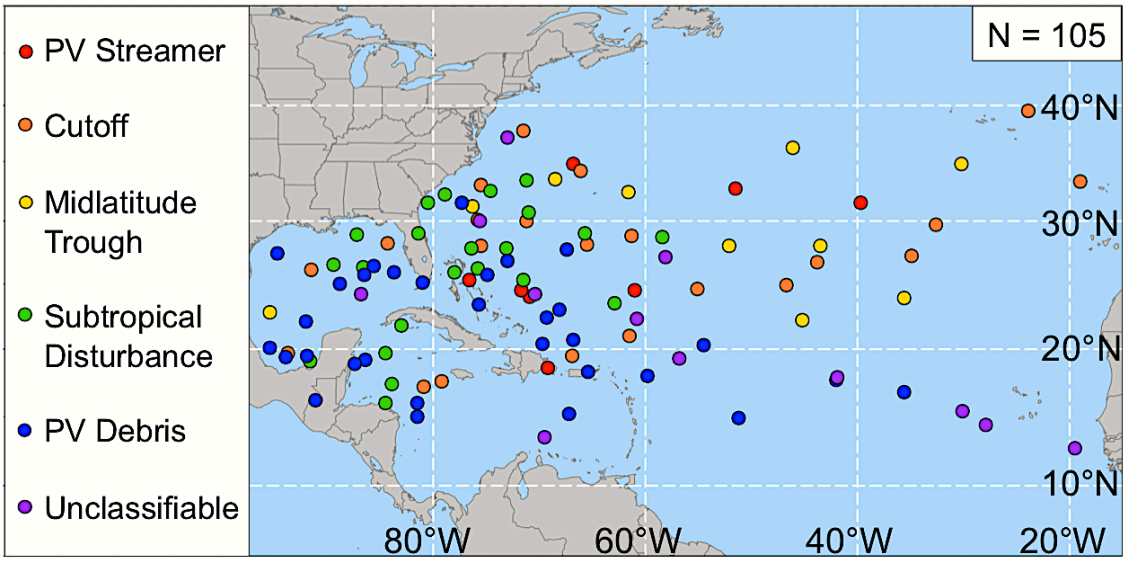

Fig 3.6. As in Fig. 3.1, except the color of each dot represents the upper-tropospheric feature linked to STC formation, according to the legend.

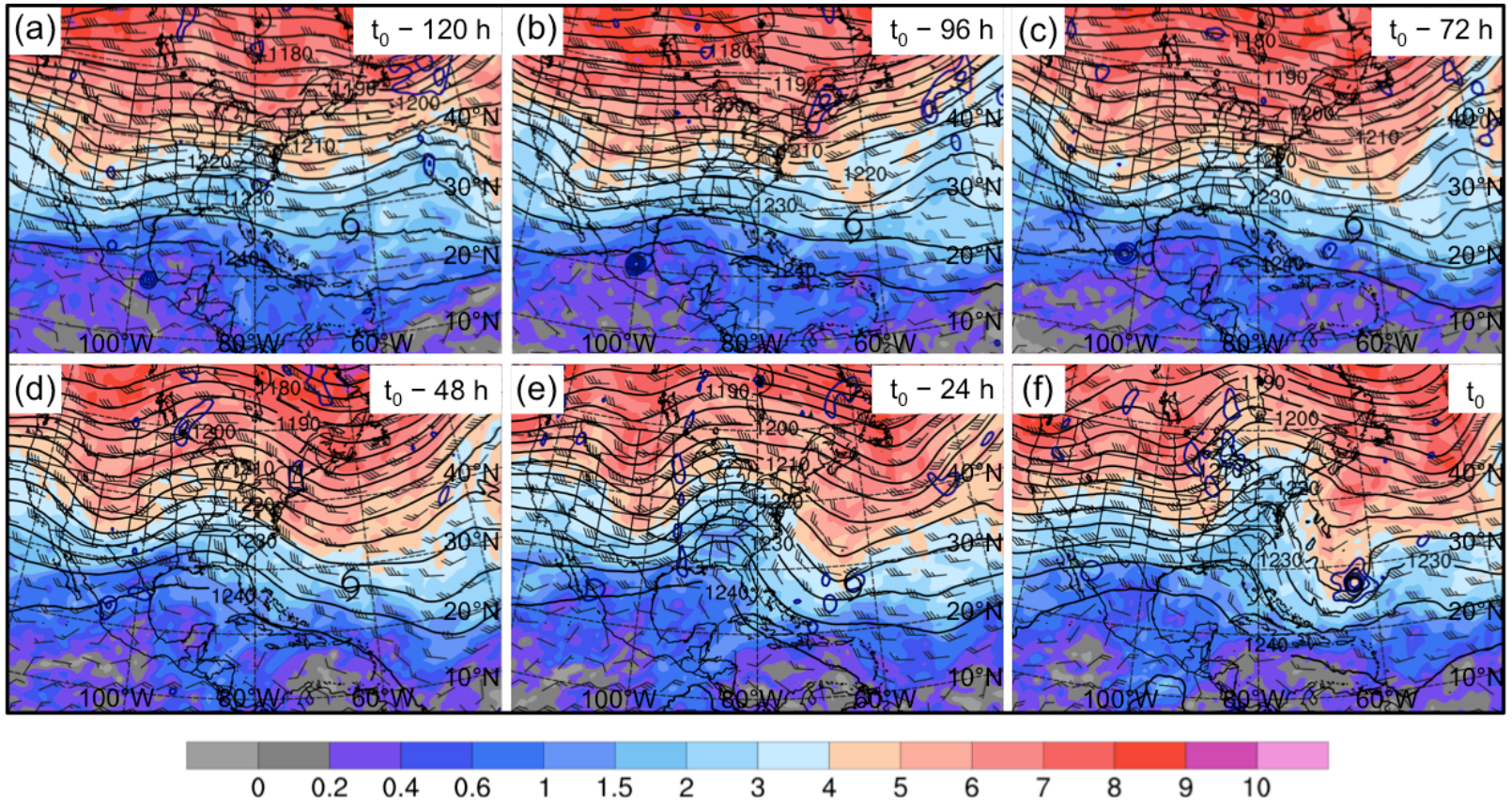

Fig 3.7. PV Streamer cluster composite (N = 8) potential vorticity (shaded, PVU) and winds (barbs, kts) on the 350 K isentropic surface, 200-hPa geopotential height (black contours, dam), and 925–850-hPa layer-averaged cyclonic relative vorticity (blue contours, every 2.5×10^{-5} s^{-1}) at (a) t_0 – 120 h, (b) t_0 – 96 h, (c) t_0 – 72 h, (d) t_0 – 48 h, (e) t_0 – 24 h, and (f) t_0. The black cyclone symbol in each panel denotes the average location of STC formation at t_0.

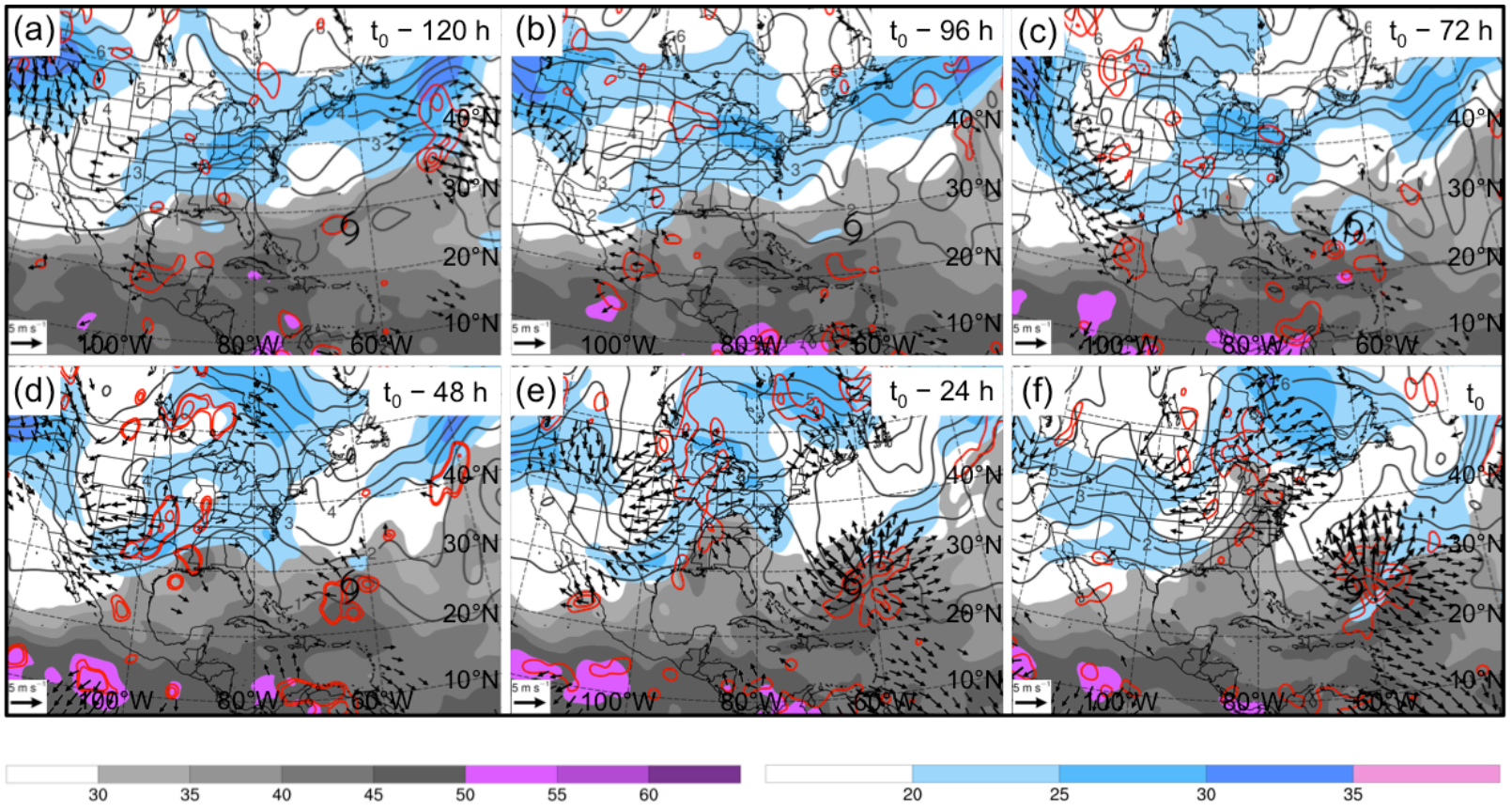

Fig 3.8. PV Streamer cluster composite (N = 8) precipitable water (gray shading, mm), 200-hPa wind speed (shaded, m s^{-1}), 200-hPa potential vorticity (gray contours, PVU), 600–400-hPa layer-averaged ascent (red contours, every 1×10^{-3} hPa s^{-1}), and 300–200-hPa layer-averaged irrotational wind (vectors, starting at 2 m s^{-1}) at (a) t_0 – 120 h, (b) t_0 – 96 h, (c) t_0 – 72 h, (d) t_0 – 48 h, (e) t_0 – 24 h, and (f) t_0. The black cyclone symbol in each panel denotes the average location of STC formation at t_0.

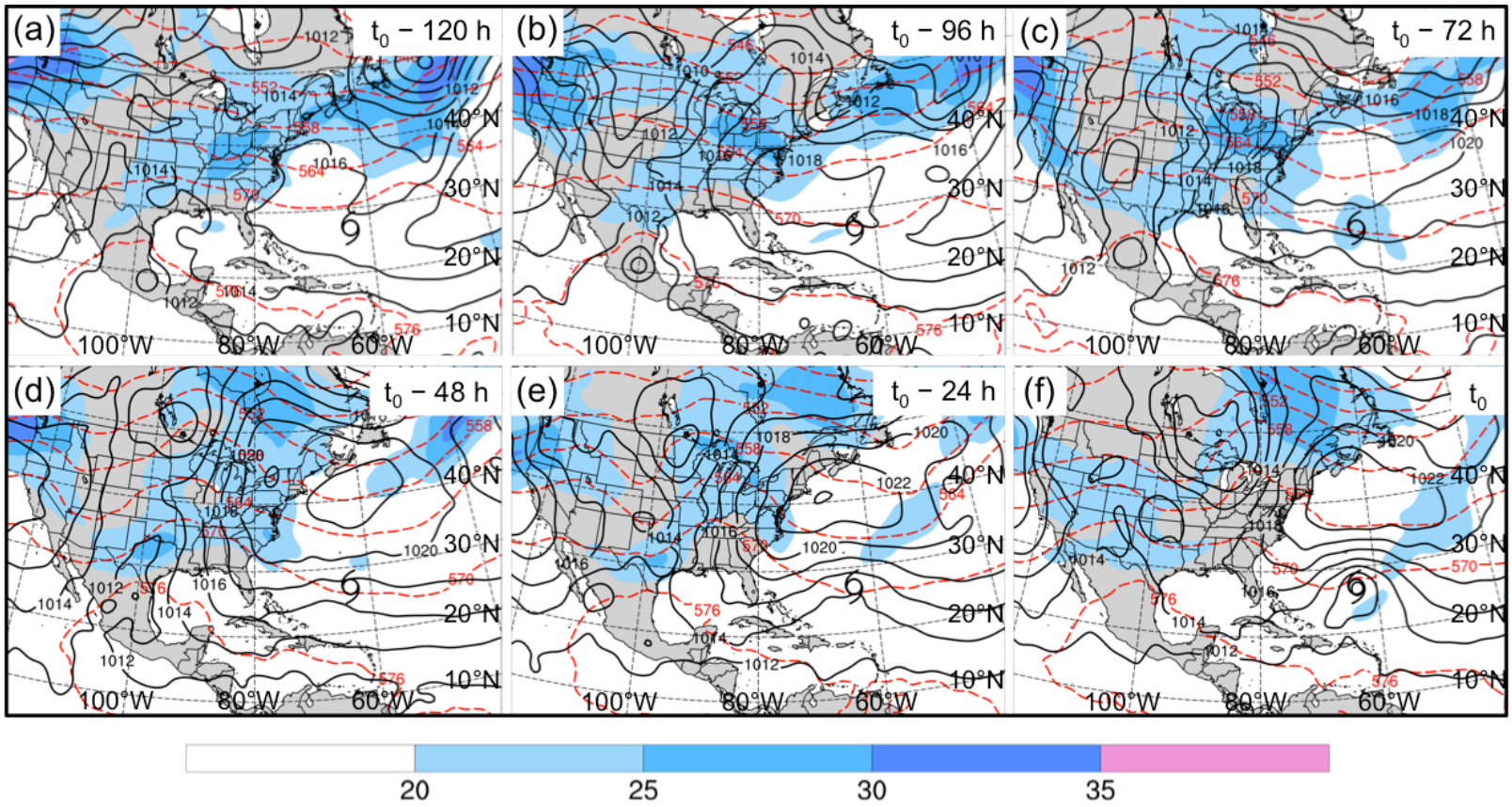

Fig 3.9. PV Streamer cluster composite (N = 8) 200-hPa wind speed (shaded, m s^{-1}), 1000–500-hPa thickness (red dashed contours, dam), and MSLP (black solid contours, hPa) at (a) t_0 – 120 h, (b) t_0 – 96 h, (c) t_0 – 72 h, (d) t_0 – 48 h, (e) t_0 – 24 h, and (f) t_0. The black cyclone symbol in each panel denotes the average location of STC formation at t_0.

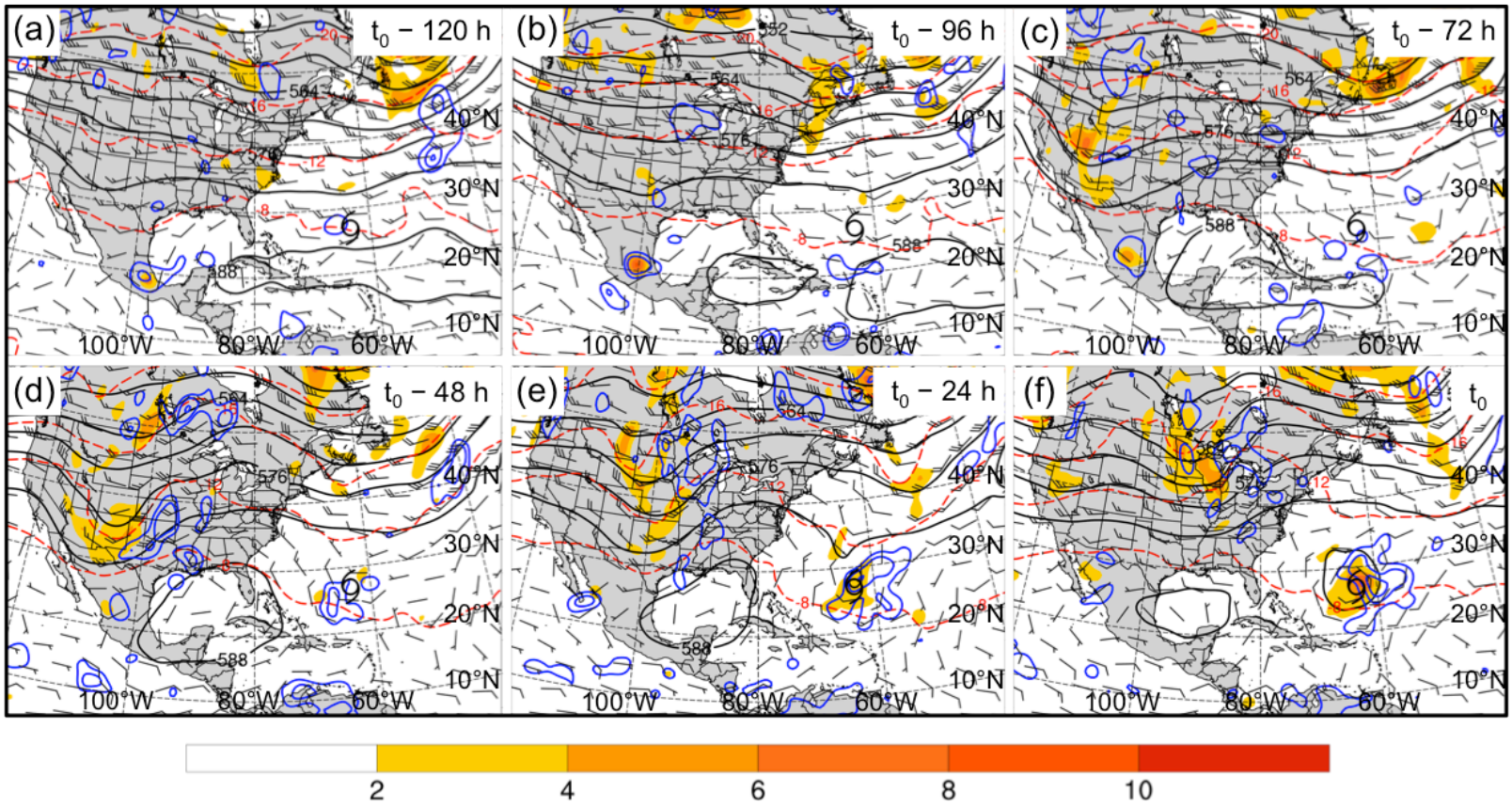

Fig 3.10. PV Streamer cluster composite (N = 8) 500-hPa cyclonic relative vorticity (shaded, 10^{-5} s^{-1}), geopotential height (black solid contours, dam), temperature (red dashed contours, °C), ascent (blue contours, every 1×10^{-3} hPa s^{-1}), and winds (barbs, kts) at (a) t_0 – 120 h, (b) t_0 – 96 h, (c) t_0 – 72 h, (d) t_0 – 48 h, (e) t_0 – 24 h, and (f) t_0. The black cyclone symbol in each panel denotes the average location of STC formation at t_0.

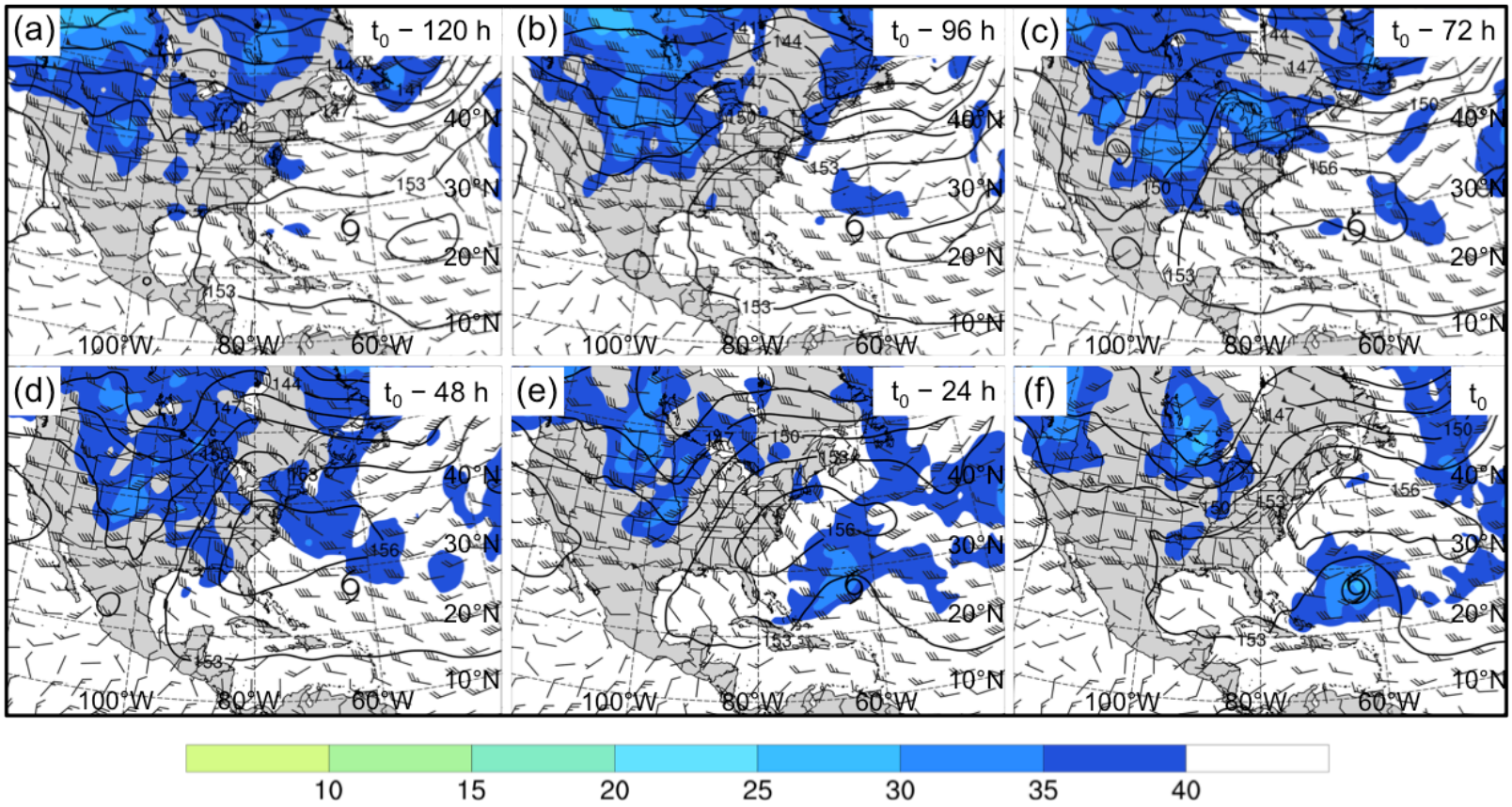

Fig 3.11. PV Streamer cluster composite (N = 8) coupling index (shaded, K), 850-hPa geopotential height (black contours, dam), and 850–200-hPa wind shear (barbs, kts) at (a) t_0 – 120 h, (b) t_0 – 96 h, (c) t_0 – 72 h, (d) t_0 – 48 h, (e) t_0 – 24 h, and (f) t_0. The black cyclone symbol in each panel denotes the average location of STC formation at t_0.

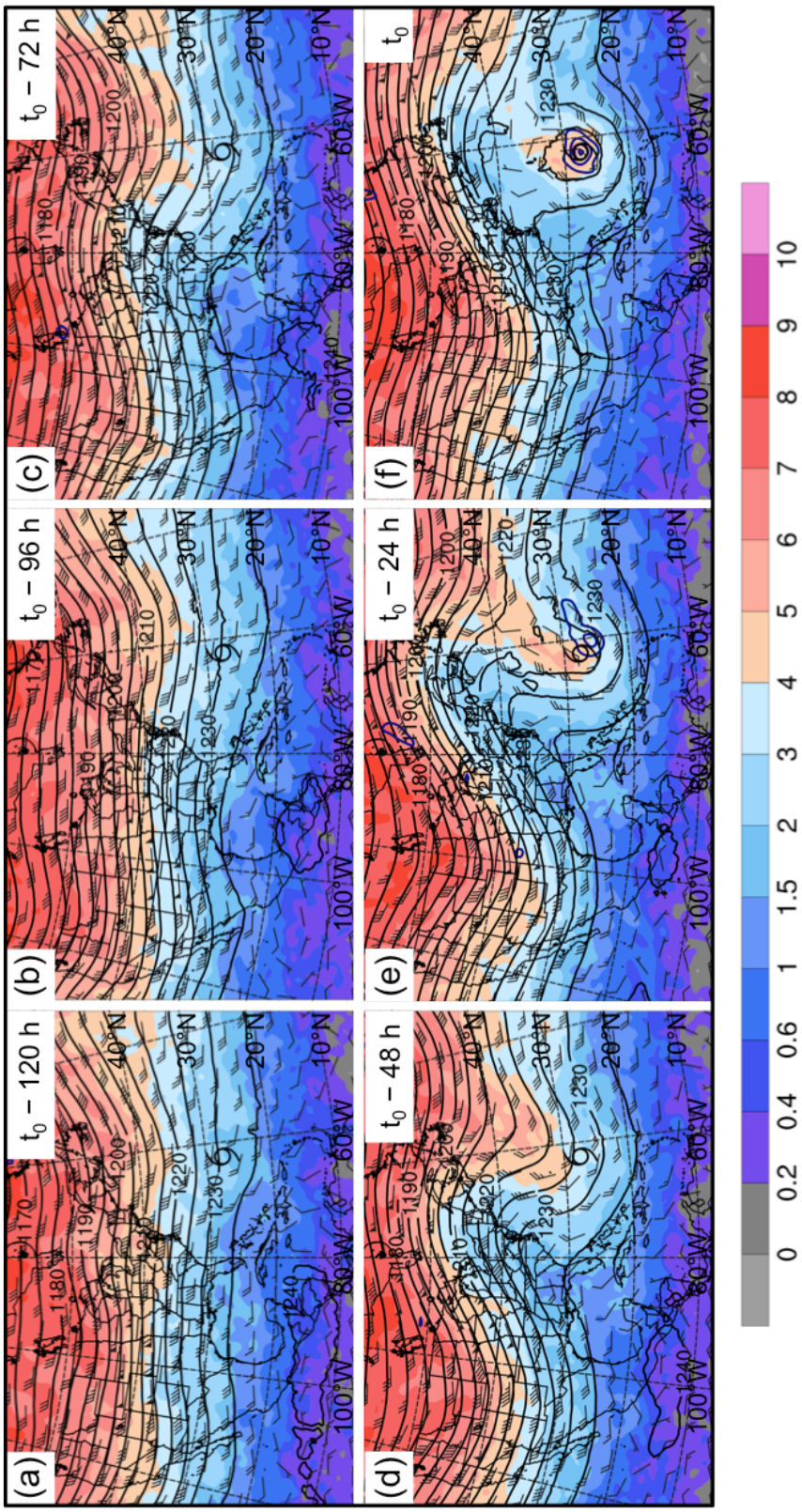

Fig 3.12. As in Fig. 3.7, except for the Cutoff cluster composite (N = 22).

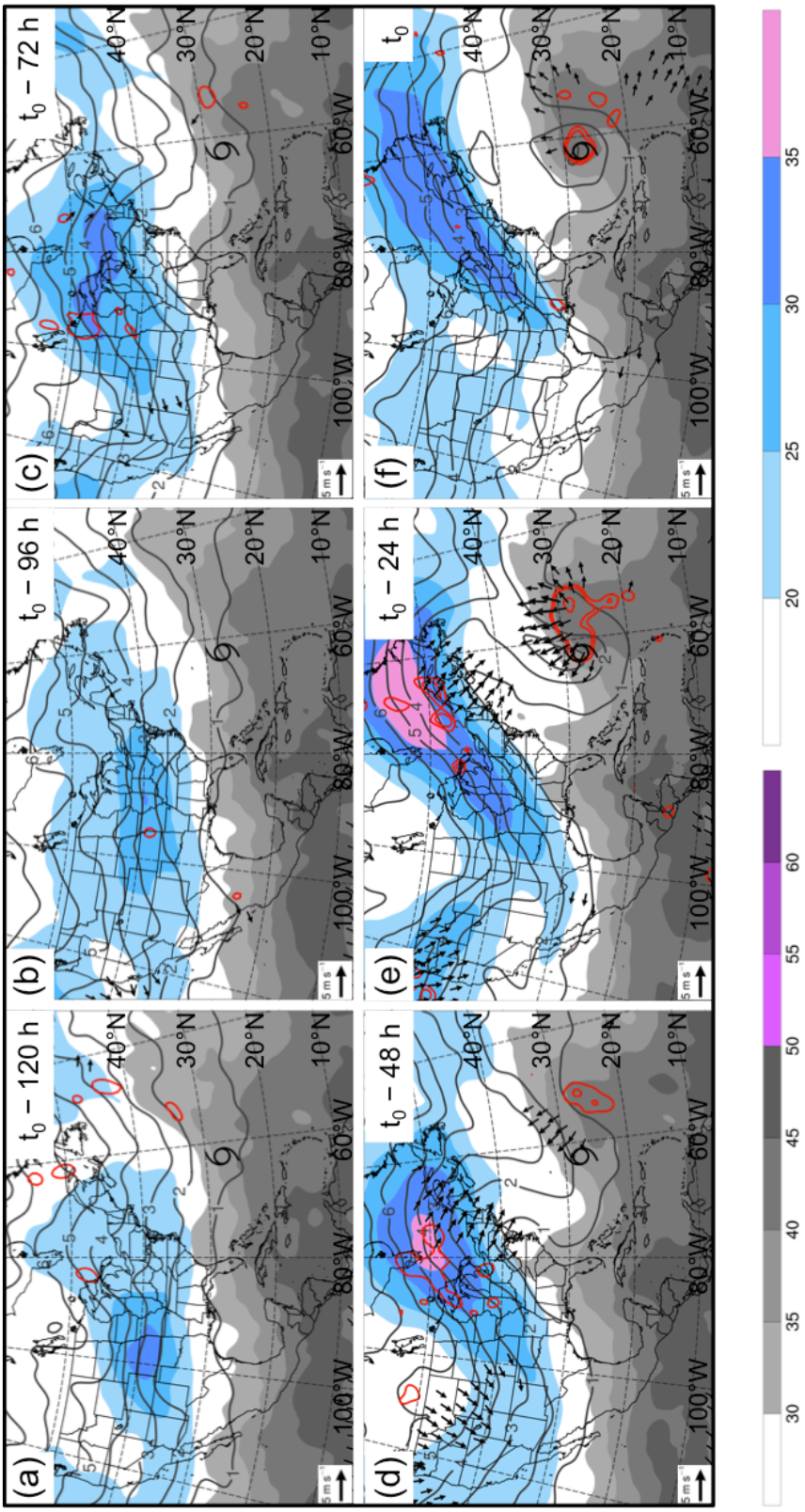

Fig 3.13. As in Fig. 3.8, except for the Cutoff cluster composite (N = 22).

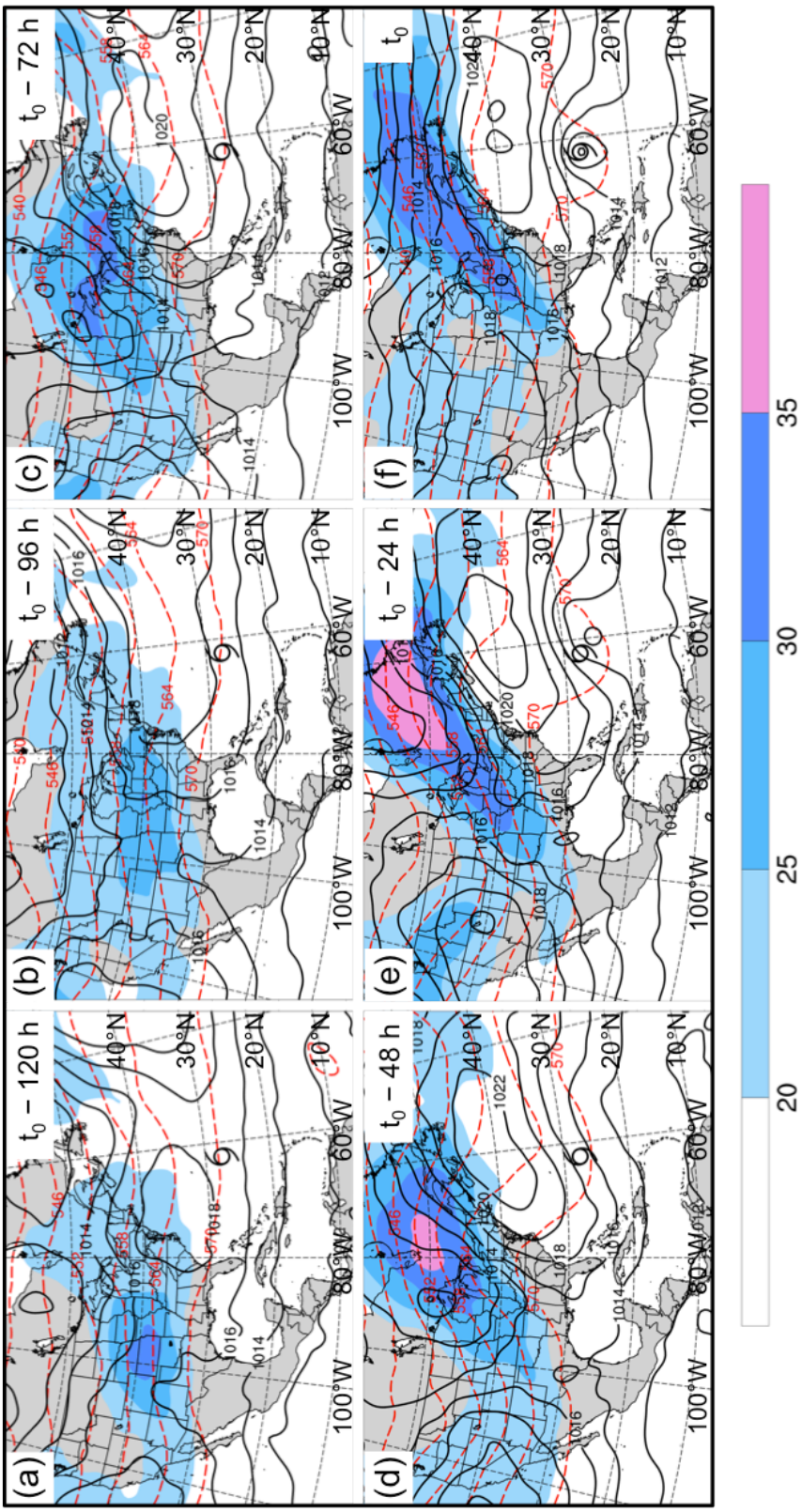

Fig 3.14. As in Fig. 3.9, except for the Cutoff cluster composite (N = 22).

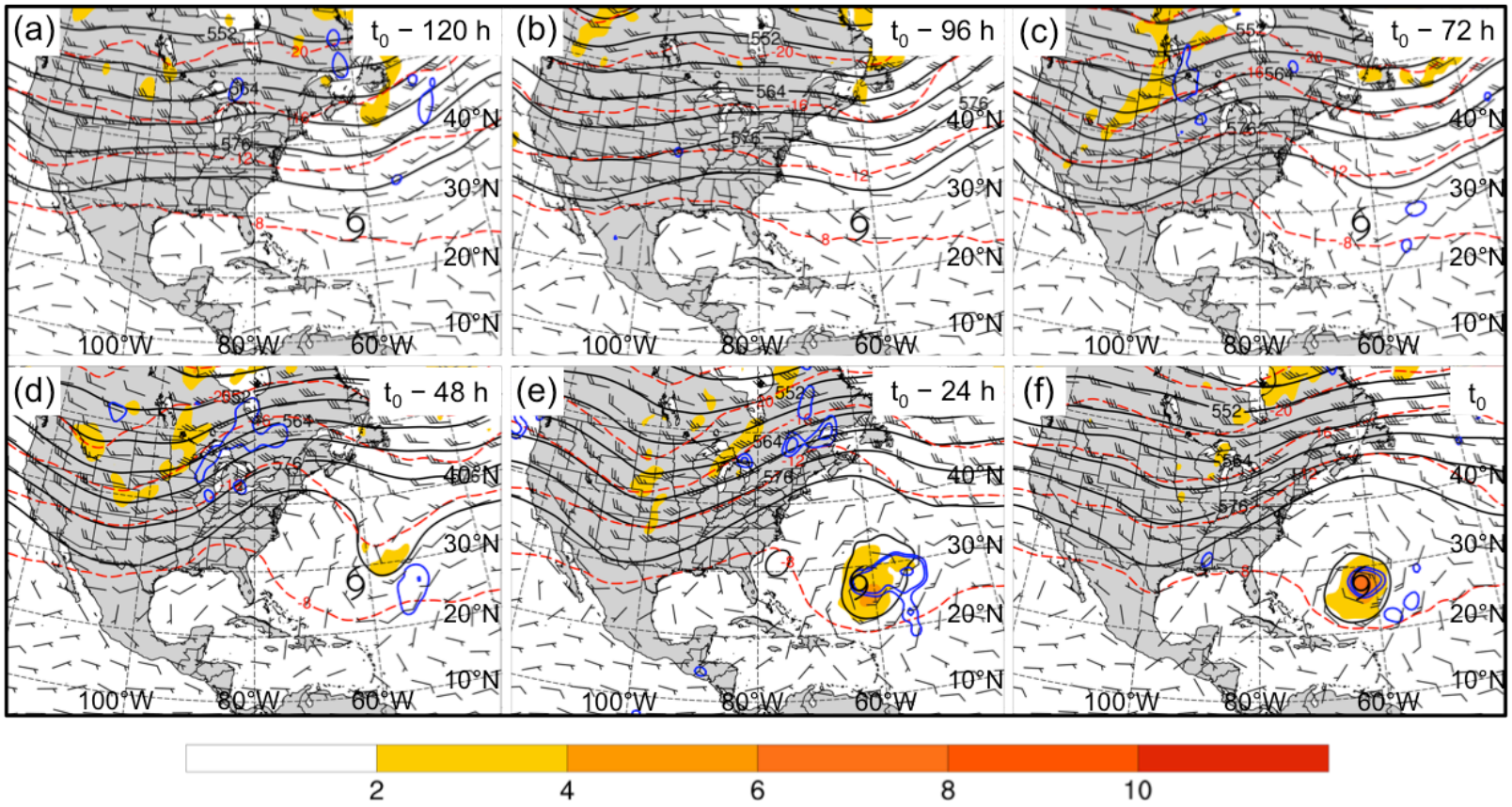

Fig 3.15. As in Fig. 3.10, except for the Cutoff cluster composite (N = 22).

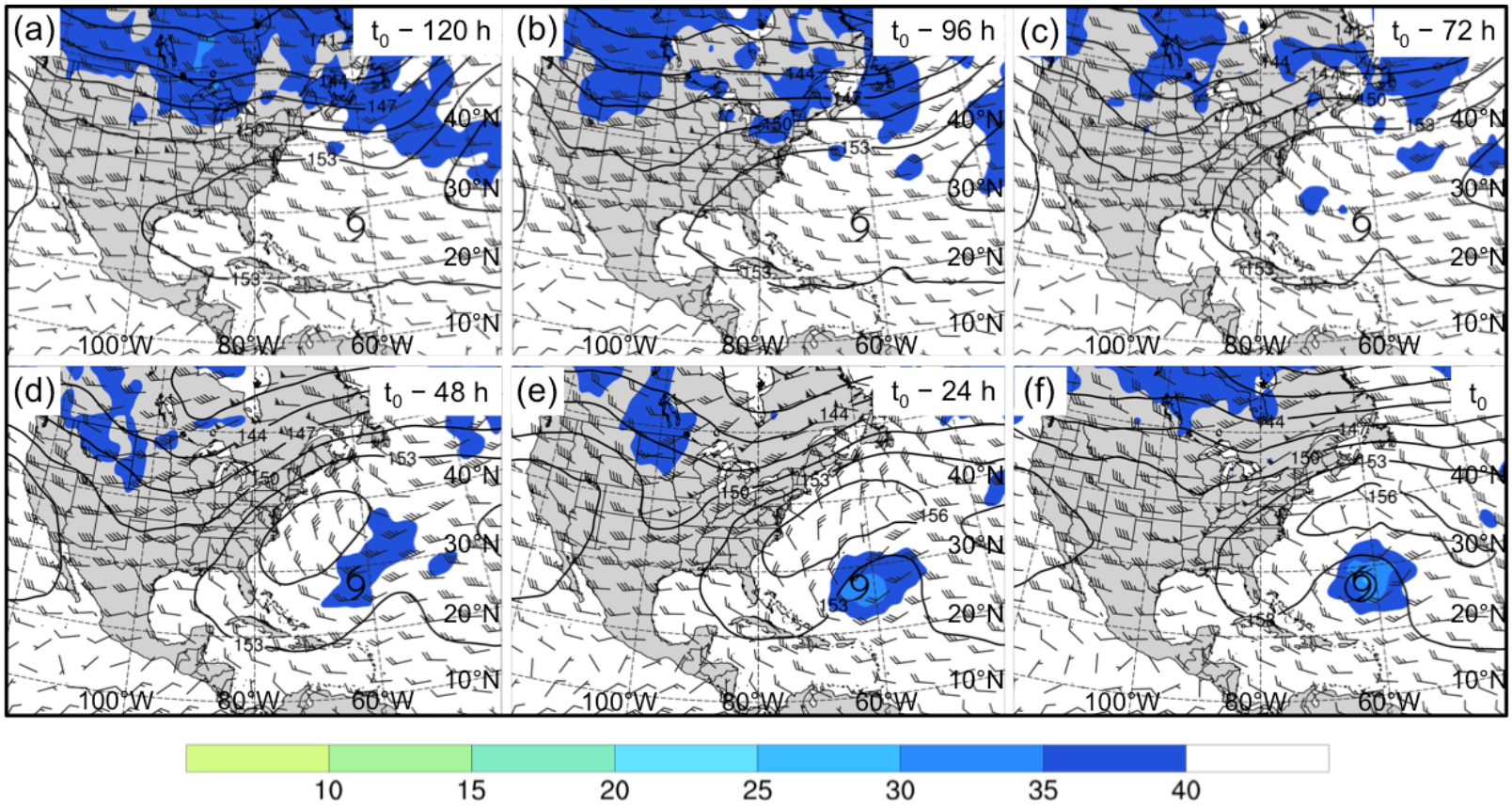

Fig 3.16. As in Fig. 3.11, except for the Cutoff cluster composite (N = 22).

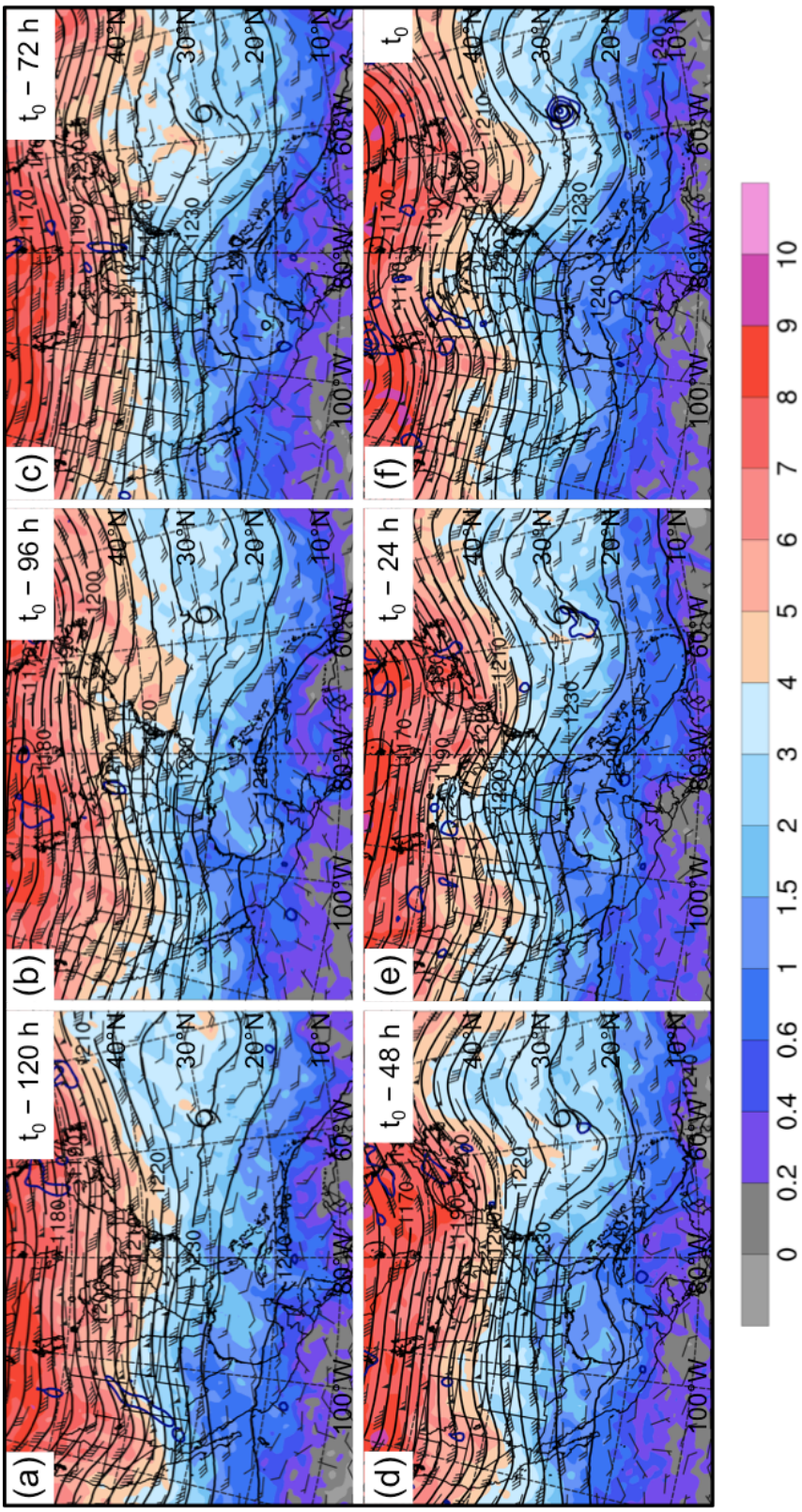

Fig 3.17. As in Fig. 3.7, except for the Midlatitude Trough cluster composite (N = 10).

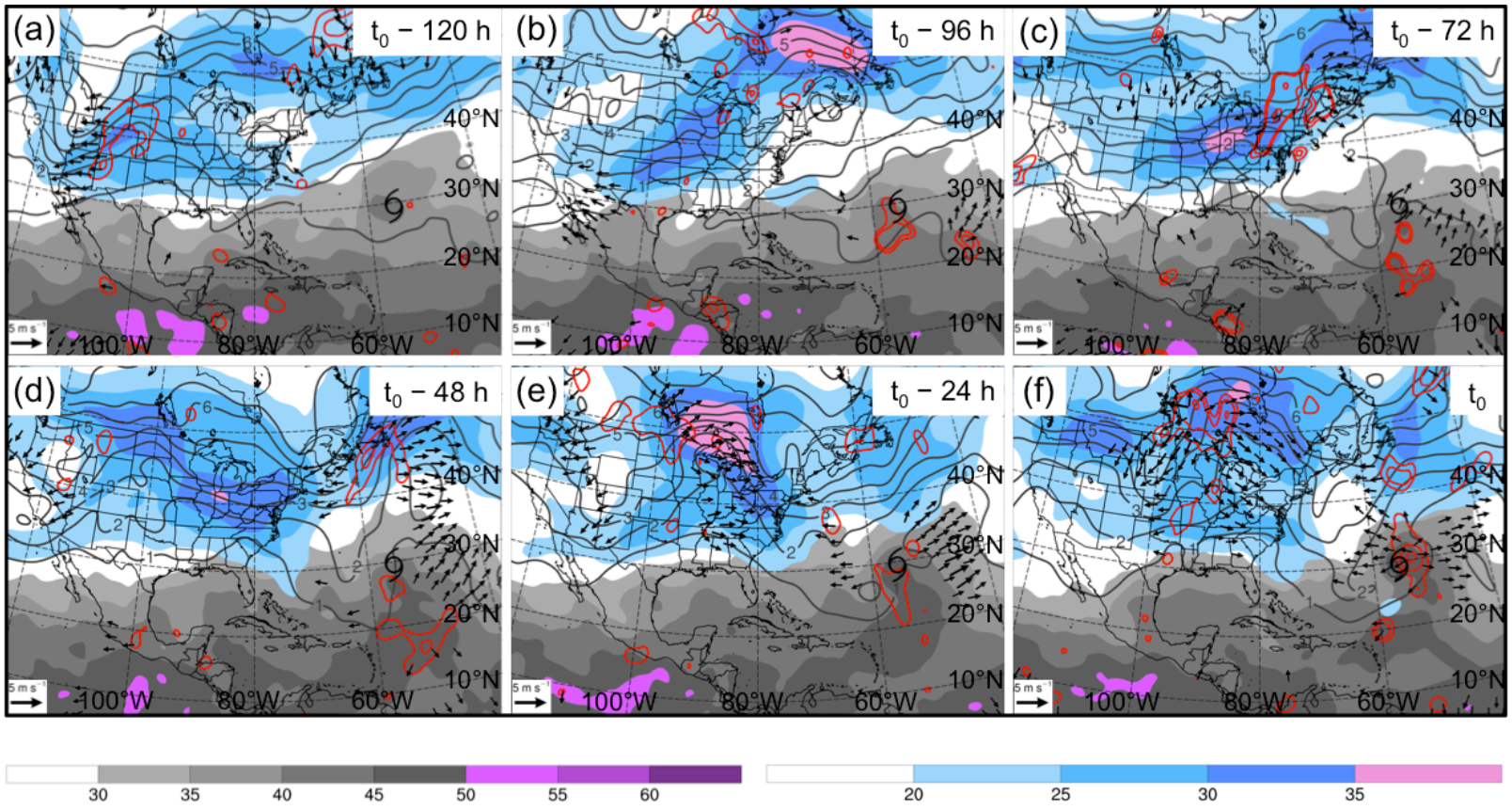

Fig 3.18. As in Fig. 3.8, except for the Midlatitude Trough cluster composite (N = 10).

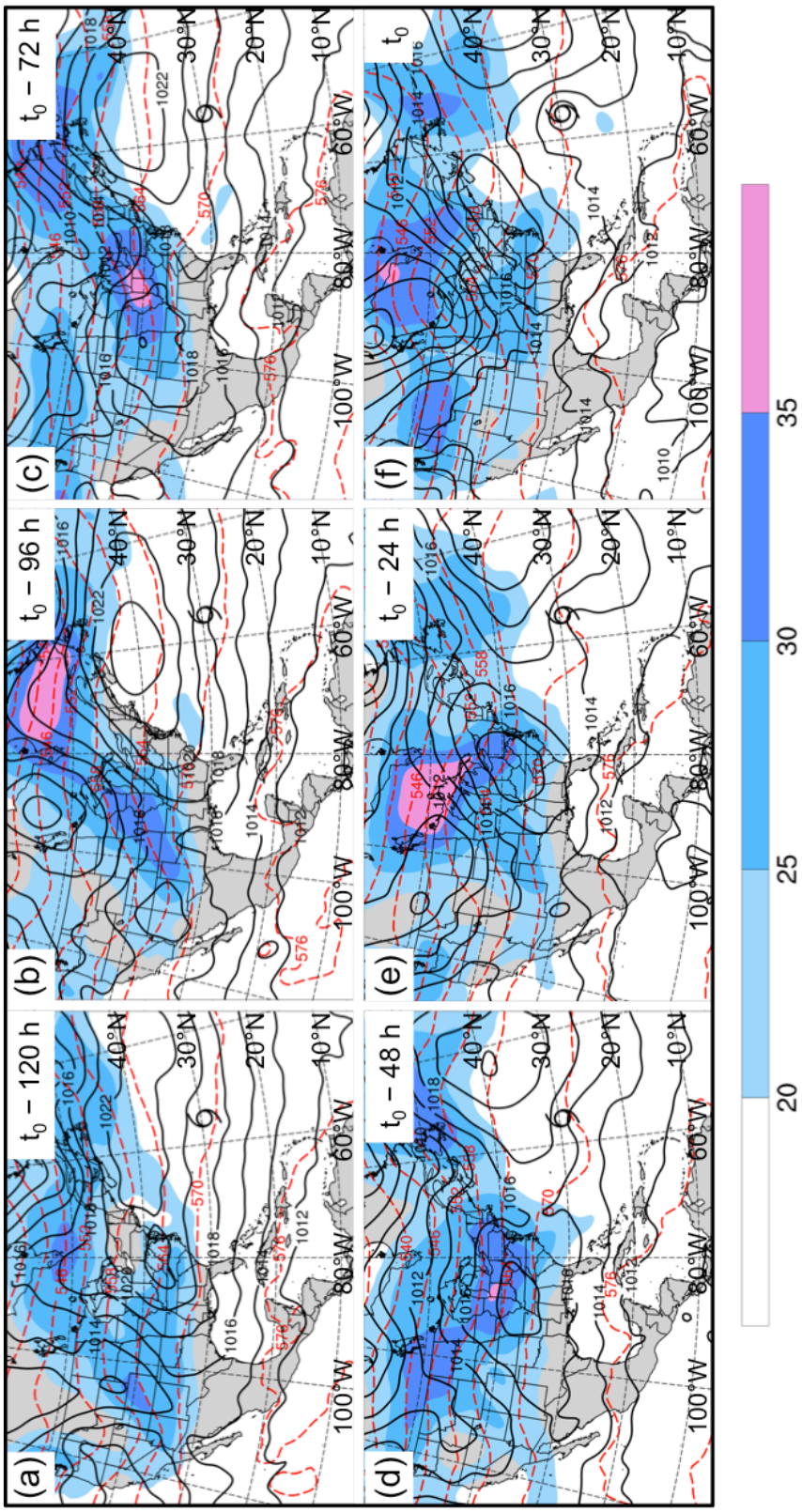

Fig 3.19. As in Fig. 3.9, except for the Midlatitude Trough cluster composite (N = 10).

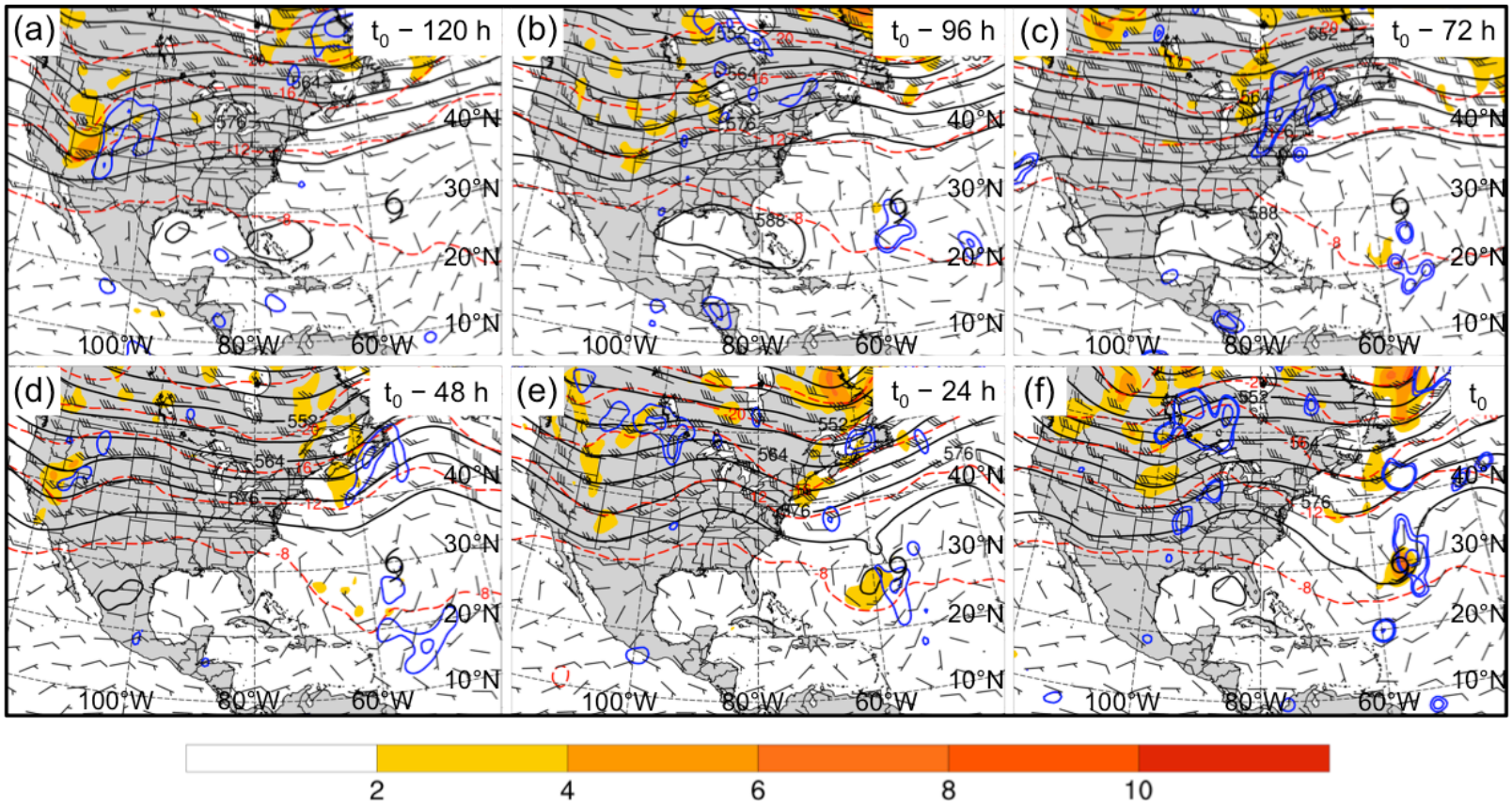

Fig 3.20. As in Fig. 3.10, except for the Midlatitude Trough cluster composite (N = 10).

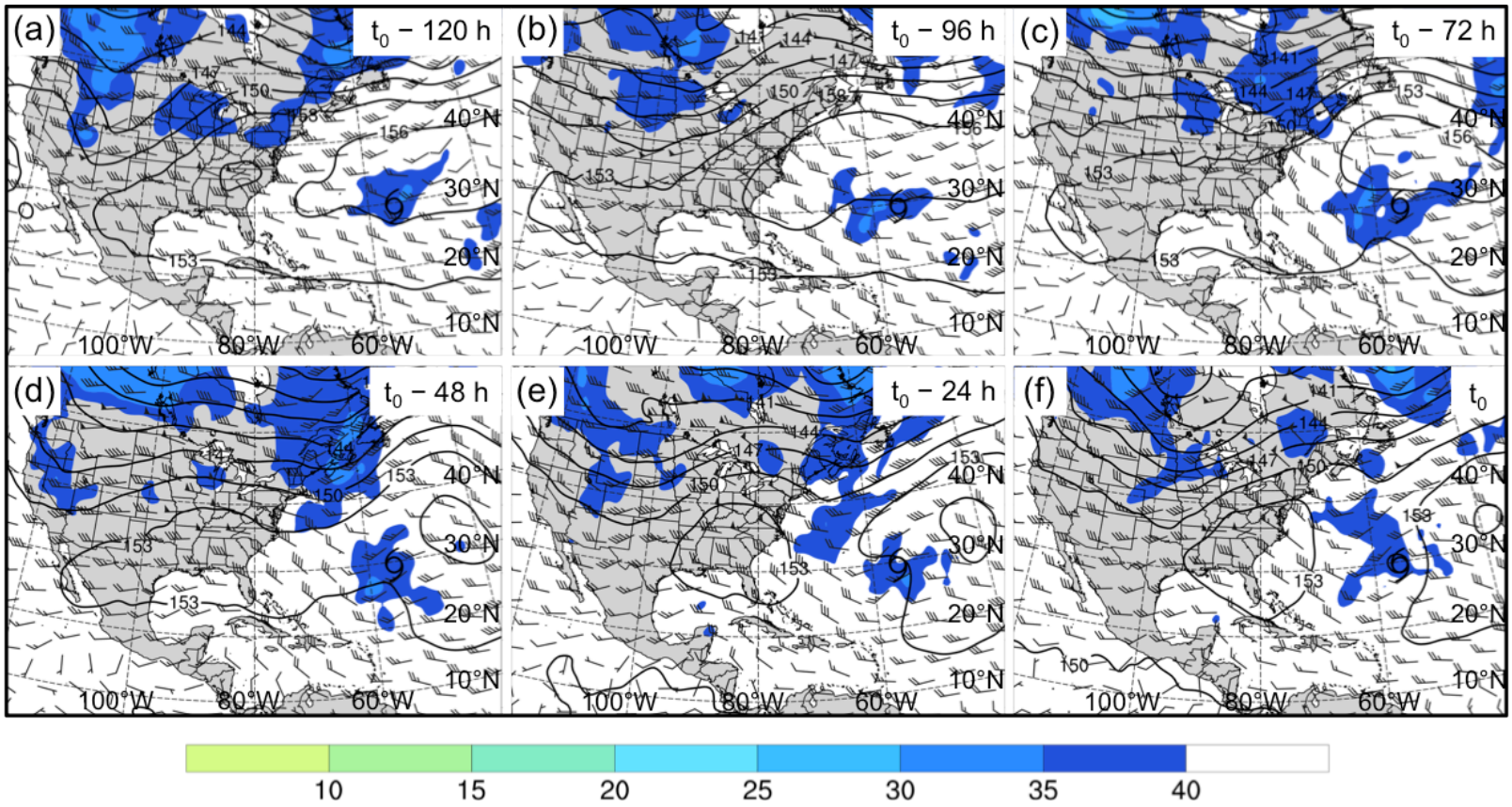

Fig 3.21. As in Fig. 3.11, except for the Midlatitude Trough cluster composite (N = 10).

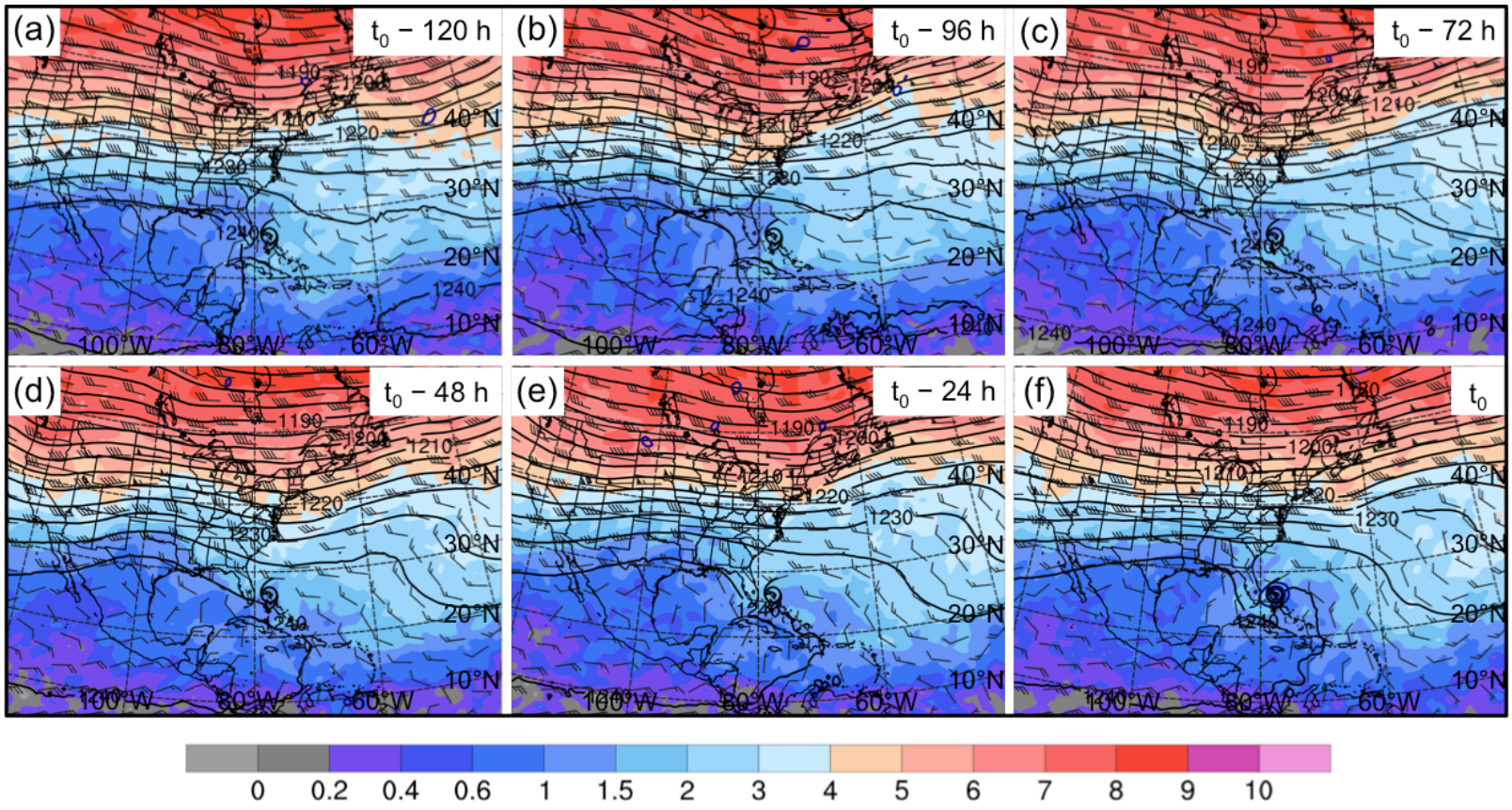

Fig 3.22. As in Fig. 3.7, except for the Subtropical Disturbance cluster composite (N = 22).

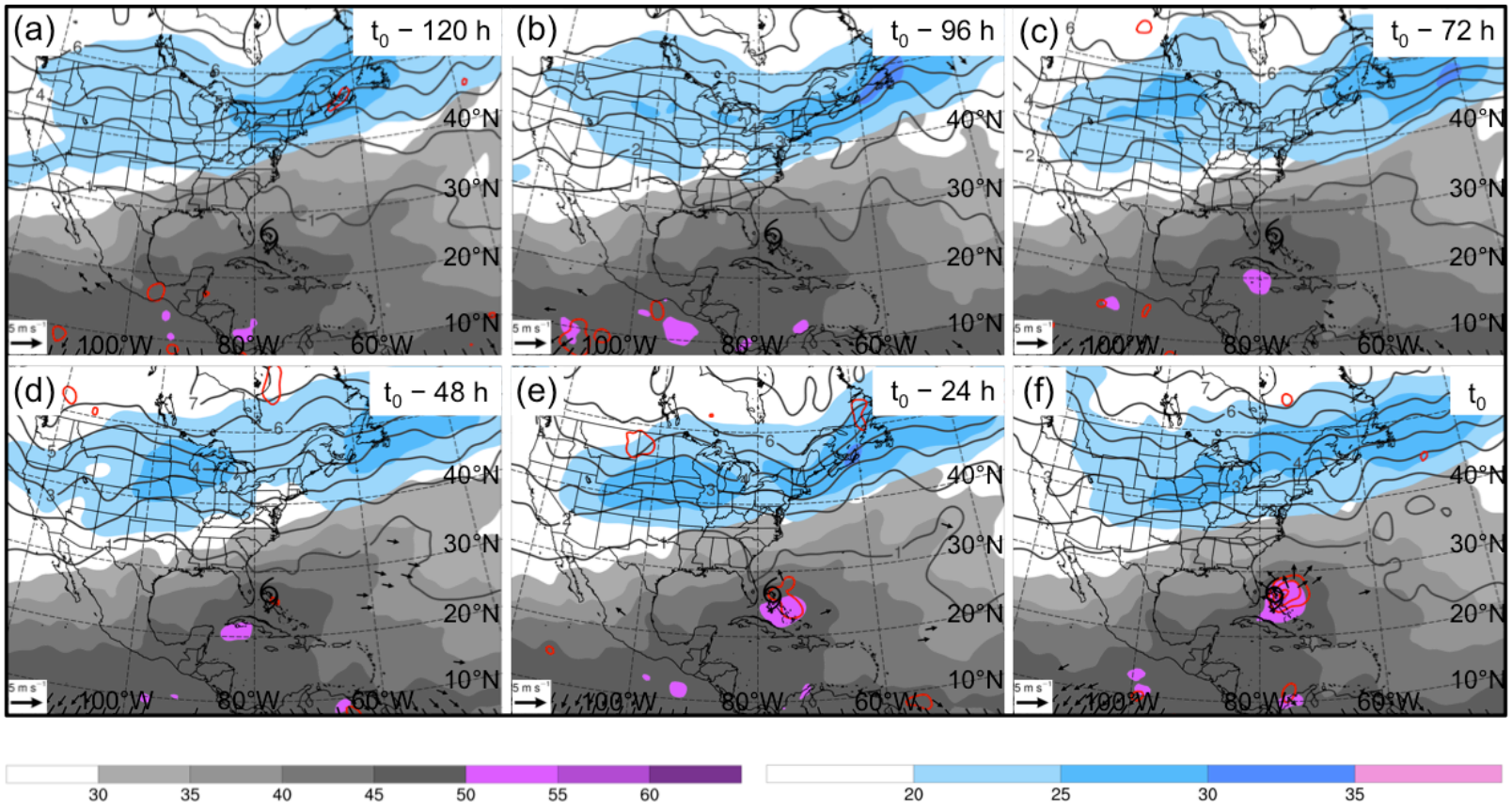

Fig 3.23. As in Fig. 3.8, except for the Subtropical Disturbance cluster composite (N = 22).

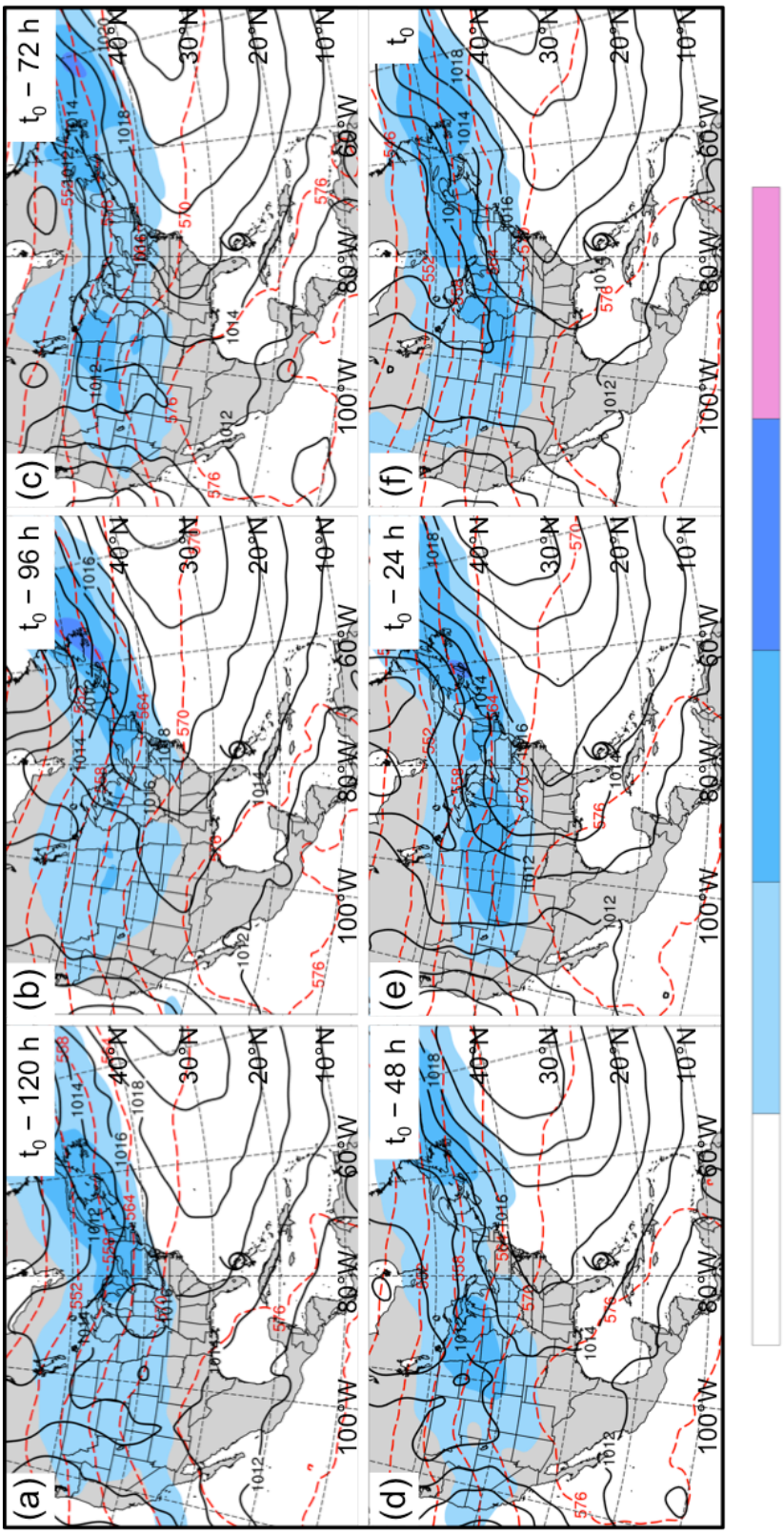

Fig 3.24. As in Fig. 3.9, except for the Subtropical Disturbance cluster composite (N = 22).

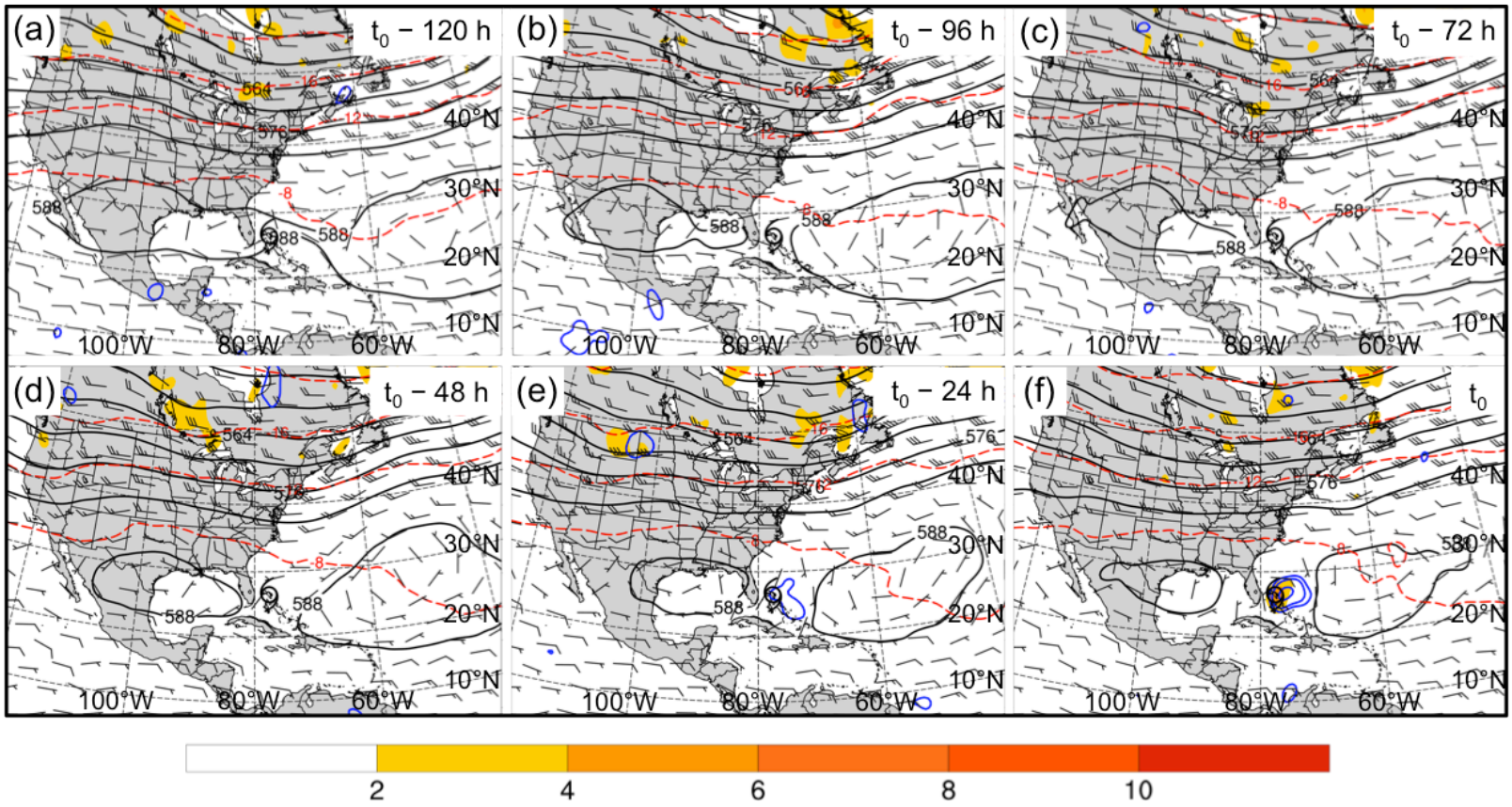

Fig 3.25. As in Fig. 3.10, except for the Subtropical Disturbance cluster composite (N = 22).

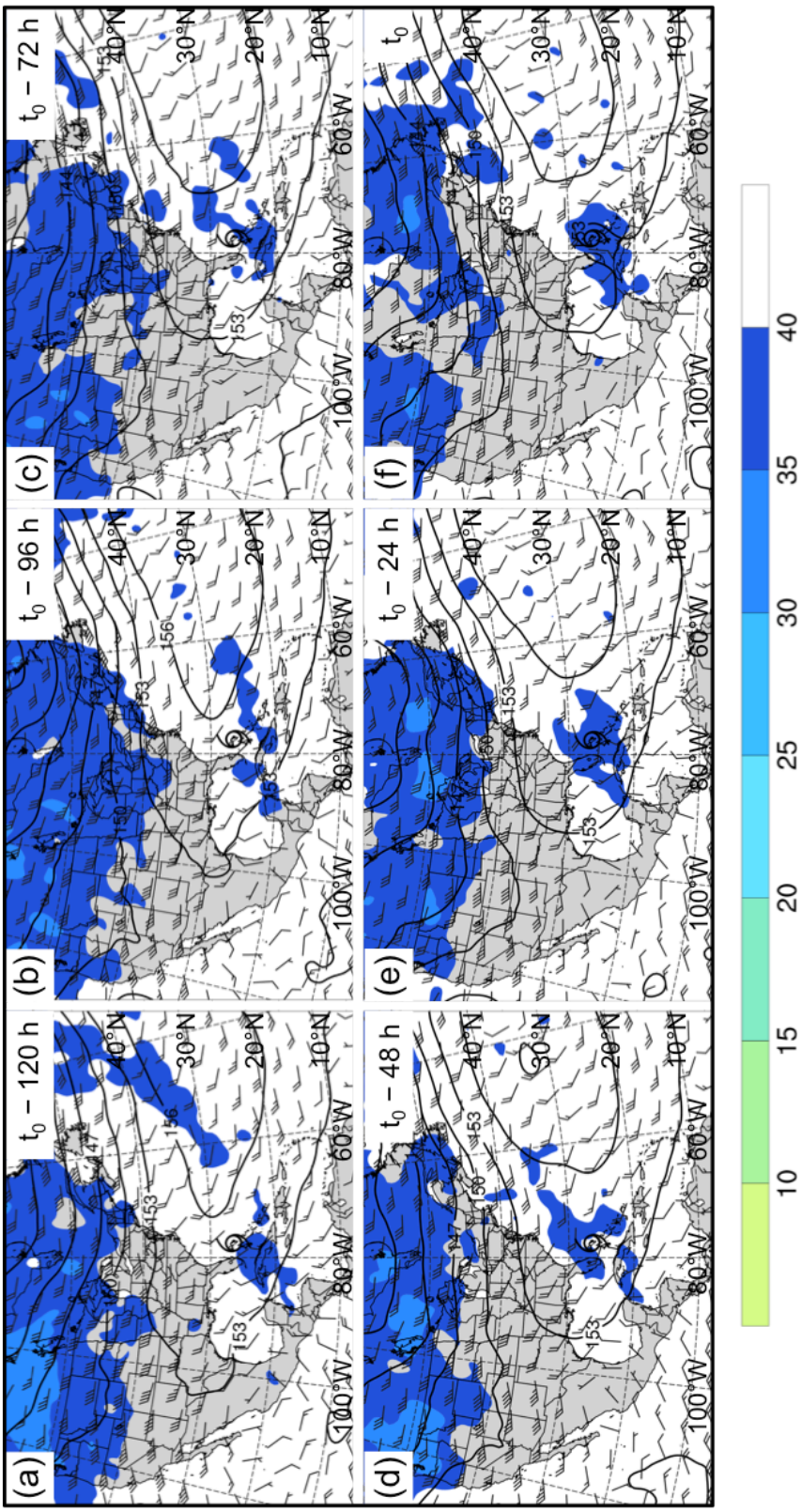

Fig 3.26. As in Fig. 3.11, except for the Subtropical Disturbance cluster composite (N = 22).

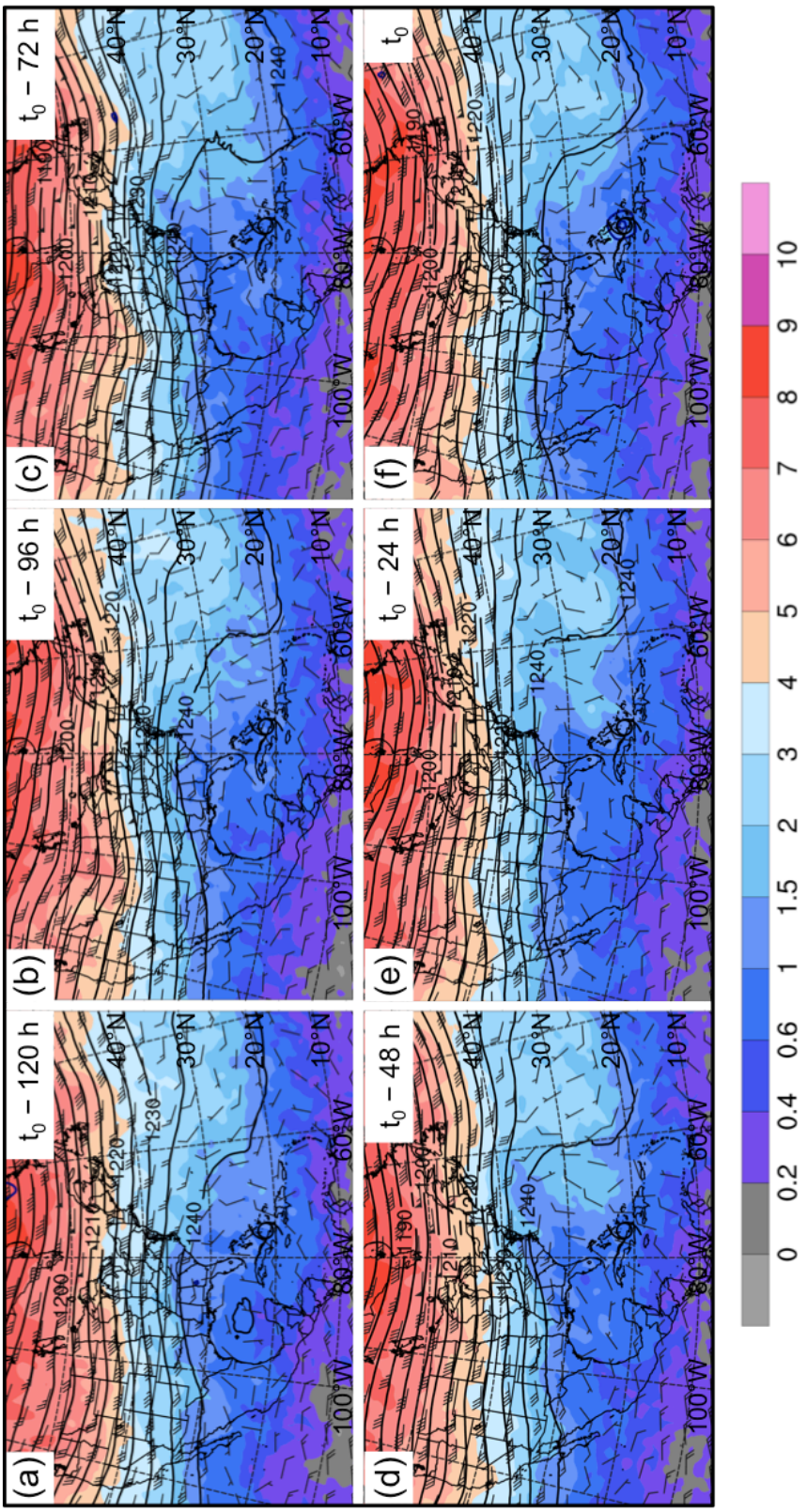

Fig 3.27. As in Fig. 3.7, except for the PV Debris cluster composite (N = 31).

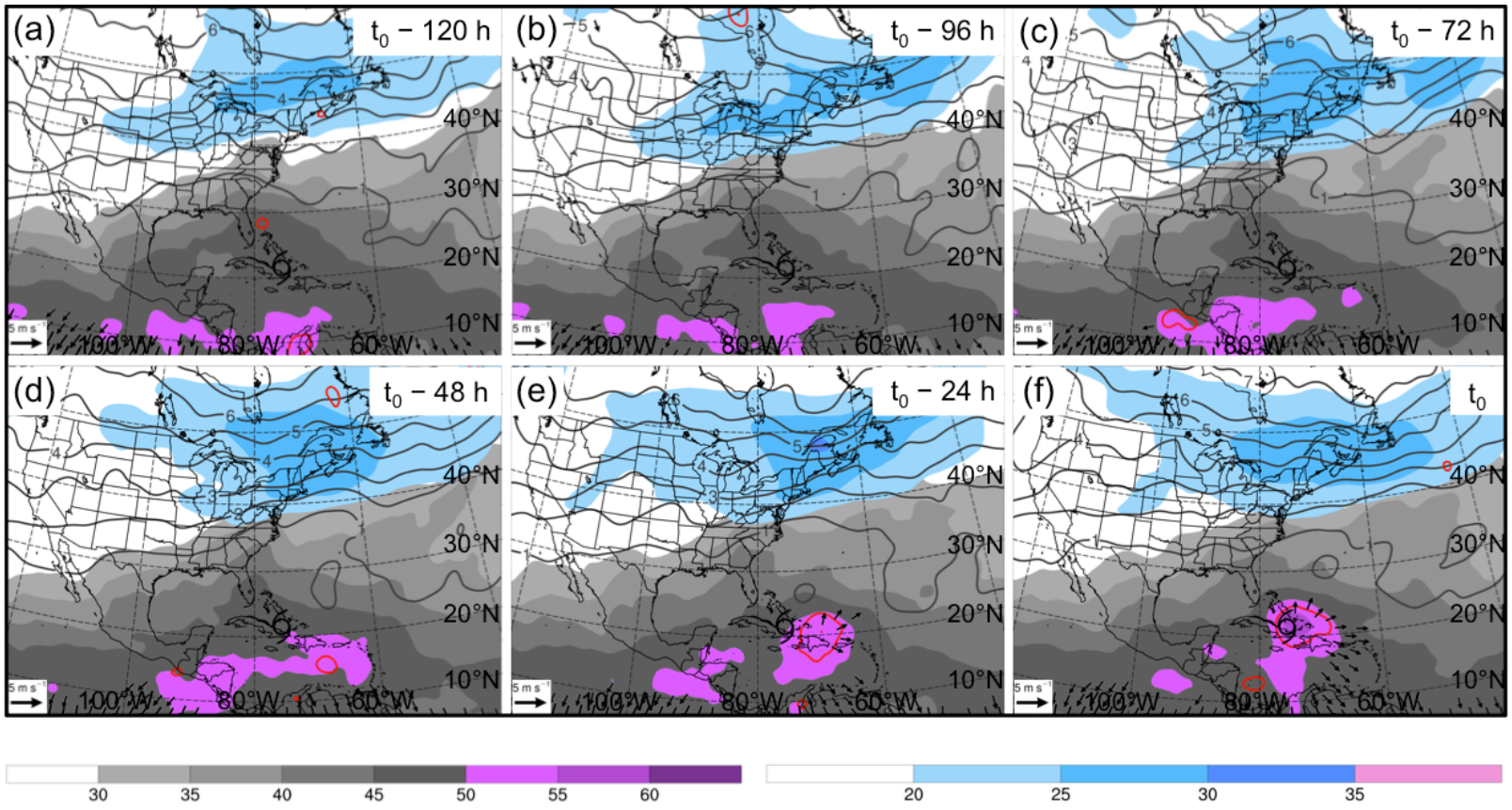

Fig 3.28. As in Fig. 3.8, except for the PV Debris cluster composite (N = 31).

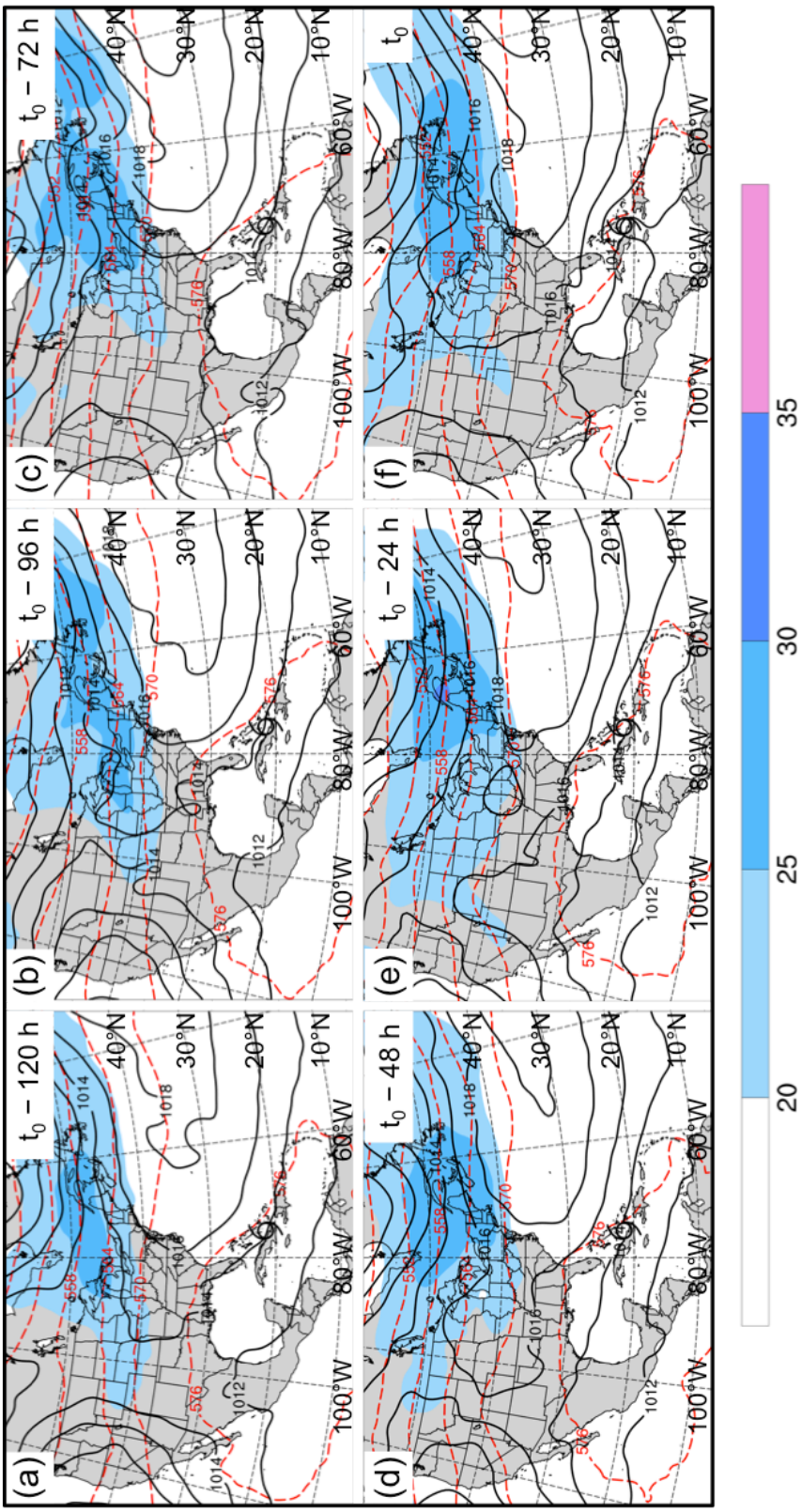

Fig 3.29. As in Fig. 3.9, except for the PV Debris cluster composite (N = 31).

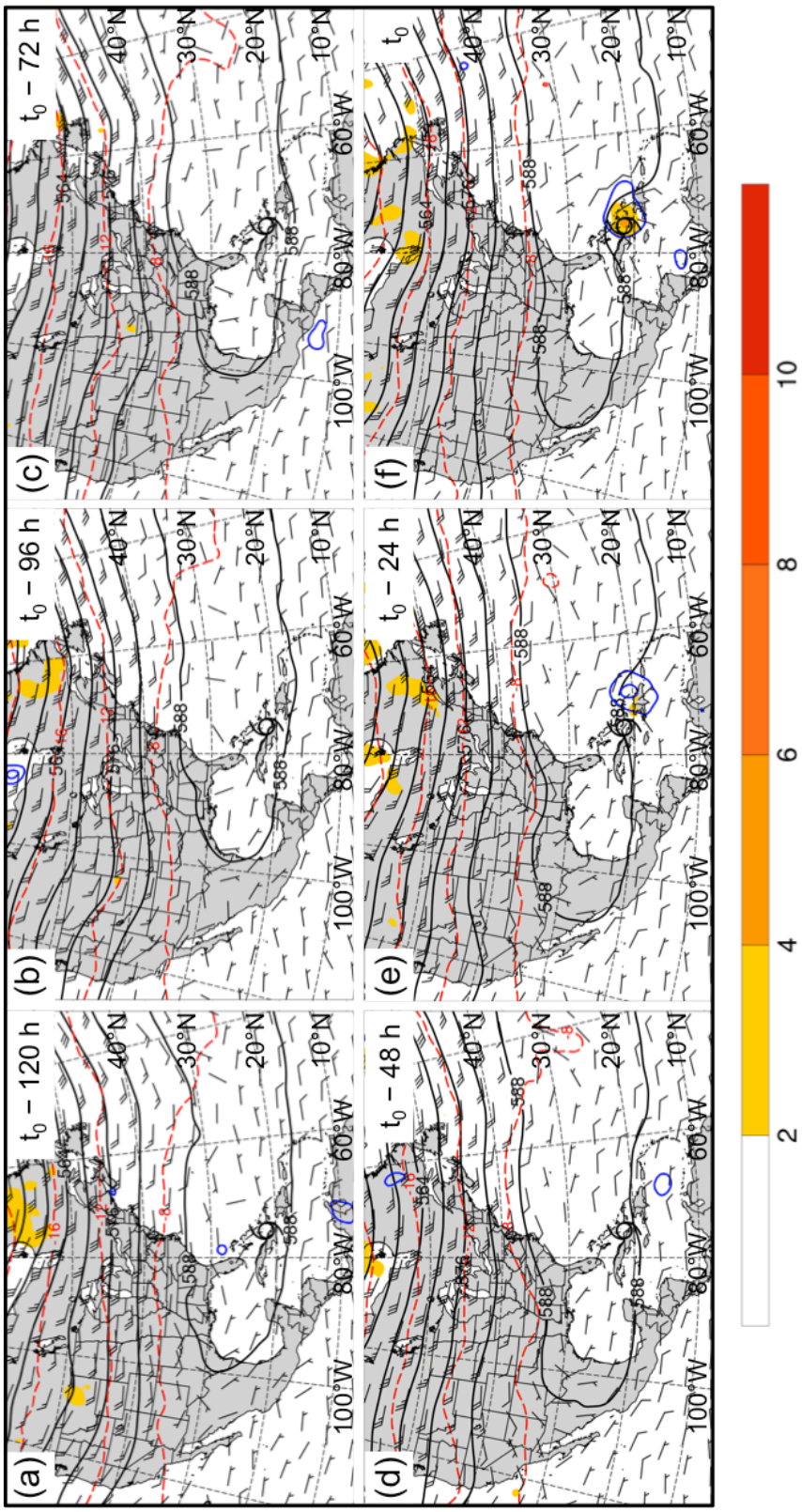

Fig 3.30. As in Fig. 3.10, except for the PV Debris cluster composite (N = 31).

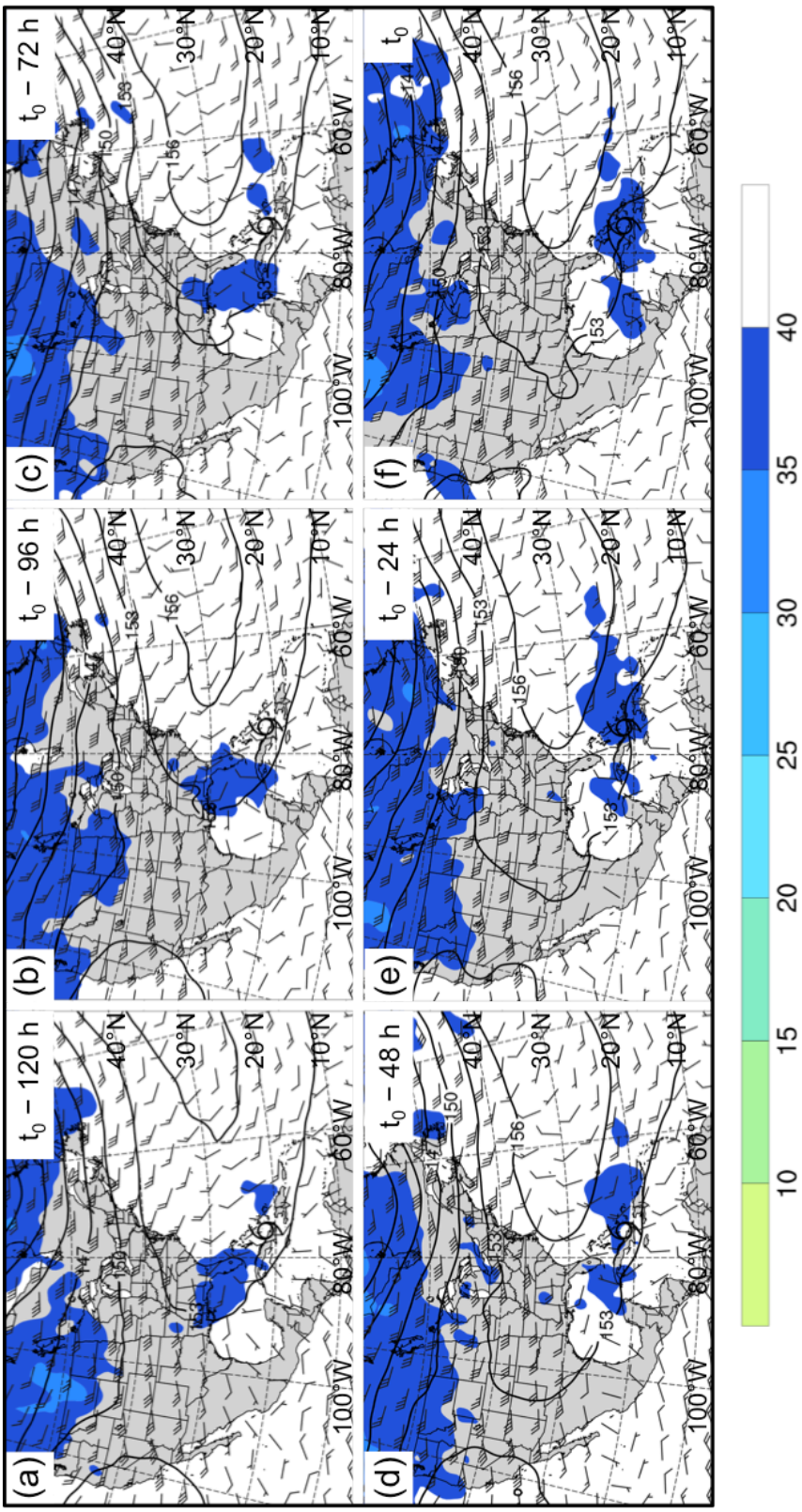

Fig 3.31. As in Fig. 3.11, except for the PV Debris cluster composite (N = 31).

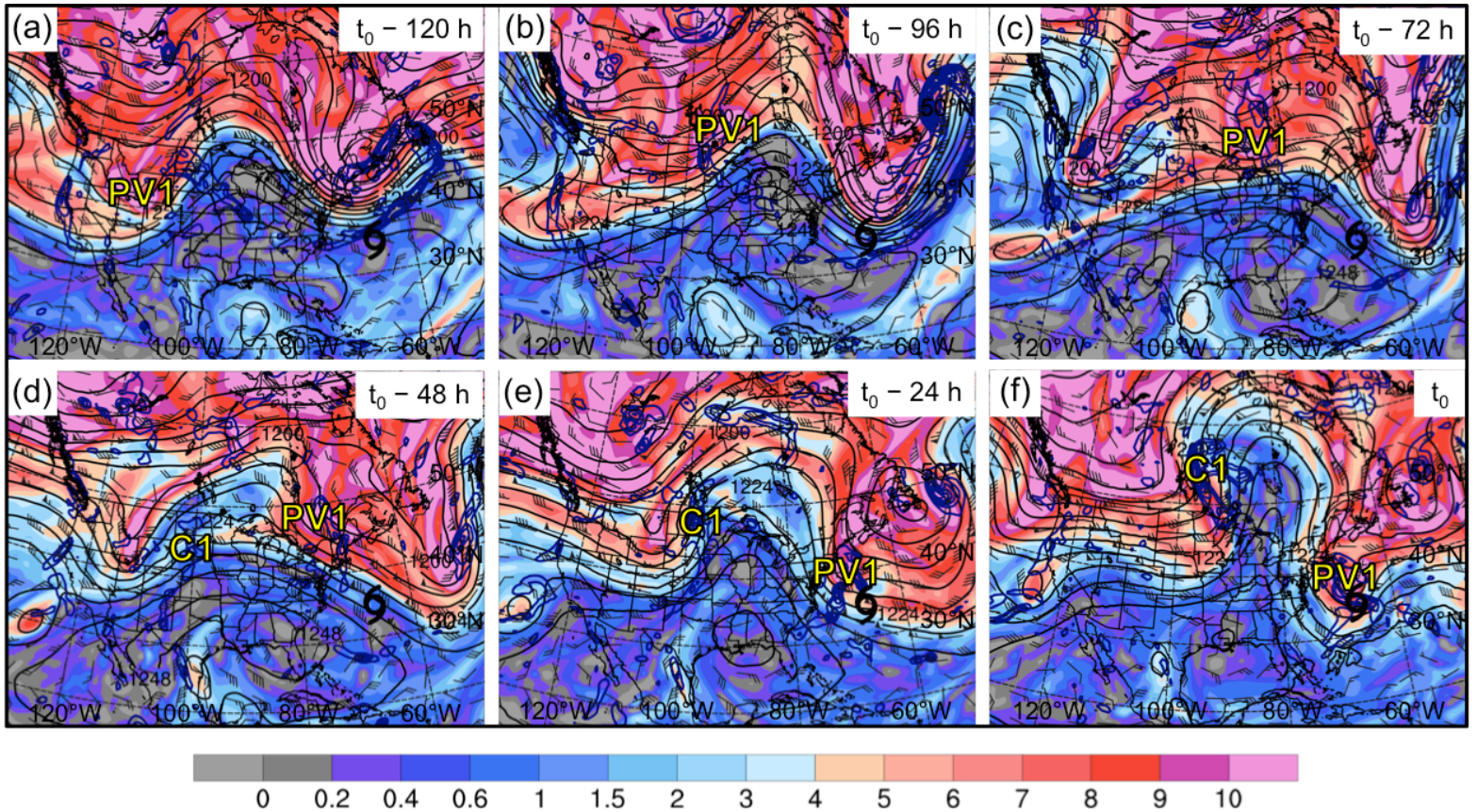

Fig 3.32. Potential vorticity (shaded, PVU) and winds (barbs, kts) on the 350 K isentropic surface, 200-hPa geopotential height (black contours, dam), and 925–850-hPa layer-averaged cyclonic relative vorticity (blue contours, every 0.5×10^{-4} s^{-1}) for an STC forming in association with a PV streamer at 1800 UTC 21 August 1980 (t_0). Panels depict the aforementioned features at (a) t_0 – 120 h, (b) t_0 – 96 h, (c) t_0 – 72 h, (d) t_0 – 48 h, (e) t_0 – 24 h, and (f) t_0. The black cyclone symbol in each panel denotes the location of STC formation at t_0. Label "PV1" indicates the position of a region of relatively high upper-tropospheric PV. Label "C1" indicates the position of a surface cyclone.

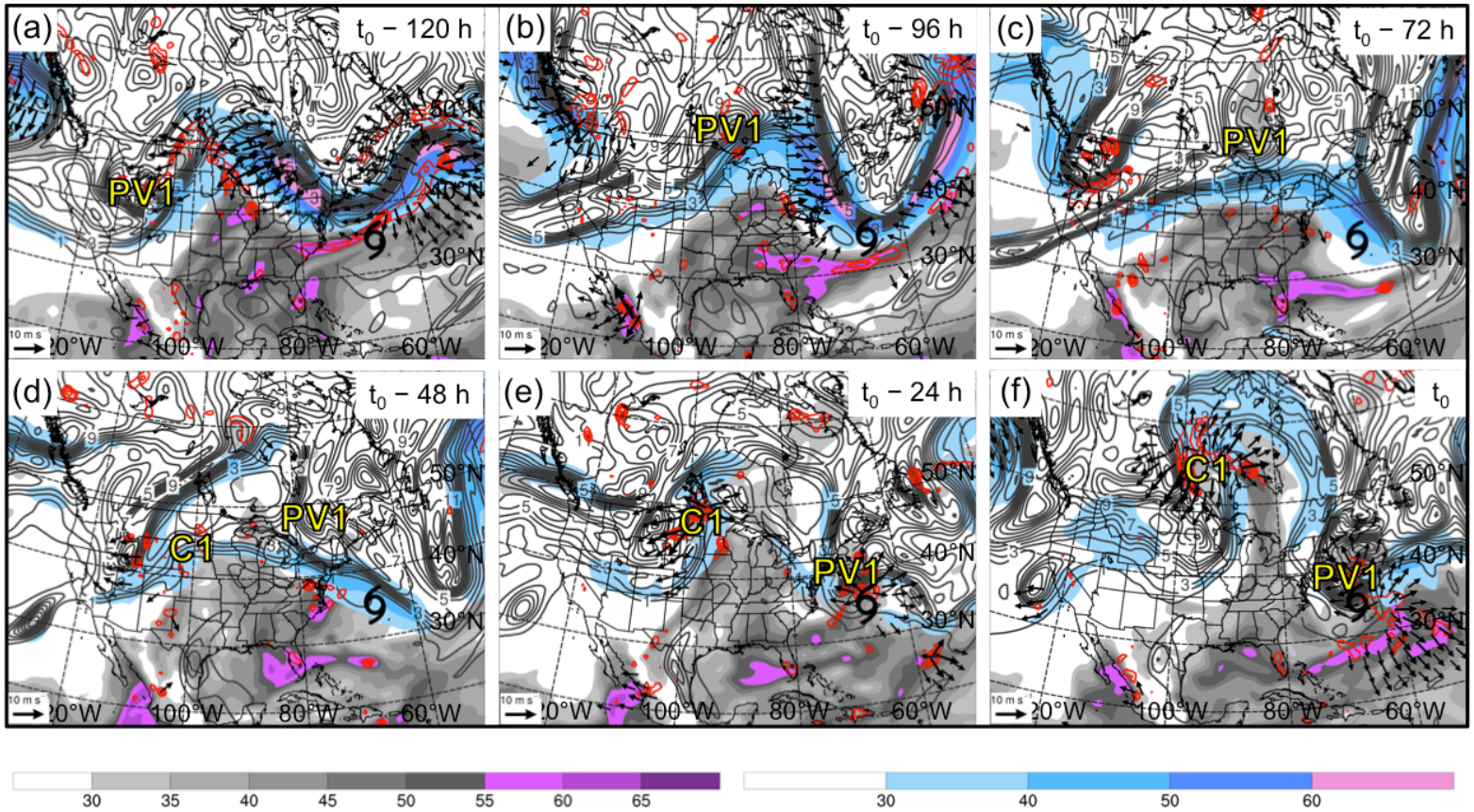

Fig 3.33. Precipitable water (gray shading, mm), 200-hPa wind speed (shaded, m s^{-1}), 200-hPa potential vorticity (gray contours, PVU), 600–400-hPa layer-averaged ascent (red contours, every 5 × 10^{-3} hPa s^{-1}), and 300–200-hPa layer-averaged irrotational wind (vectors, starting at 5 m s^{-1}) for an STC forming in association with a PV streamer at 1800 UTC 21 August 1980 (t_0). Panels depict the aforementioned features at (a) t_0 – 120 h, (b) t_0 – 96 h, (c) t_0 – 72 h, (d) t_0 – 48 h, (e) t_0 – 24 h, and (f) t_0. The black cyclone symbol in each panel denotes the location of STC formation at t_0. Label "PV1" indicates the position of a region of relatively high upper-tropospheric PV. Label "C1" indicates the position of a surface cyclone.

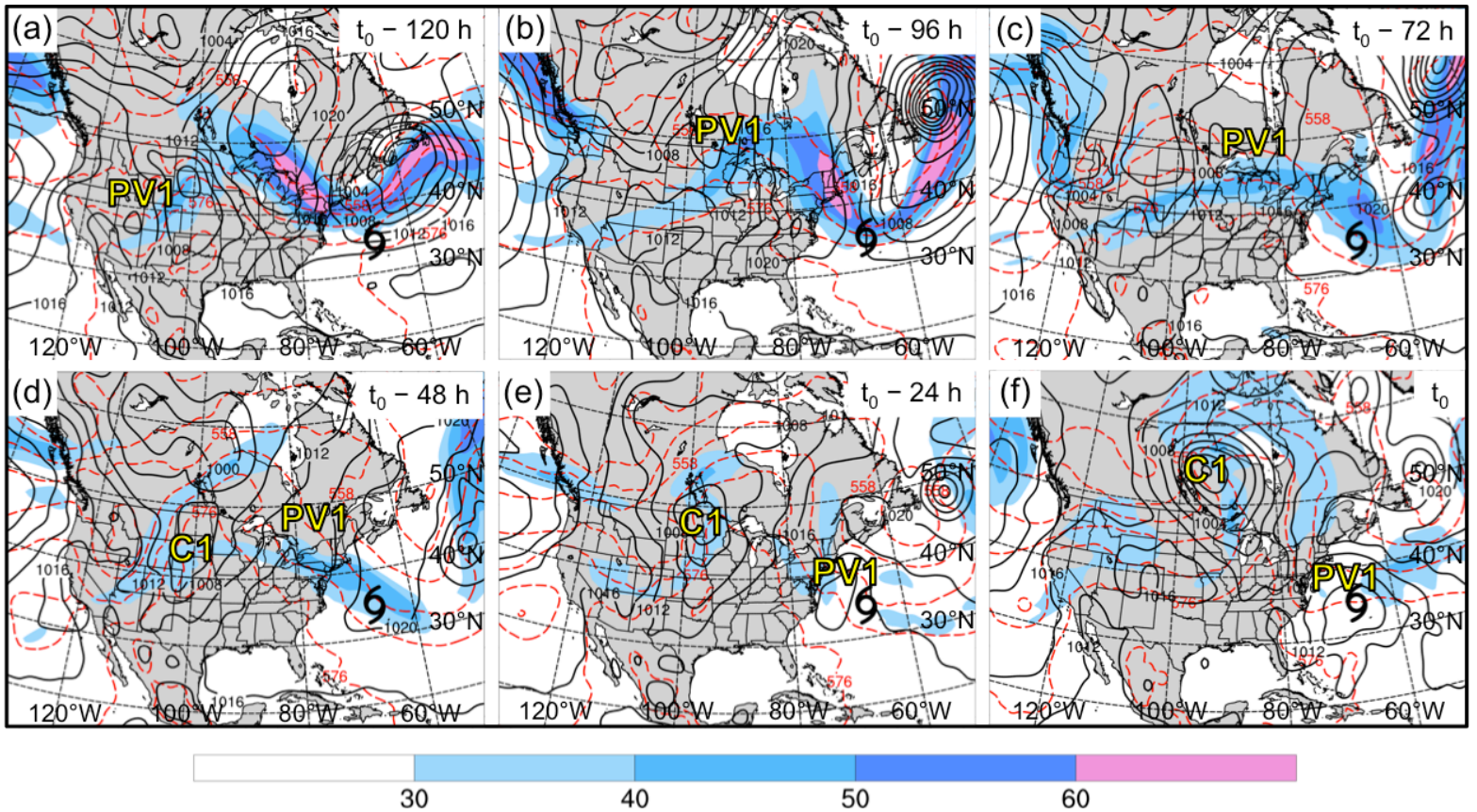

Fig 3.34. 200-hPa wind speed (shaded, m s^{-1}), 1000–500-hPa thickness (red dashed contours, dam), and MSLP (black solid contours, hPa) for an STC forming in association with a PV streamer at 1800 UTC 21 August 1980 (t_0). Panels depict the aforementioned features at (a) t_0 – 120 h, (b) t_0 – 96 h, (c) t_0 – 72 h, (d) t_0 – 48 h, (e) t_0 – 24 h, and (f) t_0. The black cyclone symbol in each panel denotes the location of STC formation at t_0. Label "PV1" indicates the position of a region of relatively high upper-tropospheric PV. Label "C1" indicates the position of a surface cyclone.

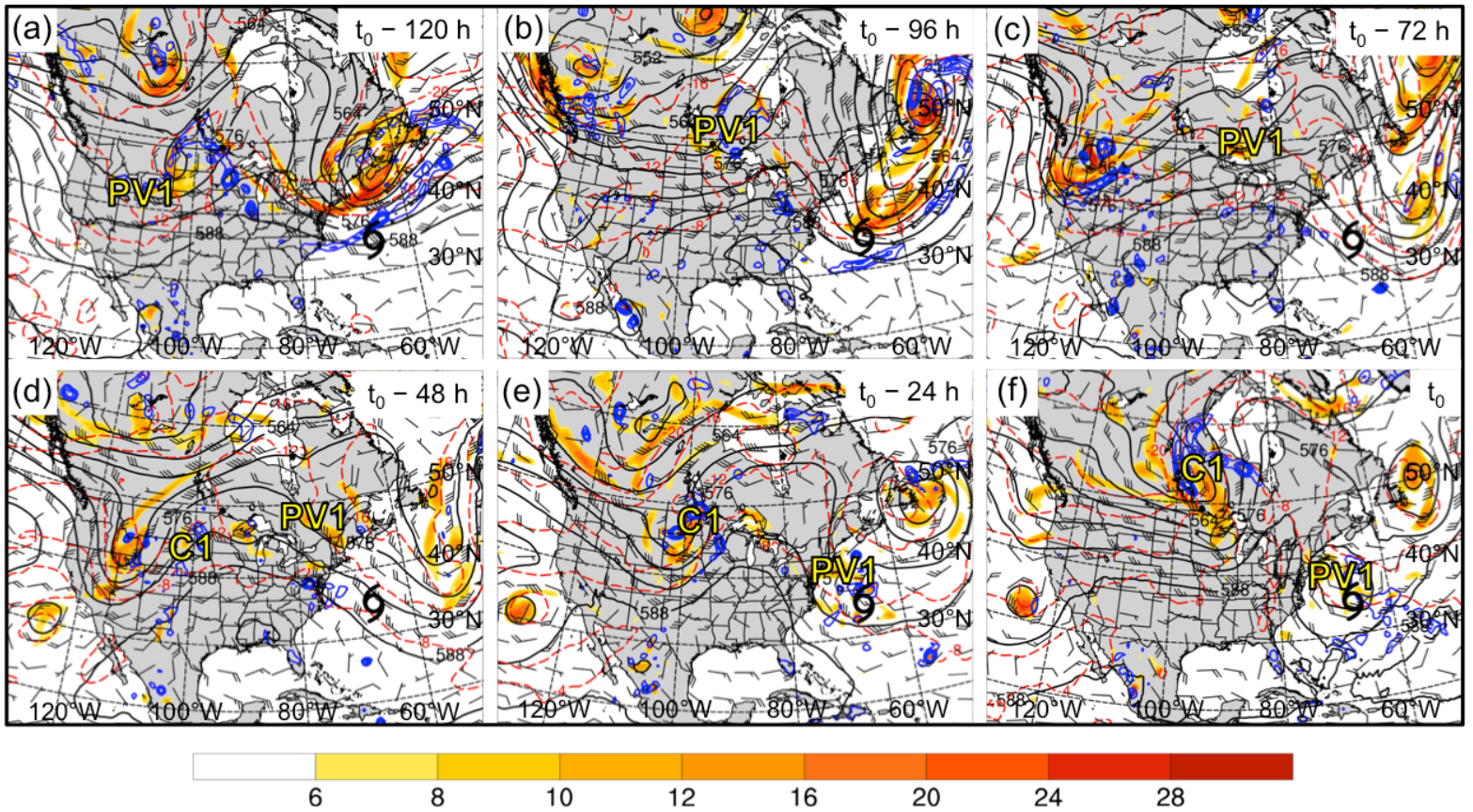

Fig 3.35. 500-hPa cyclonic relative vorticity (shaded, 10^{-5} s^{-1}), geopotential height (black solid contours, dam), temperature (red dashed contours, °C), ascent (blue contours, every 5×10^{-3} hPa s^{-1}), and winds (barbs, kts) for an STC forming in association with a PV streamer at 1800 UTC 21 August 1980 (t_0). Panels depict the aforementioned features at (a) t_0 – 120 h, (b) t_0 – 96 h, (c) t_0 – 72 h, (d) t_0 – 48 h, (e) t_0 – 24 h, and (f) t_0. The black cyclone symbol in each panel denotes the location of STC formation at t_0. Label "PV1" indicates the position of a region of relatively high upper-tropospheric PV. Label "C1" indicates the position of a surface cyclone.

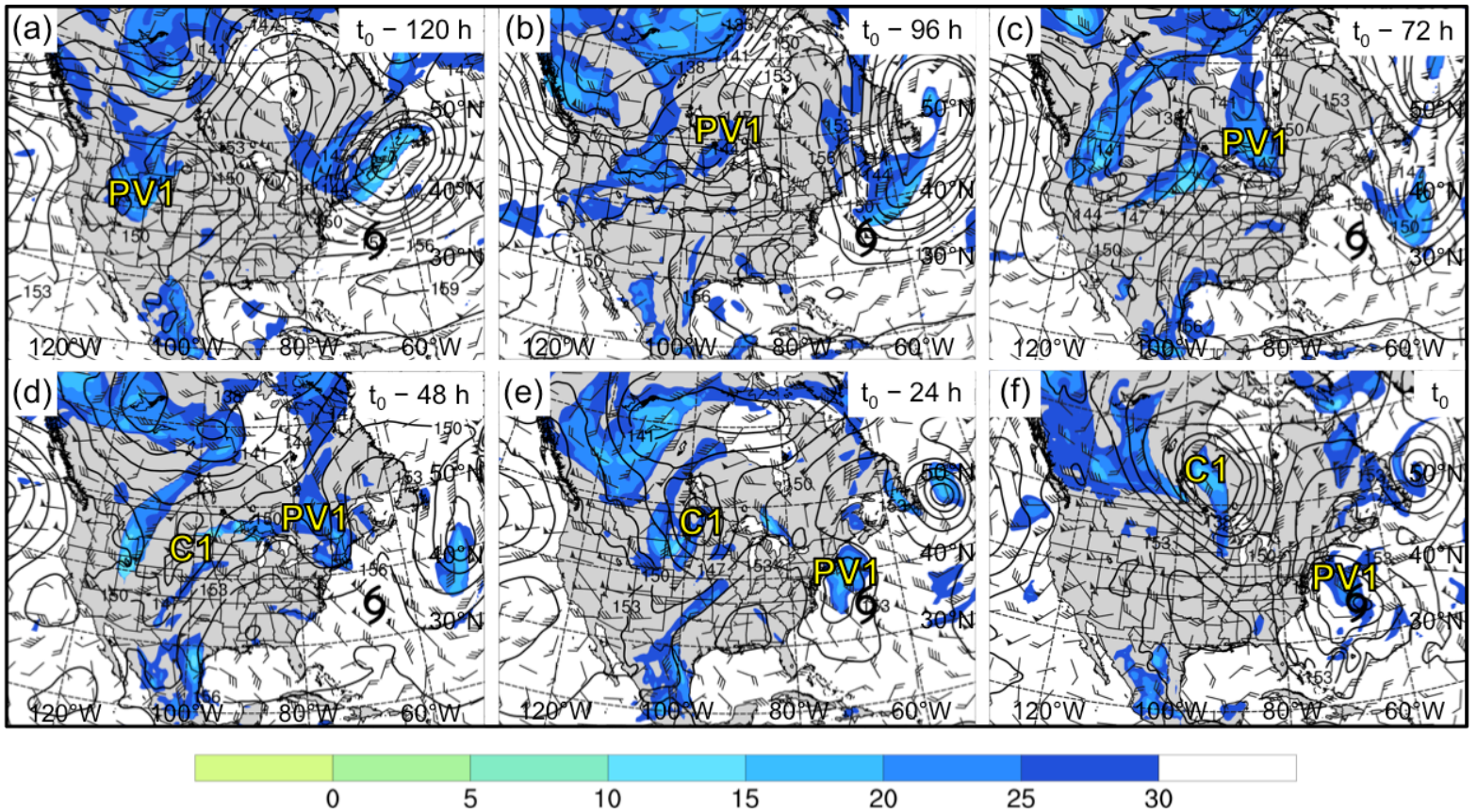

Fig 3.36. Coupling index (shaded, K), 850-hPa geopotential height (black contours, dam), and 850–200-hPa wind shear (barbs, kts) for an STC forming in association with a PV streamer at 1800 UTC 21 August 1980 (t_0). Panels depict the aforementioned features at (a) t_0 – 120 h, (b) t_0 – 96 h, (c) t_0 – 72 h, (d) t_0 – 48 h, (e) t_0 – 24 h, and (f) t_0. The black cyclone symbol in each panel denotes the location of STC formation at t_0. Label "PV1" indicates the position of a region of relatively high upper-tropospheric PV. Label "C1" indicates the position of a surface cyclone.

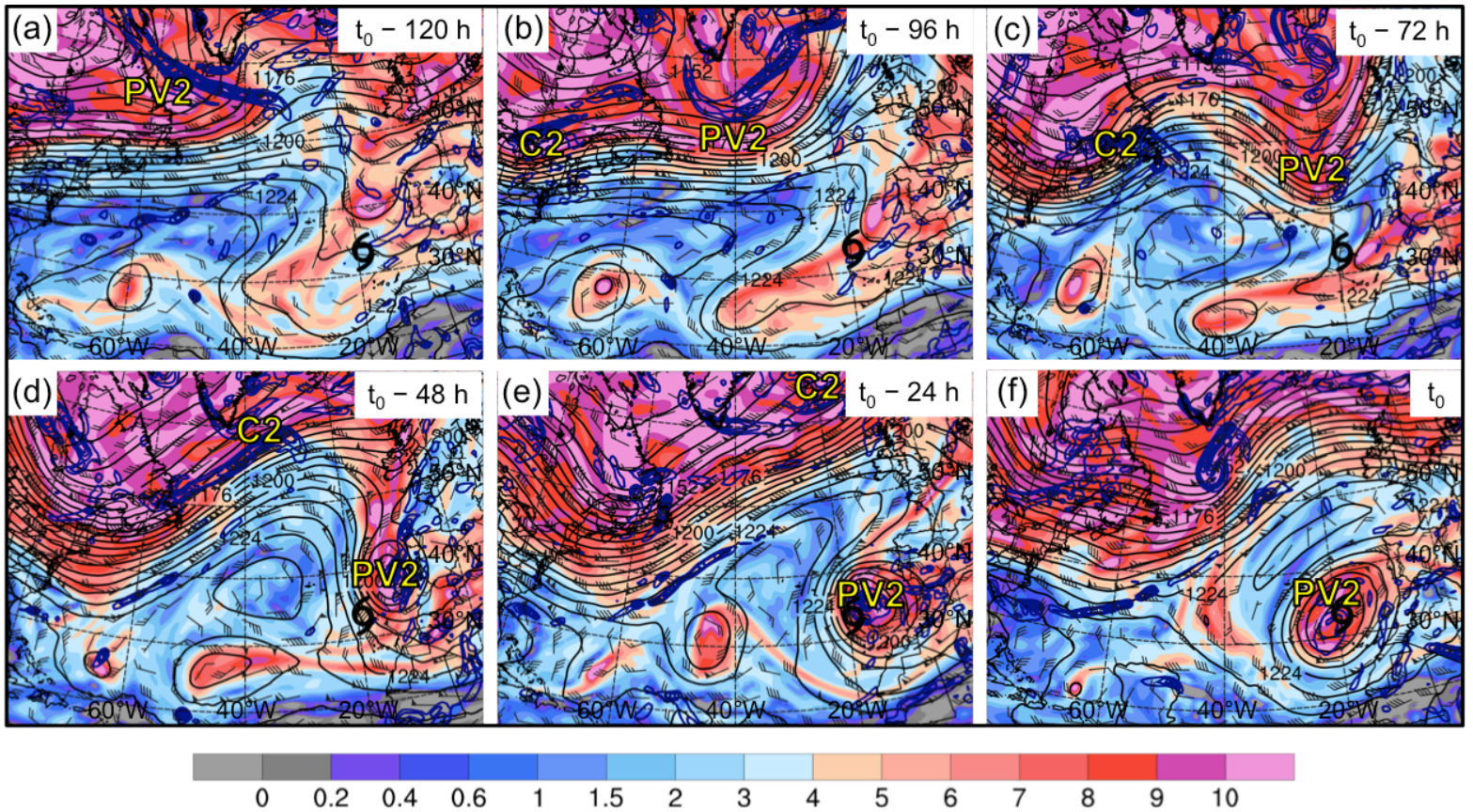

Fig 3.37. As in Fig. 3.32, except for an STC forming in association with a cutoff at 0600 UTC 30 September 1980 (t_0). Label "PV2" indicates the position of a region of relatively high upper-tropospheric PV. Label "C2" indicates the position of a surface cyclone.

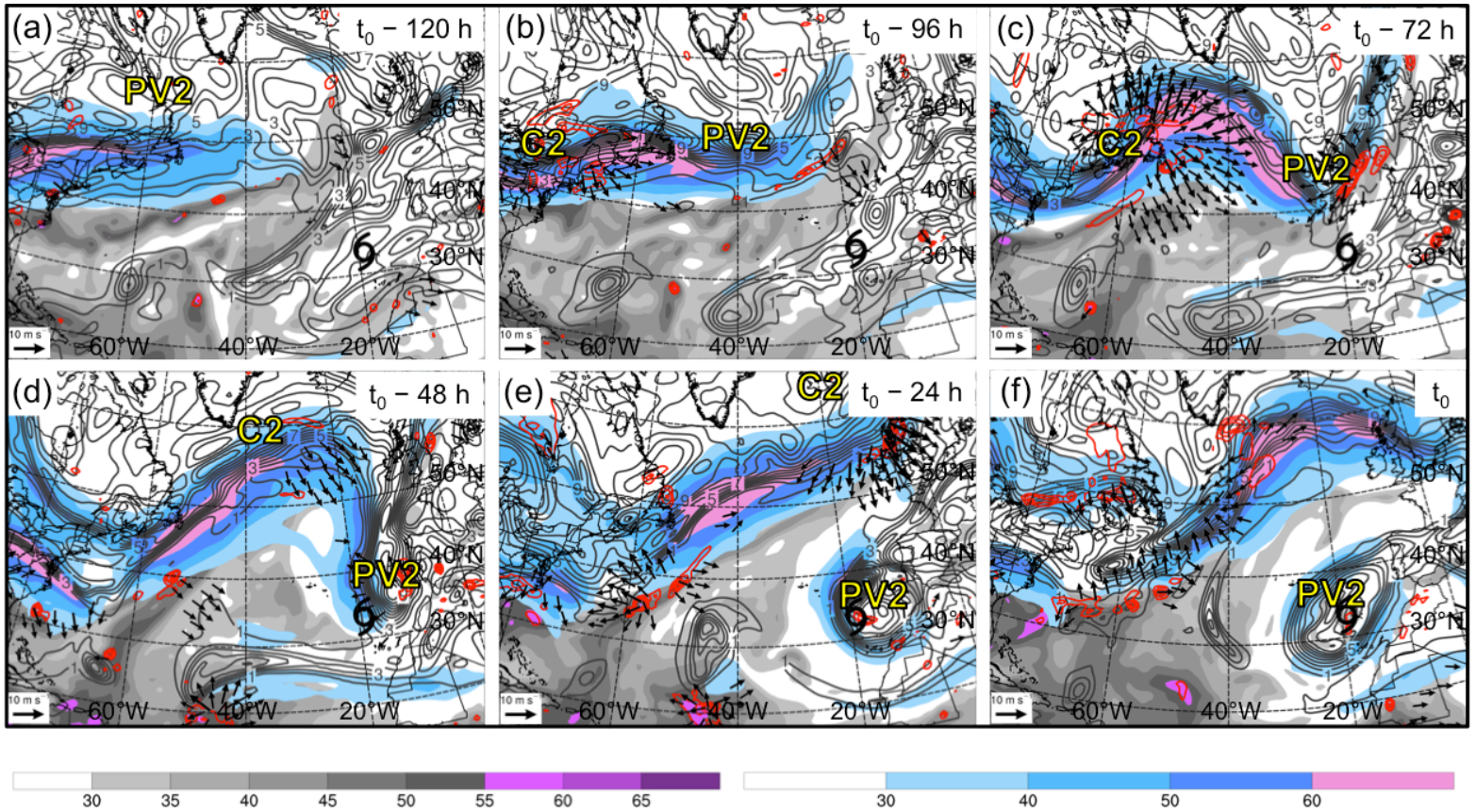

Fig 3.38. As in Fig. 3.33, except for an STC forming in association with a cutoff at 0600 UTC 30 September 1980 (t_0). Label "PV2" indicates the position of a region of relatively high upper-tropospheric PV. Label "C2" indicates the position of a surface cyclone.

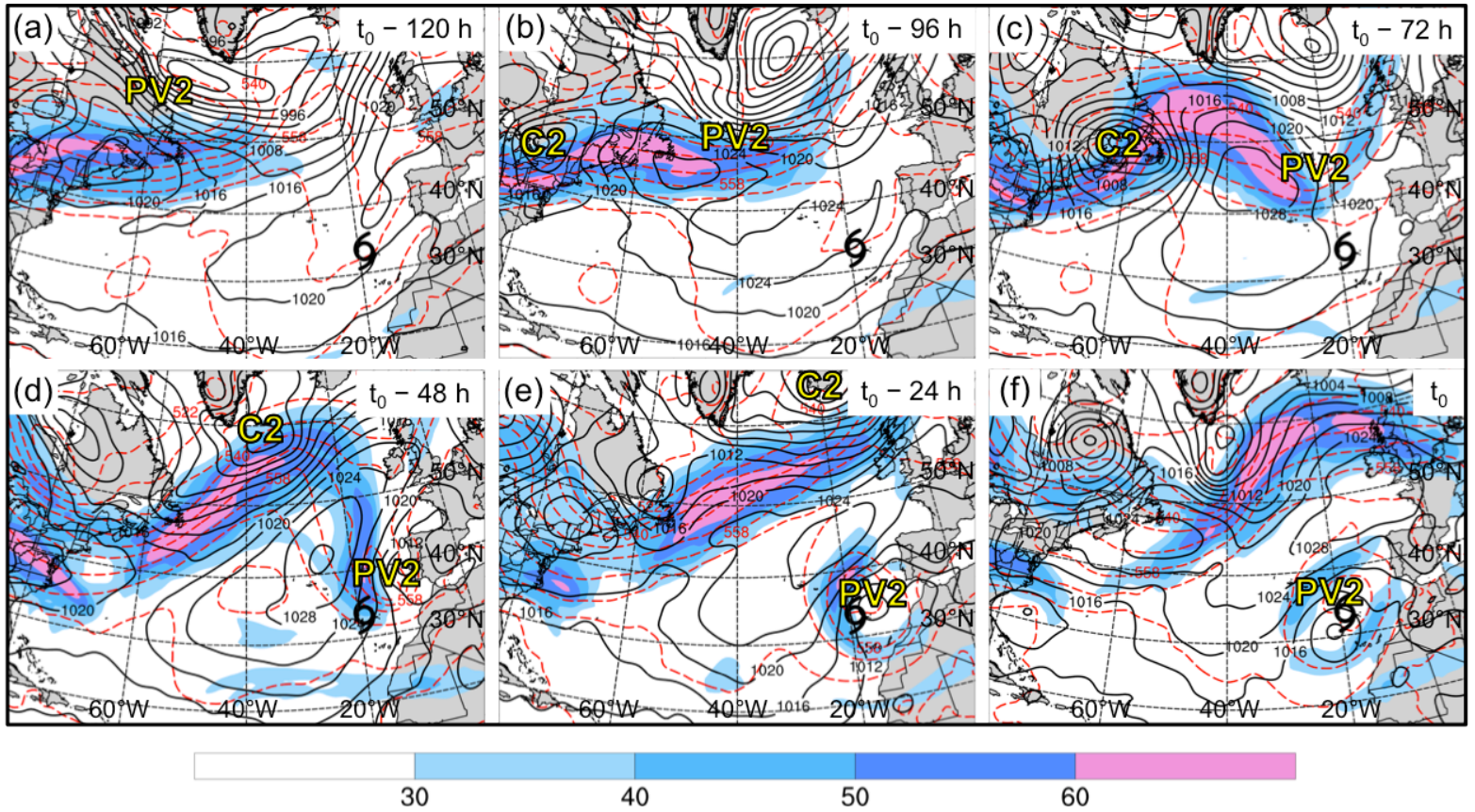

Fig 3.39. As in Fig. 3.34, except for an STC forming in association with a cutoff at 0600 UTC 30 September 1980 (t_0). Label "PV2" indicates the position of a region of relatively high upper-tropospheric PV. Label "C2" indicates the position of a surface cyclone.

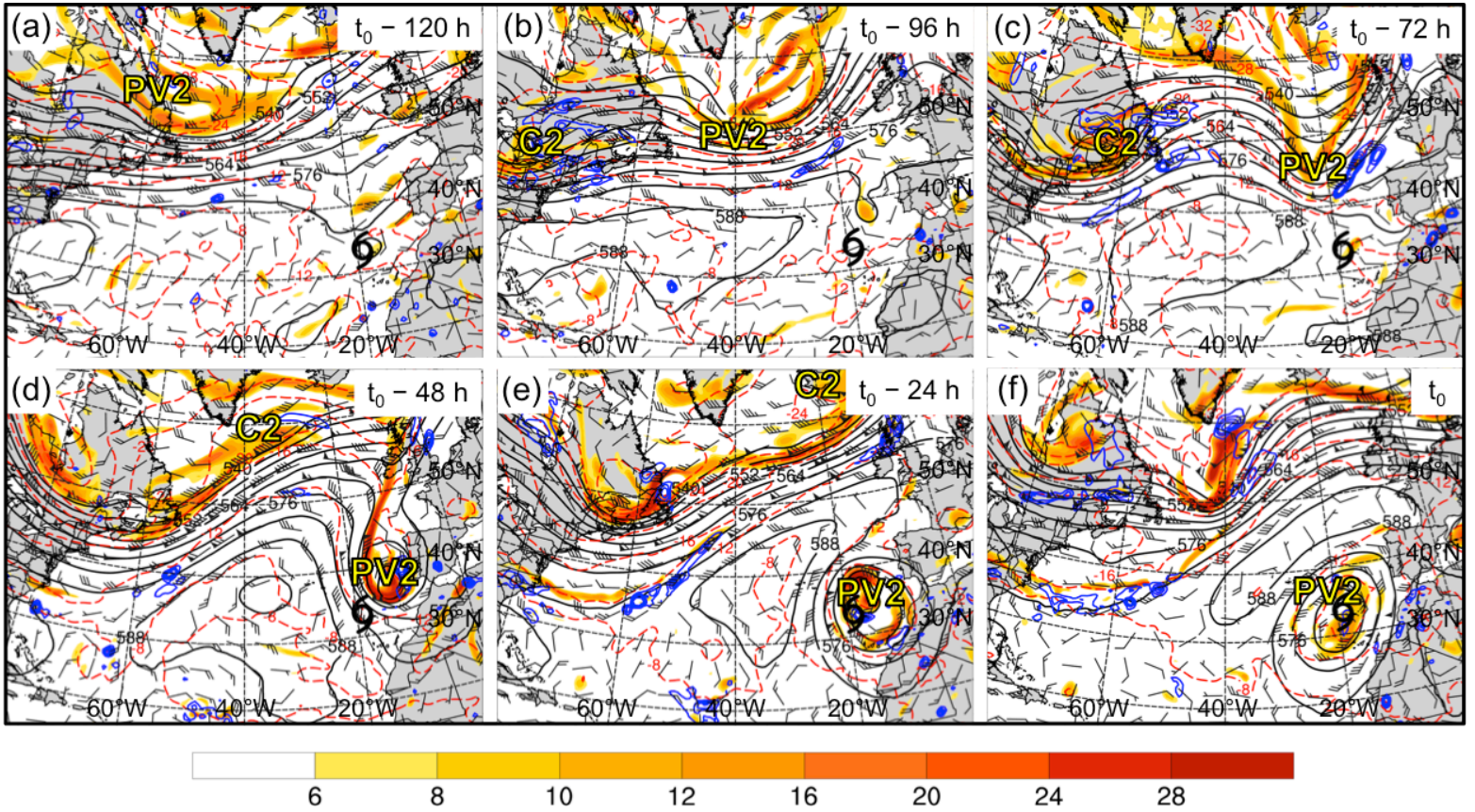

Fig 3.40. As in Fig. 3.35, except for an STC forming in association with a cutoff at 0600 UTC 30 September 1980 (t_0). Label "PV2" indicates the position of a region of relatively high upper-tropospheric PV. Label "C2" indicates the position of a surface cyclone.

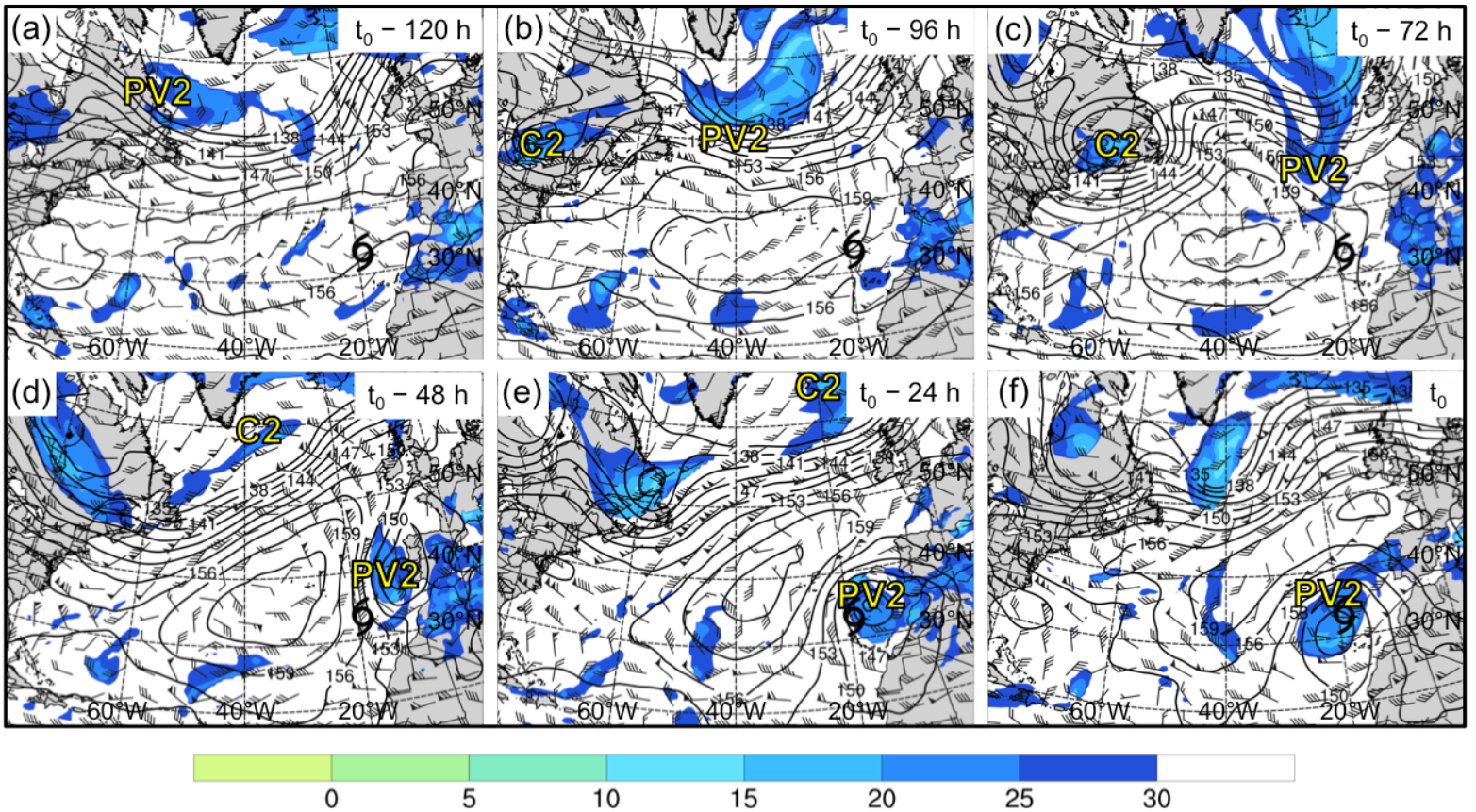

Fig 3.41. As in Fig. 3.36, except for an STC forming in association with a cutoff at 0600 UTC 30 September 1980 (t_0). Label "PV2" indicates the position of a region of relatively high upper-tropospheric PV. Label "C2" indicates the position of a surface cyclone.

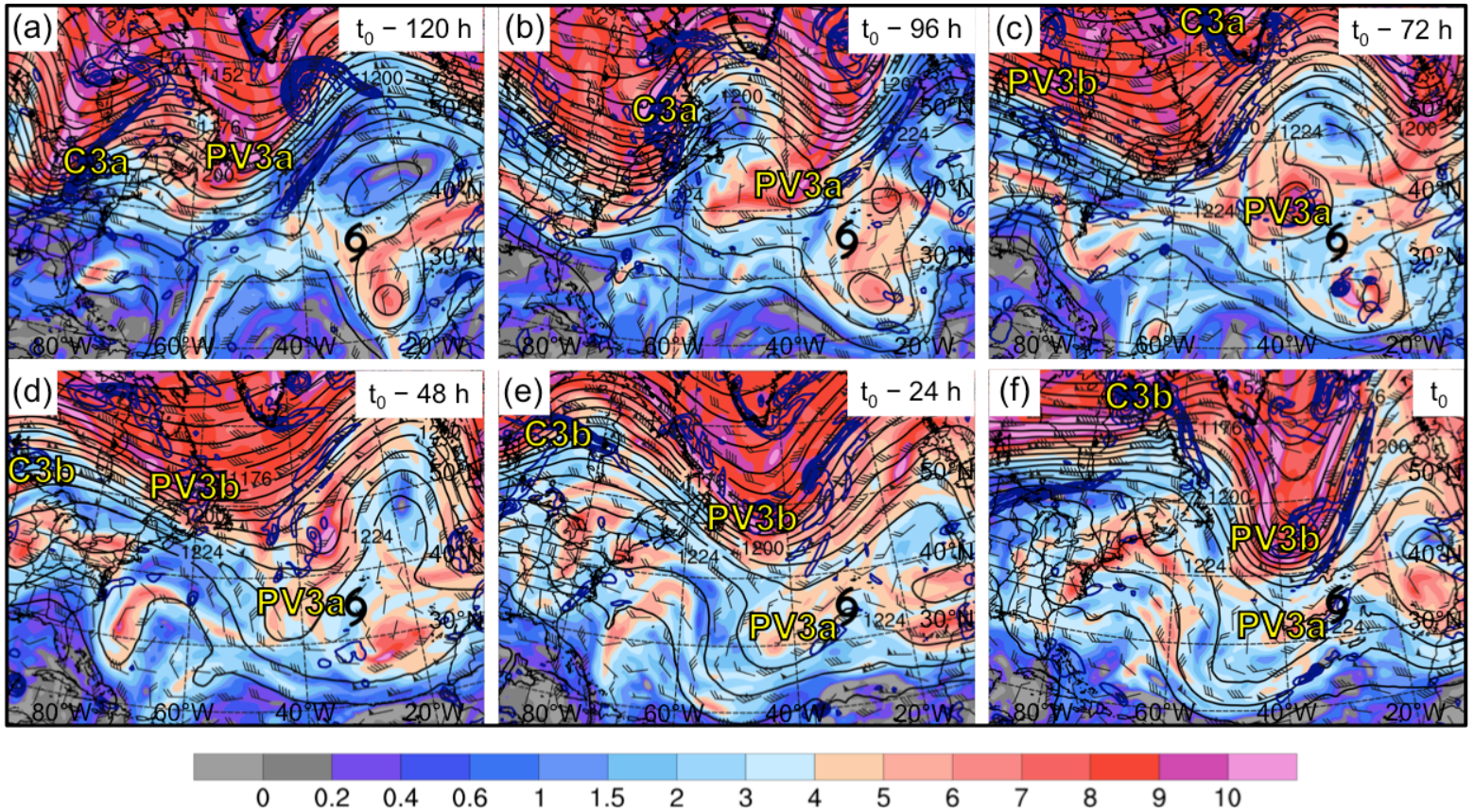

Fig 3.42. As in Fig. 3.32, except for an STC forming in association with a midlatitude trough at 0600 UTC 4 October 2005 (t_0). Labels "PV3a" and "PV3b" indicate the position of regions of relatively high upper-tropospheric PV. Labels "C3a" and "C3b" indicate the position of surface cyclones.

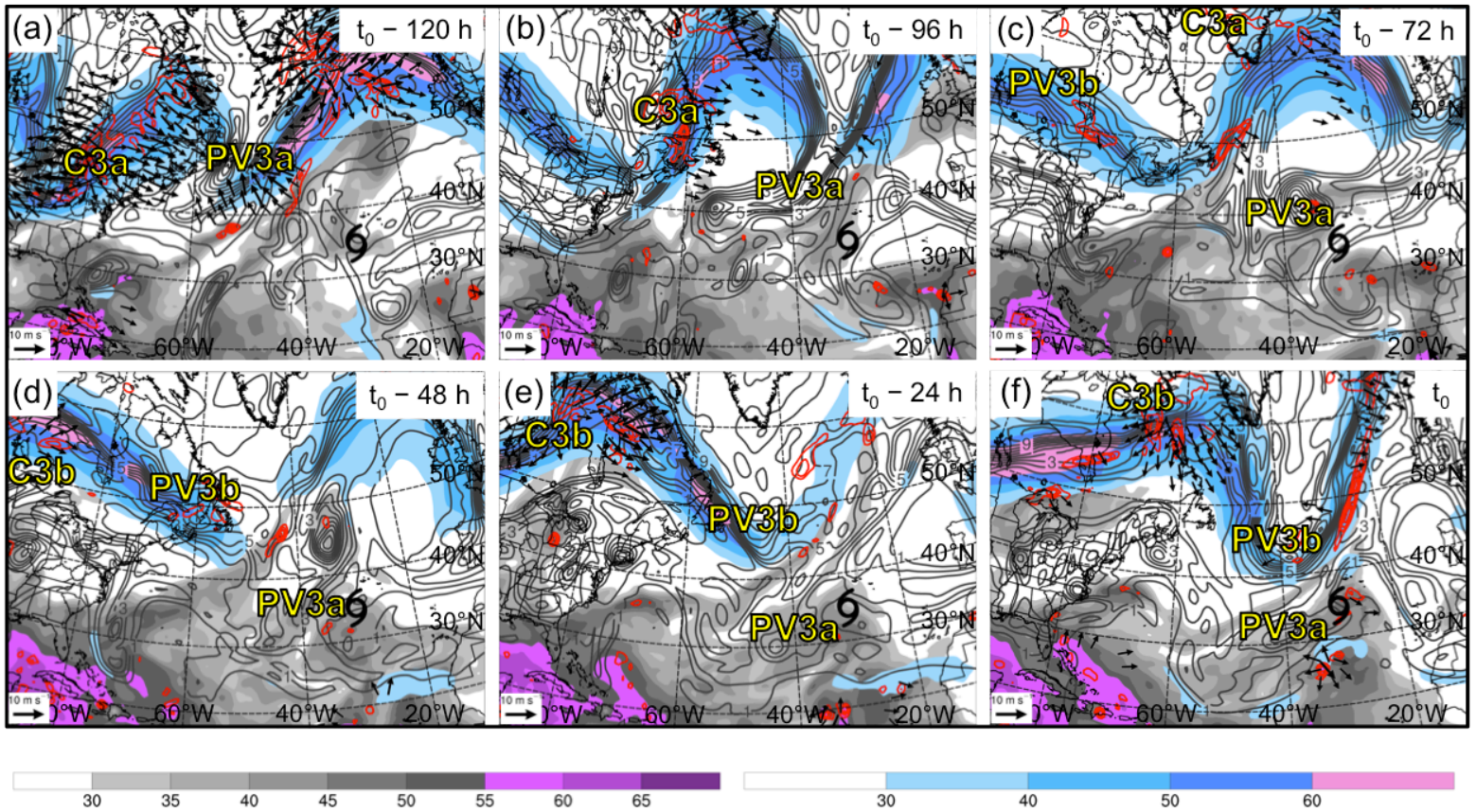

Fig 3.43. As in Fig. 3.33, except for an STC forming in association with a midlatitude trough at 0600 UTC 4 October 2005 (t_0). Labels "PV3a" and "PV3b" indicate the position of regions of relatively high upper-tropospheric PV. Labels "C3a" and "C3b" indicate the position of surface cyclones.

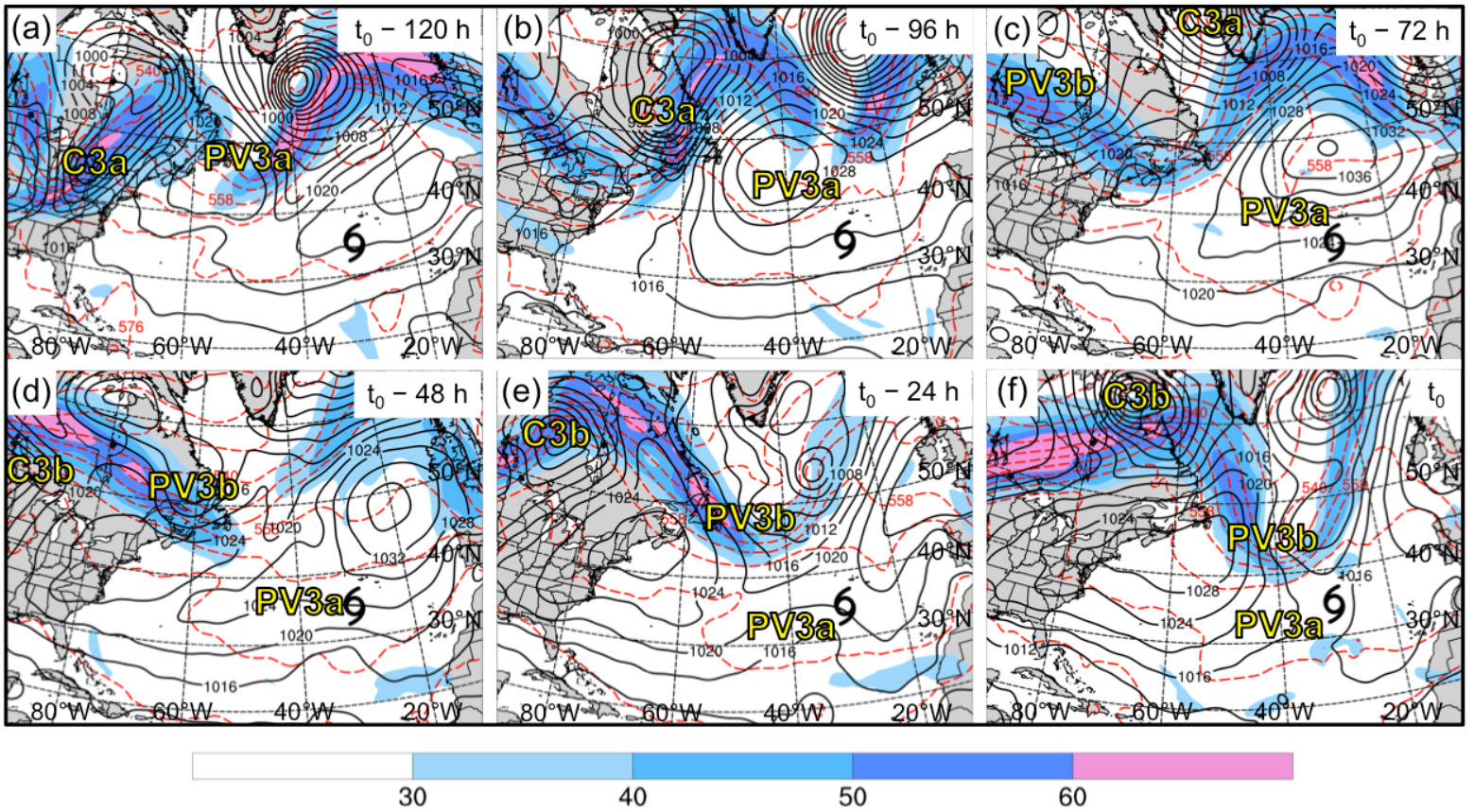

Fig 3.44. As in Fig. 3.34, except for an STC forming in association with a midlatitude trough at 0600 UTC 4 October 2005 (t_0). Labels "PV3a" and "PV3b" indicate the position of regions of relatively high upper-tropospheric PV. Labels "C3a" and "C3b" indicate the position of surface cyclones.

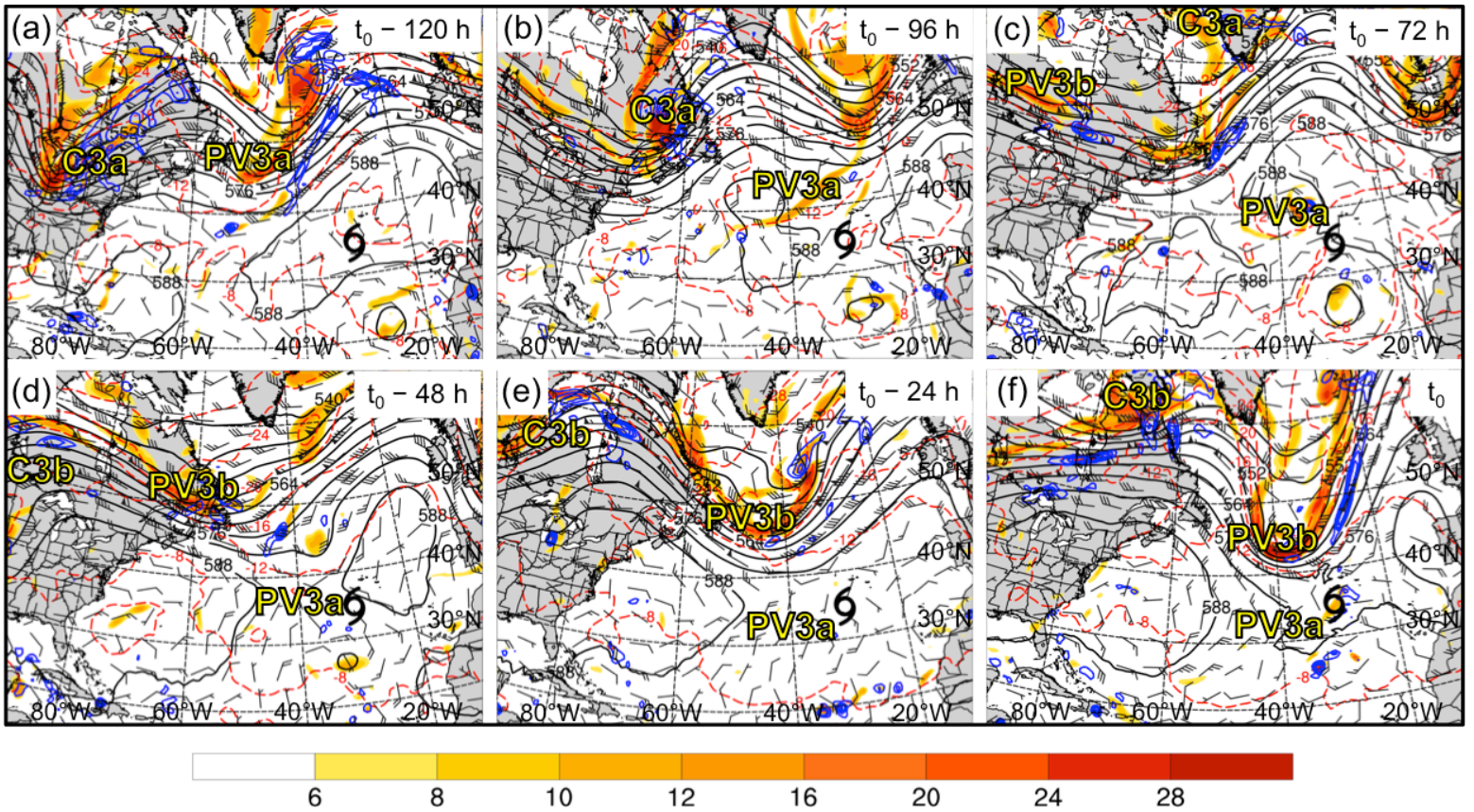

Fig 3.45. As in Fig. 3.35, except for an STC forming in association with a midlatitude trough at 0600 UTC 4 October 2005 (t_0). Labels "PV3a" and "PV3b" indicate the position of regions of relatively high upper-tropospheric PV. Labels "C3a" and "C3b" indicate the position of surface cyclones.

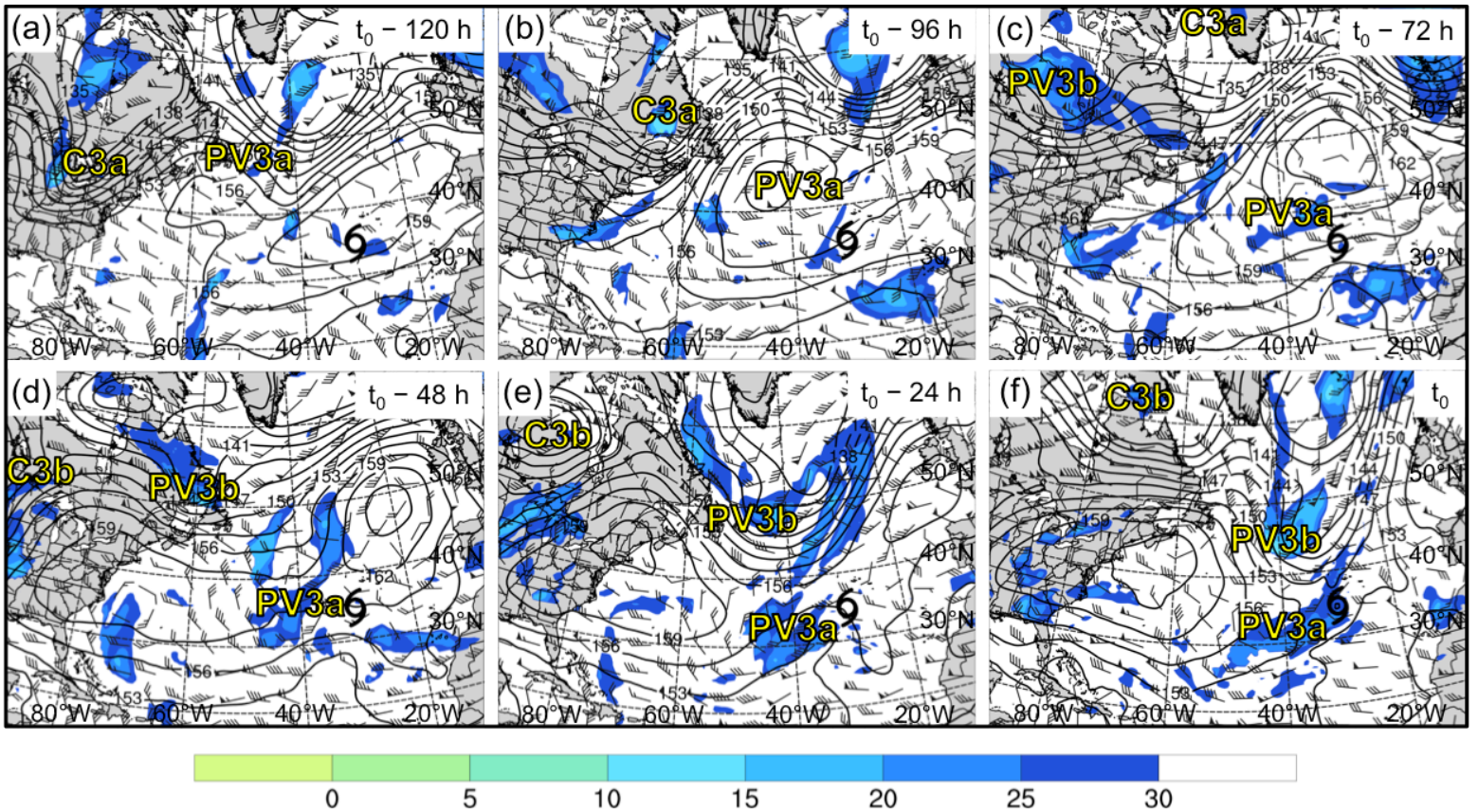

Fig 3.46. As in Fig. 3.36, except for an STC forming in association with a midlatitude trough at 0600 UTC 4 October 2005 (t_0). Labels "PV3a" and "PV3b" indicate the position of regions of relatively high upper-tropospheric PV. Labels "C3a" and "C3b" indicate the position of surface cyclones.

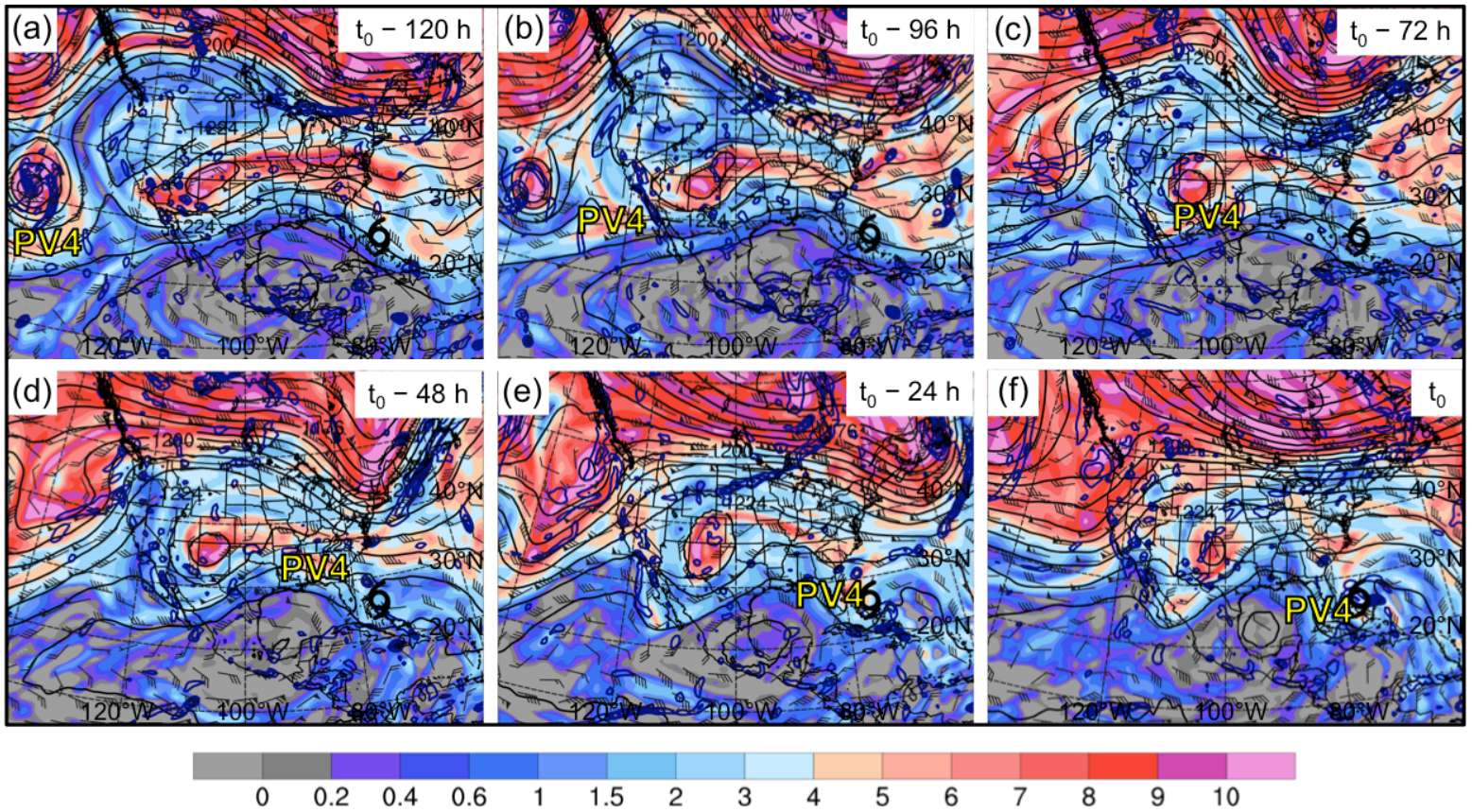

Fig 3.47. As in Fig. 3.32, except for an STC forming in association with a subtropical disturbance at 0000 UTC 5 June 1986 (t_0). Label "PV4" indicates the position of a region of relatively high upper-tropospheric PV.

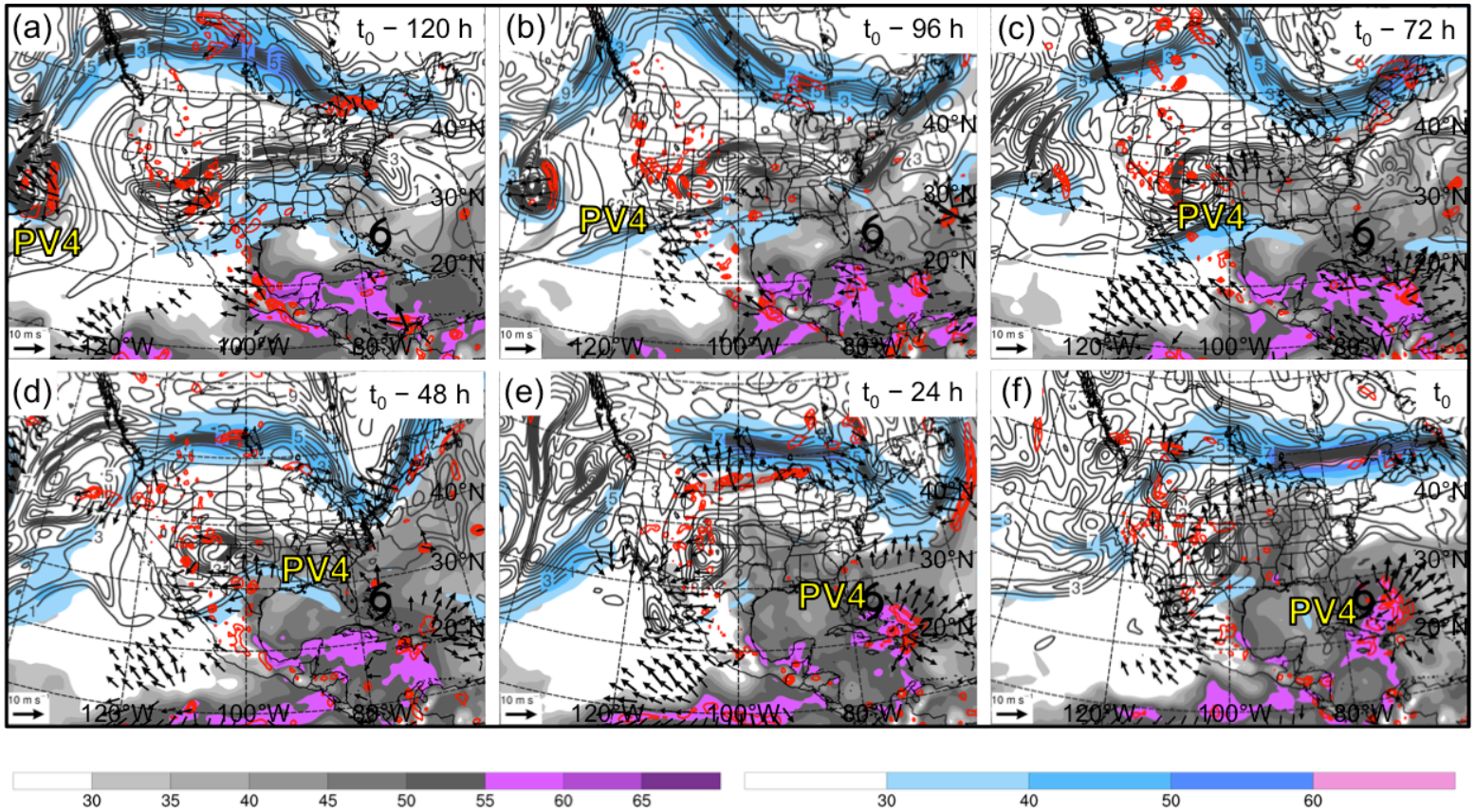

Fig 3.48. As in Fig. 3.33, except for an STC forming in association with a subtropical disturbance at 0000 UTC 5 June 1986 (t_0). Label "PV4" indicates the position of a region of relatively high upper-tropospheric PV.

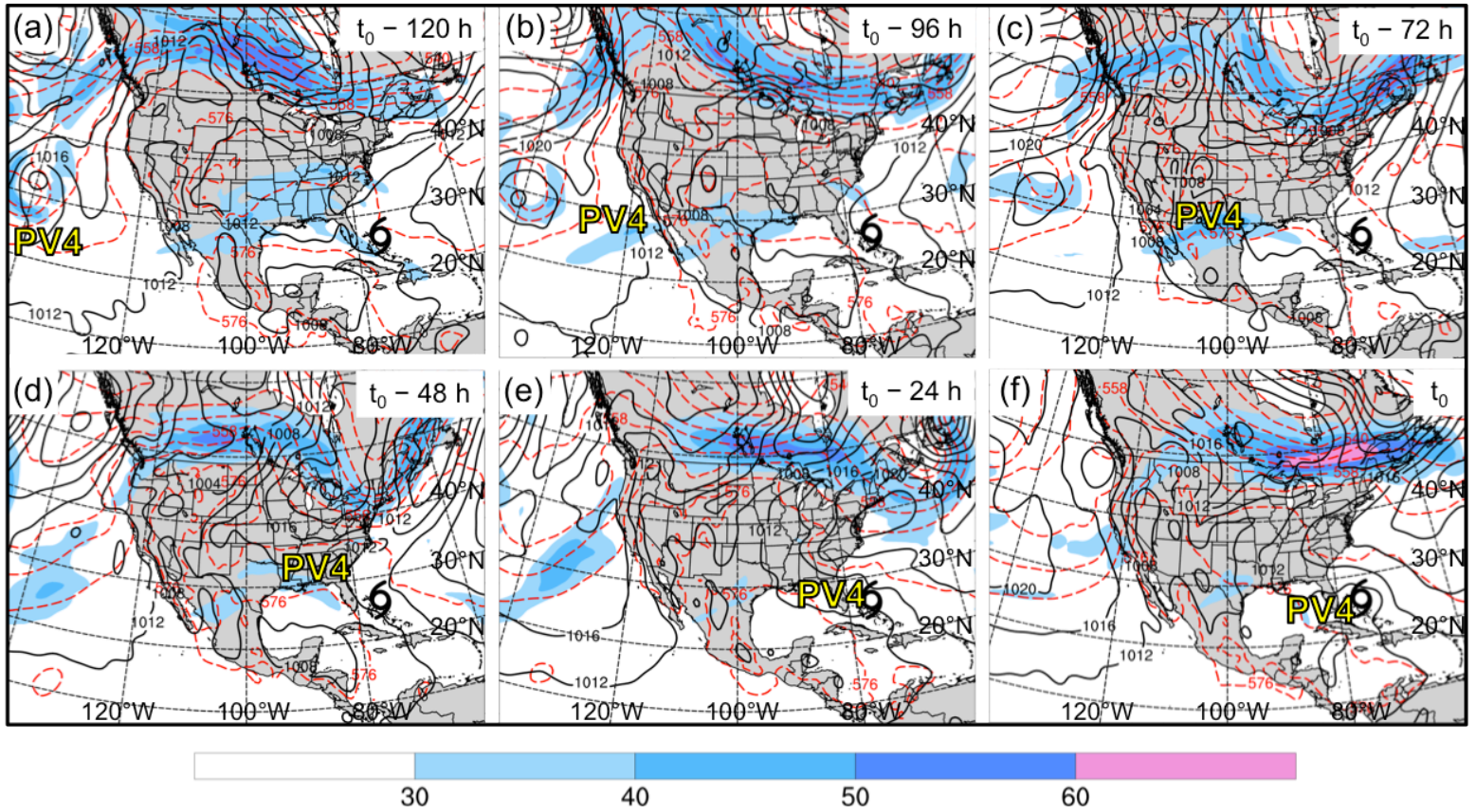

Fig 3.49. As in Fig. 3.34, except for an STC forming in association with a subtropical disturbance at 0000 UTC 5 June 1986 (t_0). Label "PV4" indicates the position of a region of relatively high upper-tropospheric PV.

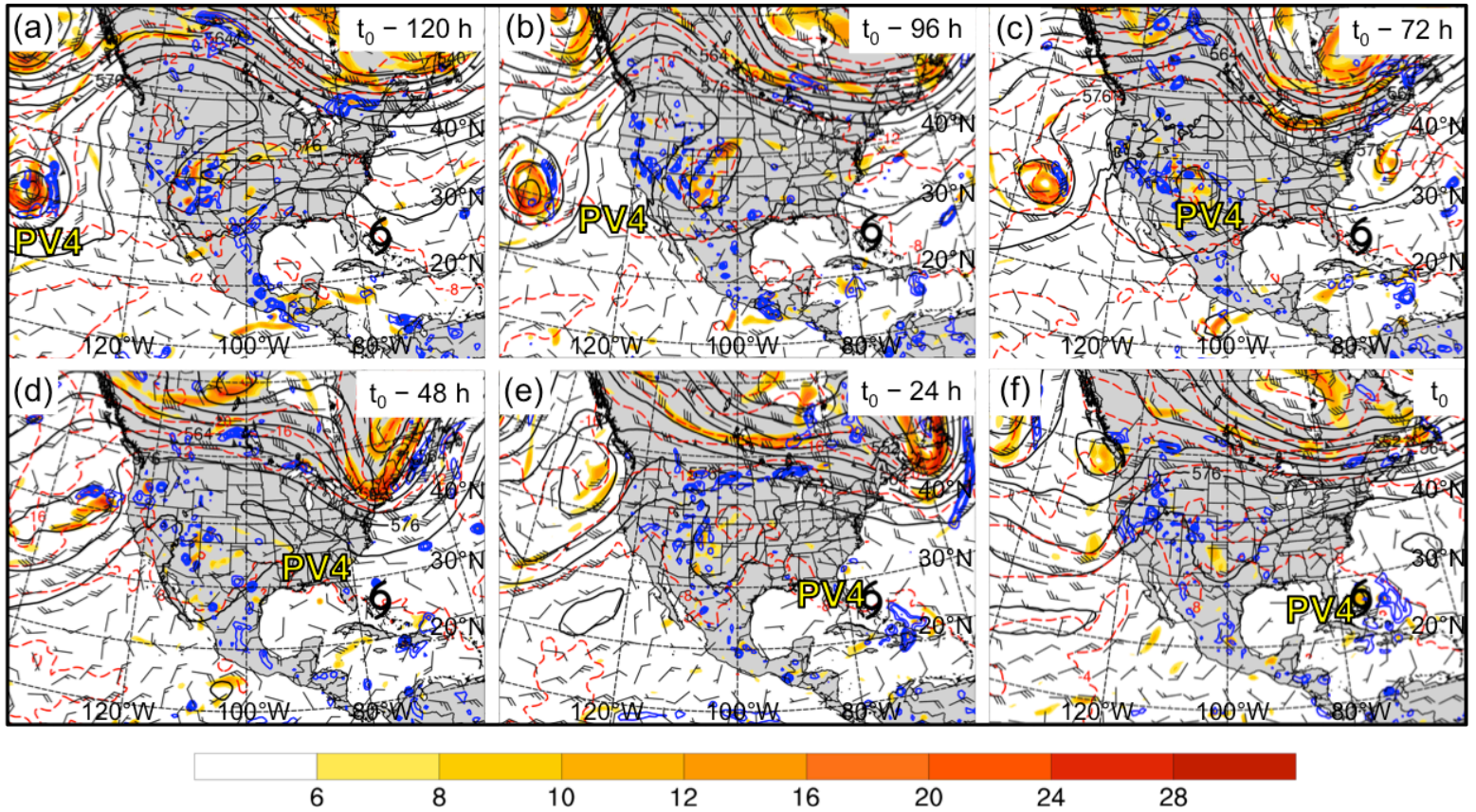

Fig 3.50. As in Fig. 3.35, except for an STC forming in association with a subtropical disturbance at 0000 UTC 5 June 1986 (t_0). Label "PV4" indicates the position of a region of relatively high upper-tropospheric PV.

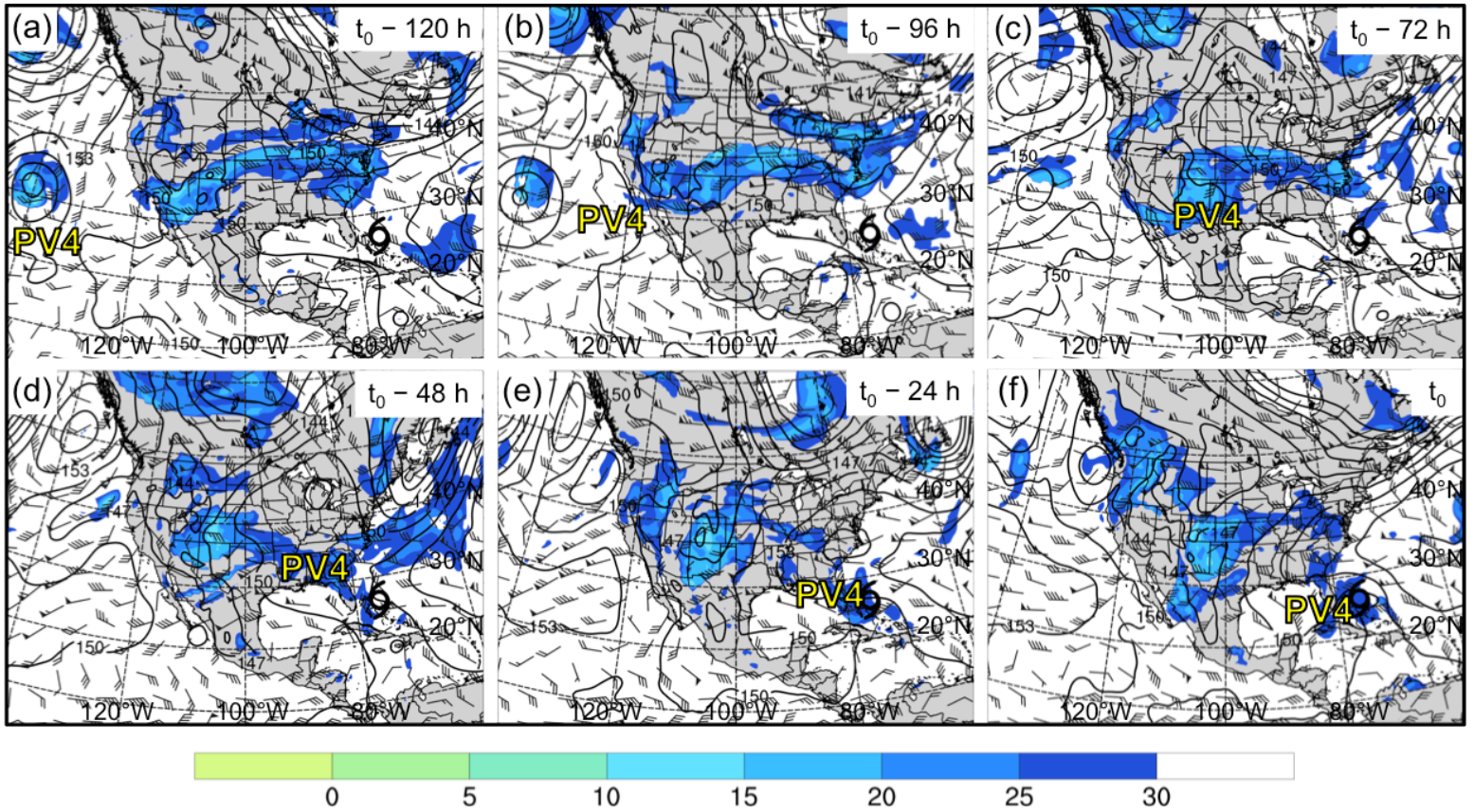

Fig 3.51. As in Fig. 3.36, except for an STC forming in association with a subtropical disturbance at 0000 UTC 5 June 1986 (t_0). Label "PV4" indicates the position of a region of relatively high upper-tropospheric PV.

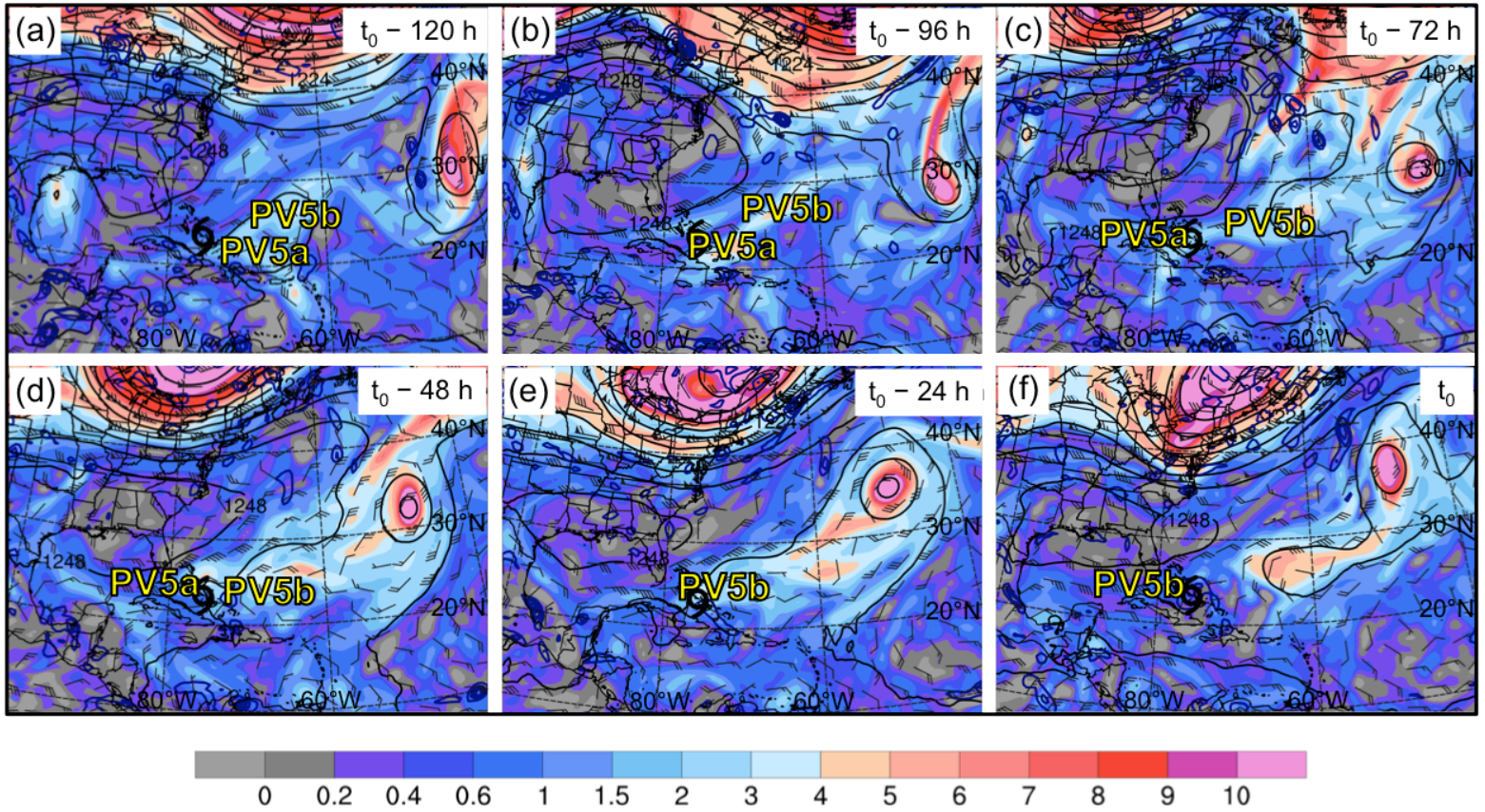

Fig 3.52. As in Fig. 3.32, except for an STC forming in association with PV debris at 0000 UTC 24 August 2005 (t_0). Labels "PV5a" and "PV5b" indicate the position of regions of relatively high upper-tropospheric PV.

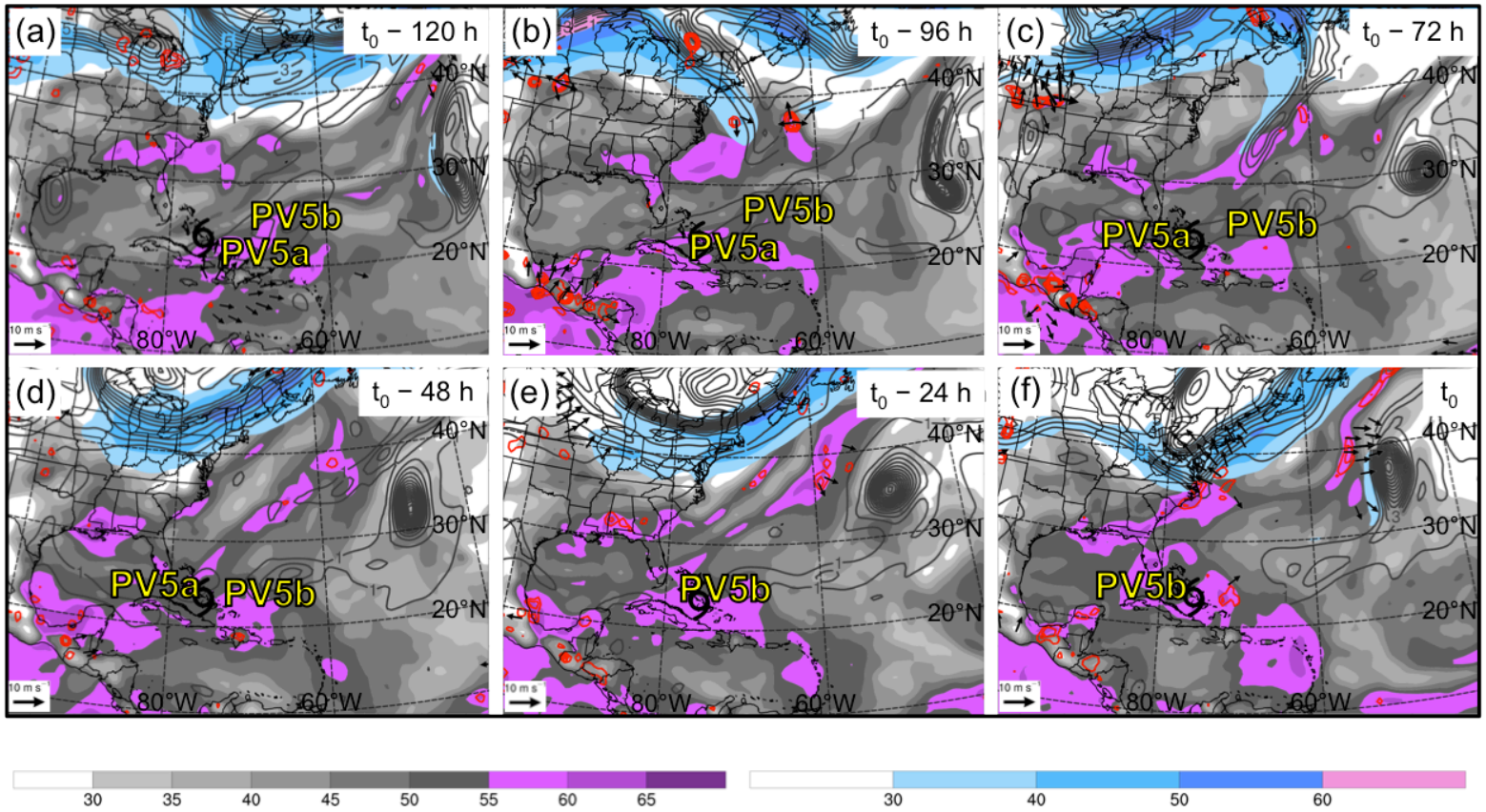

Fig 3.53. As in Fig. 3.33, except for an STC forming in association with PV debris at 0000 UTC 24 August 2005 (t_0). Labels "PV5a" and "PV5b" indicate the position of regions of relatively high upper-tropospheric PV.

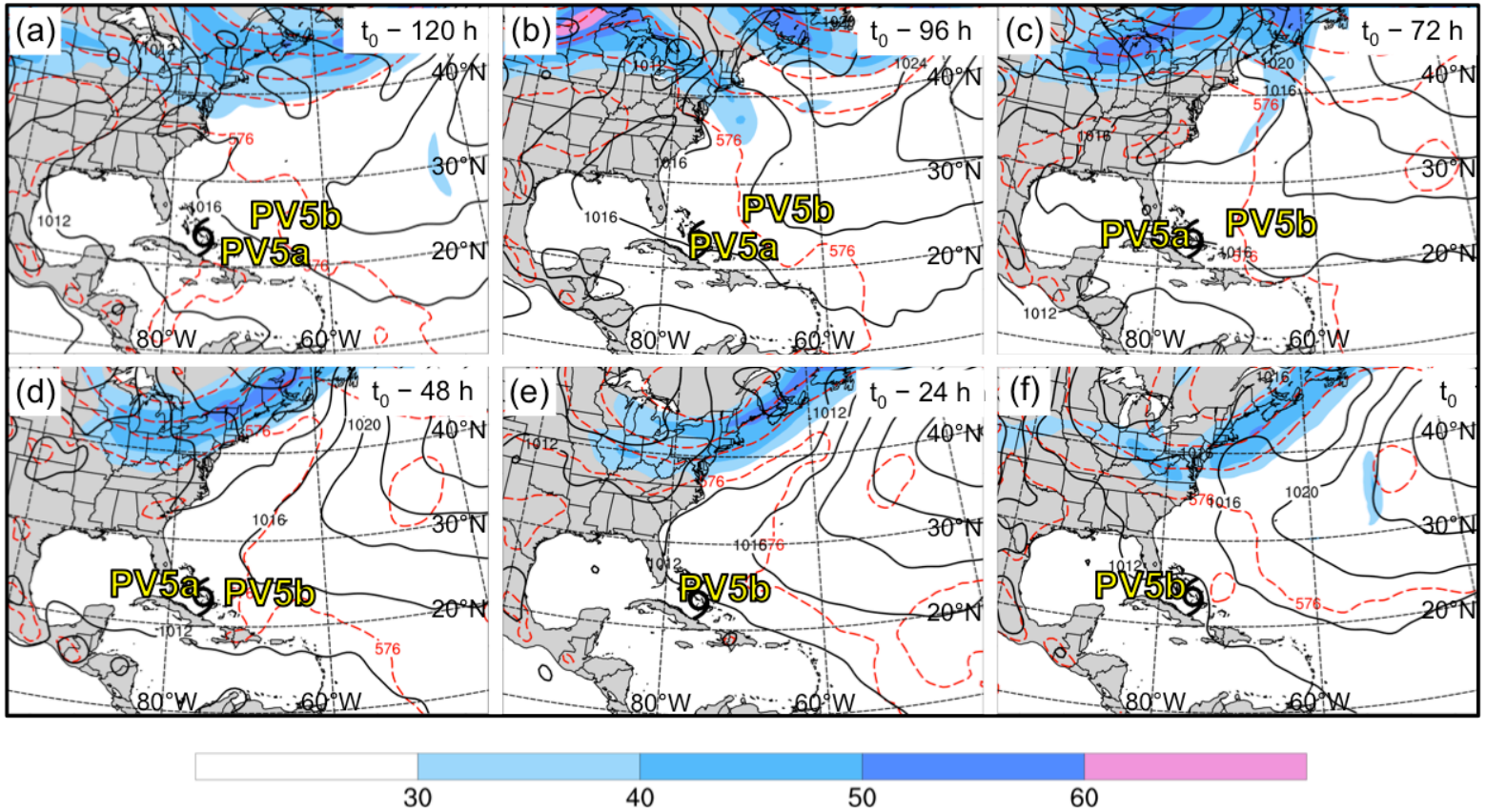

Fig 3.54. As in Fig. 3.34, except for an STC forming in association with PV debris at 0000 UTC 24 August 2005 (t_0). Labels "PV5a" and "PV5b" indicate the position of regions of relatively high upper-tropospheric PV.

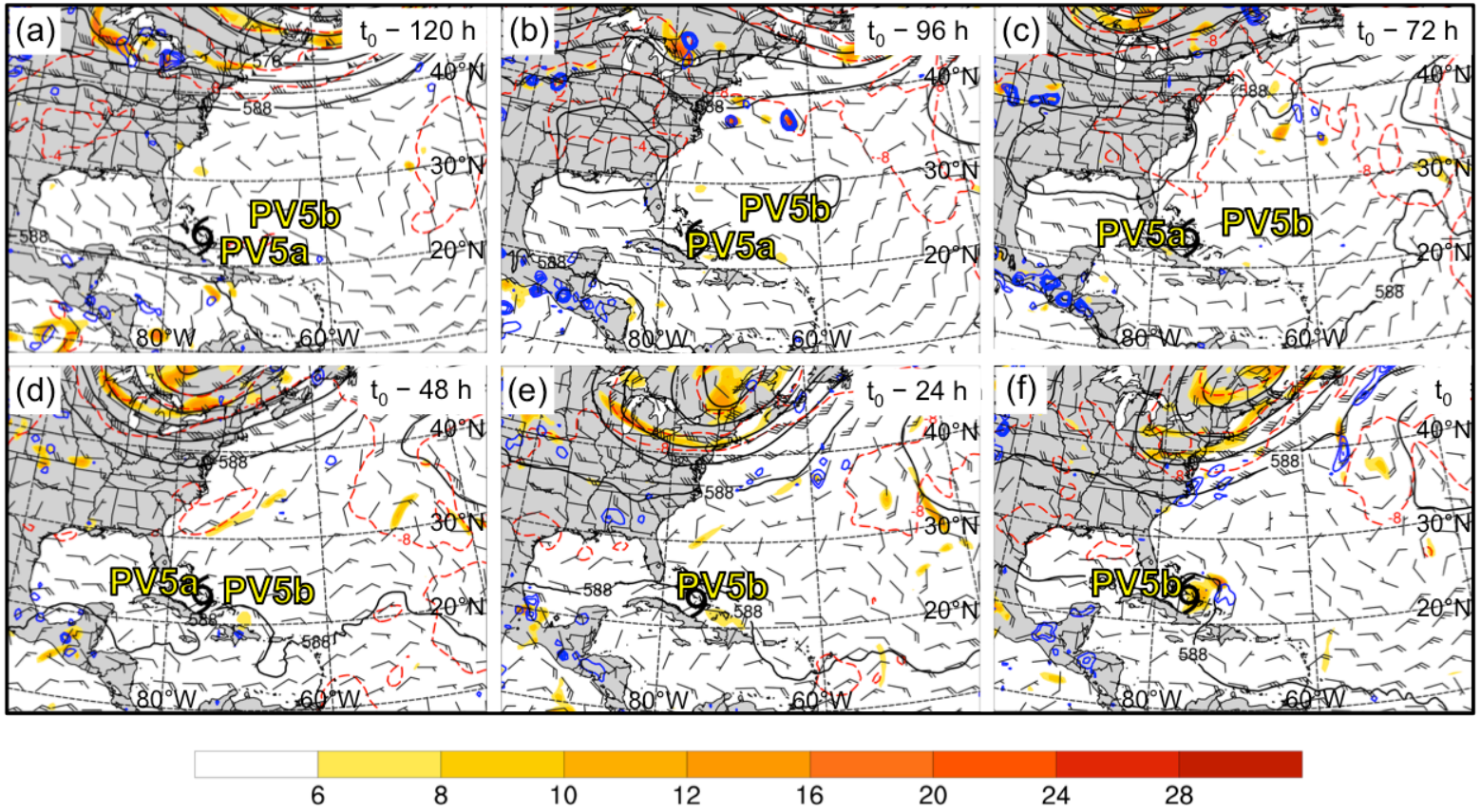

Fig 3.55. As in Fig. 3.35, except for an STC forming in association with PV debris at 0000 UTC 24 August 2005 (t_0). Labels "PV5a" and "PV5b" indicate the position of regions of relatively high upper-tropospheric PV.

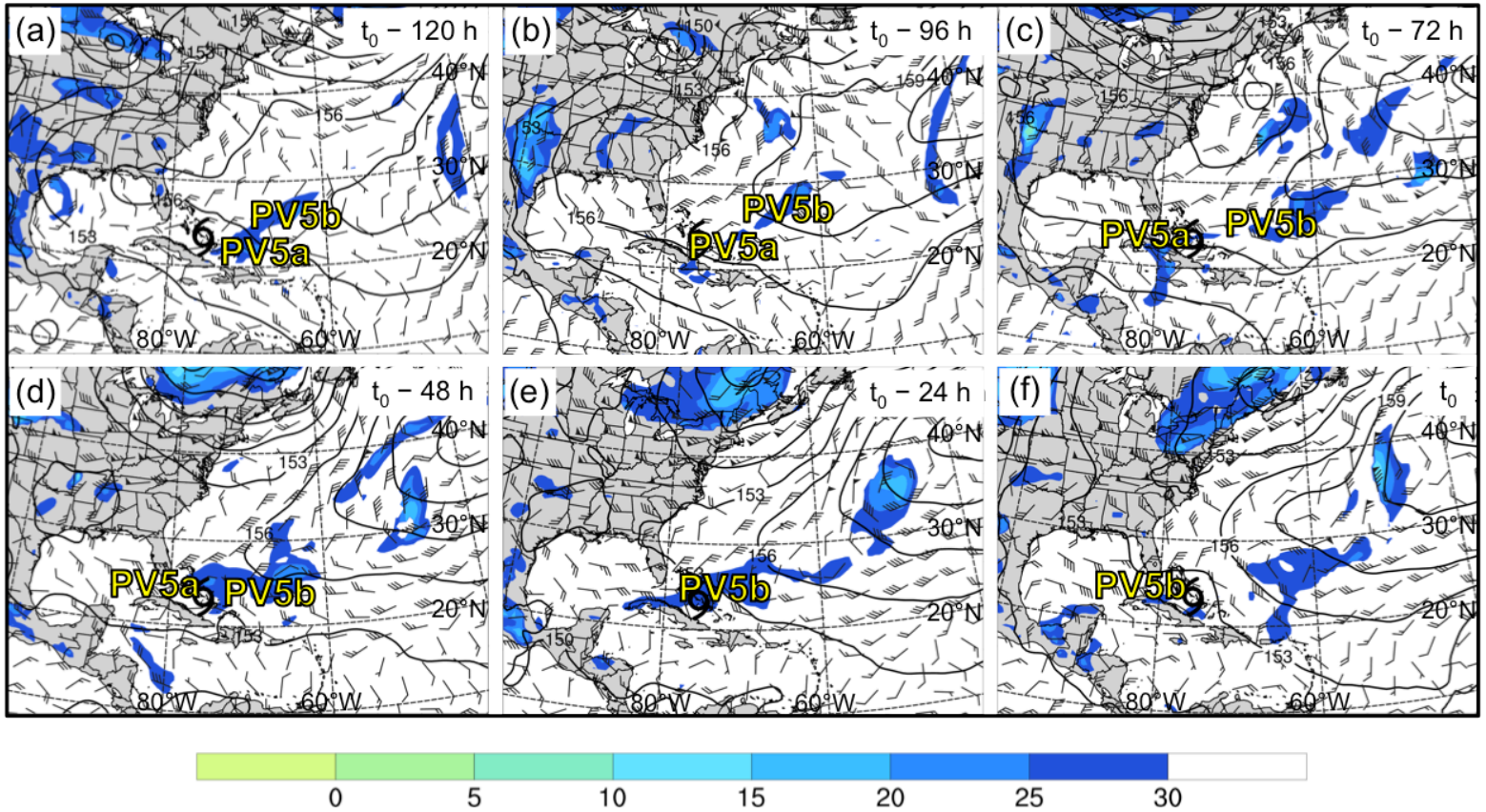

Fig 3.56. As in Fig. 3.36, except for an STC forming in association with PV debris at 0000 UTC 24 August 2005 (t_0). Labels "PV5a" and "PV5b" indicate the position of regions of relatively high upper-tropospheric PV.

4. Discussion, Conclusions, and Suggestions for Future Work

4.1 Discussion

4.1.1 STC Climatology (1979–2010)

Many of the results of the 1979–2010 North Atlantic STC climatology presented in this study complement the results of the 1957–2002 North Atlantic STC climatology presented in Guishard et al. (2009). As mentioned in section 3.1, ~3 STCs are identified per year in the present study—a similar, but not identical, number to the ~4 STCs identified per year in Guishard et al. (2009). This difference in the number of STCs identified per year may be explained by considering the 1) higher resolution reanalysis dataset, 2) smaller number of candidate cyclones, and 3) dynamically rather than structurally based STC identification technique used to construct the North Atlantic STC climatology presented in this study.

The intraseasonal variability associated with the location and frequency of North Atlantic STC formation is similar as well. STCs identified in Guishard et al. (2009) form more frequently over the western North Atlantic than over the eastern North Atlantic (Fig. 1.5), a result that is also found in the present study (Fig. 3.1). STC formation occurs most frequently in September and October in Guishard et al. (2009), with a secondary peak in June (their Fig. 6). The replication of these results in the present study (Fig. 3.3), despite the use of a dynamically rather than a structurally based STC identification technique, suggests that the results of the present study are robust.

4.1.2 STC Clusters

As mentioned in section 2.1, only North Atlantic tropical cyclogenesis cases included in the Strong TT, Weak TT, or Trough induced development pathways identified in McTaggart-Cowan et al. (2013) were selected for potential STC identification. Of the 222 candidate cyclones included in the Strong TT, Weak TT, or Trough induced development pathways, 105 were identified as STCs (34 Strong TT, 56 Weak TT, 15 Trough induced).

Approximately 76% of the STCs included in the Strong TT development pathway form in association with a PV streamer, cutoff, or midlatitude trough (Fig. 4.1a). This result suggests that the Strong TT development pathway identified in McTaggart-Cowan et al. (2013) is primarily comprised of TCs forming in association with a midlatitude disturbance—unsurprising considering the "high" values of **Q** and Th that the Strong TT development pathways requires (Table 1).

Approximately 25% of the STCs included in the Weak TT development pathway form in association with a PV streamer, cutoff, or midlatitude trough (Fig. 4.1b). However, the majority of the STCs included in the Weak TT development pathway (~64%) form in association with a subtropical disturbance or a disorganized region of relatively high upper-tropospheric PV deposited in the subtropics several days prior to STC formation (i.e., PV debris) (Fig. 4.1b). These results suggest that the Weak TT development pathway identified in McTaggart-Cowan et al. (2013) is comprised of TCs forming in association with midlatitude *and* subtropical disturbances and that a variety of upper-tropospheric features can be linked to tropical cyclogenesis within this development pathway.

Approximately 20% of the STCs included in the Trough induced development pathway form in association with a subtropical disturbance (Fig. 4.1c). However, the majority of the STCs included in the Trough induced development pathway (~73%) form in association with PV debris (Fig. 4.1c). These results suggest that the Trough induced development pathway identified in McTaggart-Cowan et al. (2013) is primarily comprised of TCs forming in association with relatively weak disturbances in the subtropics—specifically those that lack appreciable lower-tropospheric thermal gradients (Table 1).

The results stated above suggest that a variety of upper-tropospheric features can be linked to TC formation within each of the development pathways identified in McTaggart-Cowan et al. (2013). STCs included in the Strong TT (Trough induced) development pathway have the most (least) evident midlatitude connection (Figs. 4.1a,c), where as STCs included in the Weak TT development pathway form in association with a combination of midlatitude and subtropical disturbances (Fig. 4.1b). These findings suggest that the subjectively constructed clusters discussed in section 3.2 accurately represent the spectrum of the most common upper-tropospheric features linked to STC formation and substantiate the results of the present study.

4.1.3 Composite Analysis

McTaggart-Cowan et al. (2013) suggested that their global climatology of baroclinically influenced tropical cyclogenesis events could "serve as a baseline for future composites and process studies that enhance our understanding of the role of

baroclinic influences on TC formation**...**." The cyclone-relative composite analysis presented in this study is a natural extension of McTaggart-Cowan et al. (2013), performed on subjectively constructed clusters of STCs that represent the most common upper-tropospheric features linked to STC formation.

As mentioned in section 3.3, some of the cyclone-relative composites presented in this study have similarities to each other. STCs forming in association with PV streamers and cutoffs have a well-defined midlatitude connection, developing near a region of relatively high upper-tropospheric PV injected into the subtropics during an upstream AWB event. However, Figs. 3.7d–f reveal that STCs forming in association with PV streamers develop ~48 h earlier during upstream AWB events than STCs forming in association with cutoffs (Figs. 3.12b–f). STCs forming in association with midlatitude troughs also have a well-defined midlatitude connection (Fig. 3.17f), but do not develop as a result of upstream AWB.

Unlike STCs included in the first three clusters, STCs forming in association with subtropical disturbances do not have a well-defined midlatitude connection (Fig. 3.22f). As mentioned in section 3.3.4, the progressive PV filament associated with subtropical disturbances is considerably smaller in meridional extent than the upper-tropospheric disturbances associated with PV streamers, cutoffs, or midlatitude troughs. This difference in meridional extent causes the cyclone-relative composites associated with subtropical disturbances to be less distinct than those associated with PV streamers, cutoffs, or midlatitude troughs.

STCs forming in association with a disorganized region of relatively high upper-tropospheric PV deposited in the subtropics several days prior to STC formation (i.e., PV

debris) do not have a well-defined midlatitude connection (Fig. 3.27f). Much like subtropical disturbances, the disorganized nature of PV debris results in less distinct cyclone-relative composites than those associated with PV streamers, cutoffs, or midlatitude troughs.

Although not discussed in section 3.3.5, the author speculates that the disorganized regions of PV debris associated with STC formation may have been injected into the subtropics prior to t_0 – 120 h during an upstream AWB event (not shown). If true, the cyclone-relative composites presented in this study would suggest that STC formation can occur during the *initial stages* of, *latter stages* of, and *following* an upstream AWB event.

4.1.4 Case Studies

The upper-tropospheric features linked to STC formation in the PV Streamer case study closely resemble those in the PV Streamer cluster composite. Rapid ridge amplification begins upstream of the location of STC formation at t_0 – 48 h in the case study (Fig. 3.32d) and composite (Fig. 3.7d), in the warm sector of a surface cyclone (Fig. 3.34d and Fig. 3.9d, respectively). Negative PV advection by the 300–200-hPa layer-averaged irrotational wind contributes to rapid ridge amplification between t_0 – 48 h and t_0 – 24 h in the case study (Figs. 3.33d,e) and composite (Figs. 3.8d,e), slows the eastward progression of the ridge, and enhances northwesterly flow downstream of the ridge axis.

Enhanced northwesterly flow downstream of the ridge axis leads to the formation and amplification of an upper-tropospheric trough over the western North Atlantic between t_0 – 48 h and t_0 – 24 h in the case study (Figs. 3.32d,e) and composite (Figs. 3.7d,e). Persistent upstream ridge amplification and enhanced northerly flow over eastern North America between t_0 – 24 h and t_0 in the case study (Figs. 3.32e,f) and composite (Figs. 3.7e,f) leads to the stretching and thinning of the upper-tropospheric trough into the PV streamer linked to STC formation. Relatively cold upper-tropospheric air, manifested as lower 200-hPa geopotential heights in the case study (Figs. 3.32e,f) and composite (Figs. 3.7e,f), accompanies the PV streamer into the subtropics and decreases the value of the coupling index over the location of STC formation in the case study (Figs. 3.36e,f) and composite (Figs. 3.11e,f) between t_0 – 24 h and t_0.

Many of the upper-tropospheric features linked to STC formation in the Cutoff case study resemble those in the Cutoff cluster composite. Rapid ridge amplification begins upstream of the location of STC formation at t_0 – 96 h in the case study (Fig. 3.37b) and composite (Fig. 3.12b), in the warm sector of a surface cyclone (Fig. 3.39b and Fig. 3.14b, respectively). Negative PV advection by the 300–200-hPa layer-averaged irrotational wind contributes to rapid ridge amplification between t_0 – 96 h and t_0 – 48 h in the case study (Figs. 3.38b–d)—a process that is considerably less pronounced in the corresponding composite (Figs. 3.13b–d).

Enhanced northwesterly flow downstream of the ridge axis contributes to the formation and amplification of an upper-tropospheric trough downstream between t_0 – 96 h and t_0 – 72 h in the case study (Figs. 3.12b,c) and composite (Figs. 3.37b,c) and the stretching and thinning of that trough into a PV streamer between t_0 – 72 h and t_0 – 48 h

(Figs. 3.12c,d and Figs. 3.37c,d, respectively). Persistent ridge amplification leads to AWB and the cutting off of a region of relatively high upper-tropospheric PV in the subtropics between t_0 – 24 h and t_0 in the case study (Figs. 3.37e,f) and composite (Figs. 3.12e,f). Relatively cold upper-tropospheric air, manifested as lower 200-hPa geopotential heights in the case study (Figs. 3.37e,f) and composite (Figs. 3.12e,f), accompanies this region of relatively high upper-tropospheric PV into the subtropics and decreases the value of the coupling index over the location of STC formation in the case study (Figs. 3.41e,f) and composite (Figs. 3.16e,f) between t_0 – 24 h and t_0.

The upper-tropospheric features linked to STC formation in the Midlatitude Trough case study bear some resemblance to those in the Midlatitude Trough cluster composite. A precursor disturbance in the upper troposphere preconditions the region surrounding the location of STC formation for the development of deep convection in the case study (Figs. 3.42b,c) and composite (Figs. 3.17b,c) between t_0 – 96 h and t_0 – 72 h. The midlatitude origin of this precursor disturbance, attributed to upstream AWB, is easily identifiable in the case study (Figs. 3.42b,c), but is considerably less evident in the composite (Figs. 3.17b,c). The muddled nature of the precursor disturbance in the composite (Figs. 3.17b,c) suggests that precursor disturbances included in the composite may be 1) injected into the subtropics at different times or 2) oriented in different directions when injected into the subtropics.

Relatively high PW values move poleward downstream of the upper-tropospheric disturbance between t_0 – 48 h and t_0 – 24 h, helping to precondition the region surrounding the location of STC formation for the development of deep convection in the case study (Figs. 3.43d,e) and composite (Figs. 3.18d,e). A broad midlatitude trough

begins to develop upstream of the precursor disturbance between t_0 – 48 h and t_0 – 24 h in the case study (Figs. 3.42d,e) and composite (Figs. 3.17d,e) in response to rapid ridge amplification over eastern North America in the warm sector of a surface cyclone (Figs. 3.44d,e and Figs. 3.19d,e, respectively). Persistent ridge amplification enhances northwesterly flow downstream of the ridge axis between t_0 – 24 h and t_0 in the case study (Figs. 3.42e,f) and composite (Figs. 3.17e,f), leading to the deepening of the broad midlatitude trough as it approaches the location of STC formation. This broad midlatitude trough contributes to the organization of deep convection over the location of STC formation in the case study (Figs. 3.43e,f) and composite (Figs. 3.18e,f) between t_0 – 24 h and t_0.

The upper-tropospheric features linked to STC formation in the Subtropical Disturbance case study bear little resemblance to those in the Subtropical Disturbance cluster composite prior to t_0 – 48 h. Although the progression of a small-scale PV filament around the northern edge of a subtropical anticyclone is detectable in the Subtropical Disturbance case study beginning at t_0 – 120 h (Fig. 3.47a), varying translation speeds of the small-scale PV filament cause it to be undetectable in the composite mean until t_0 – 48 h (Fig. 3.22d). The small-scale PV filament progresses southeastward on the northeastern edge of a subtropical anticyclone between t_0 – 48 h and t_0 in the case study (Figs. 3.42d–f) and composite (Figs. 3.22d–f) in response to northwesterly winds on the 350 K isentropic surface. Relatively high PW values move poleward downstream of the small-scale PV filament between t_0 – 48 h and t_0 – 24 h in the case study (Figs. 3.43d,e) and composite (Figs. 3.23d,e), making the region surrounding the location of STC formation favorable for the development of deep

convection. Deep convection, represented by a region of divergent outflow in the 300–200-hPa layer-averaged irrotational wind field, has developed near the location of STC formation at t_0 in the case study (Fig. 3.43f) and composite (Fig. 3.23f).

The upper-tropospheric features linked to STC formation in the PV Debris case study bear little resemblance to those in the PV Debris cluster composite prior to t_0 – 48 h. Although a disorganized region of relatively high upper-tropospheric PV deposited in the subtropics several days prior to STC formation (i.e., PV debris) is detectable in the PV Debris case study to the east of the location of STC formation beginning at t_0 – 120 h (Fig. 3.52a), the amorphous nature of this feature causes it to be undetectable in the composite until t_0 – 48 h (Fig. 3.27d). A disorganized region of PV debris moves southwestward on the southeastern edge of a broad upper-tropospheric subtropical anticyclone between t_0 – 48 h and t_0 in the case study (Figs. 3.52d–f) and composite (Figs. 3.27d–f) in response to northeasterly winds on the 350 K isentropic surface. Relatively high PW values move westward to the east of the disorganized region of PV debris between t_0 – 48 h and t_0 – 24 h in the case study (Figs. 3.53d,e) and composite (Figs. 3.28d,e), making the region surrounding the location of STC formation favorable for the development of deep convection. Deep convection, represented by a region of divergent outflow in the 300–200-hPa layer-averaged irrotational wind field, has developed near the location of STC formation at t_0 in the case study (Fig. 3.53f) and composite (Fig. 3.28f).

4.1.5 Applications of Research to Operational Forecasting

The case studies presented in section 3.4 provide evidence that STC formation can occur close to the east coast of the United States and the west coast of Portugal. Therefore, as discussed in section 1.1, the ability to anticipate and recognize the upper-tropospheric features linked to STC formation could benefit operational forecasters. Conceptual models of the upper-tropospheric features linked to STCs forming in association with 1) PV streamers, 2) cutoffs, 3) midlatitude troughs, 4) subtropical disturbances, and 5) PV debris are shown in Figs. 4.2–4.6. By summarizing the common upper-tropospheric features, the conceptual models provide a basis for pattern recognition prior to STC formation.

The adapted Davis (2010) methodology for STC identification presented in this study has the potential to be applied to oceanic cyclones in real time. The real-time application of this methodology would benefit operational forecasters and research scientists by providing further insight into the relative contributions of baroclinic and diabatic processes occurring during the evolution of individual cyclones, as well as providing an additional tool for forecasting the TT of STCs. The adapted Davis (2010) methodology for STC identification, depicted graphically in Fig. 2.2, is well-designed for implementation in an ensemble-forecasting framework due to its ability to illustrate the changing contributions of baroclinic and diabatic processes during the evolution of individual cyclones. Utilizing the adapted Davis (2010) methodology for STC identification in an ensemble-forecasting framework would allow operational forecasters to better assess the timing of STC formation and the likelihood of TT.

4.2 Conclusions

The NHC STC definition, specified in section 1.1, suggests that both baroclinic and diabatic processes contribute to STC formation. The 1979–2010 North Atlantic STC climatology presented in this study is the first STC climatology to consider baroclinic and diabatic processes in conjunction with the NHC STC definition, using the adapted Davis (2010) methodology for STC identification to quantify the relative contributions of these processes during the evolution of individual cyclones.

As hypothesized in section 1.3, considerable intraseasonal variability is associated with the location and frequency of North Atlantic STC formation that is similar, but not identical, to the intraseasonal variability associated with the location and frequency of North Atlantic TCs. Like TC formation (not shown), STC formation primarily occurs over the southern Gulf Stream and western Caribbean Sea during the spring and early summer (Fig. 3.1), coinciding with the highest mean SSTs in the North Atlantic basin (Fig. 3.2a). TC formation becomes more frequent over the MDR and Cape Verde Islands during the late summer and fall (not shown) as African easterly wave activity increases. In contrast to the location of TC formation, STC formation becomes more frequent over the central and eastern North Atlantic during the late summer and fall (Fig. 3.1) as mean SSTs increase (Figs. 3.2a,b) and more of the basin becomes favorable for the development of deep convection following an intrusion of relatively cold upper-tropospheric air accompanying an upper-tropospheric disturbance.

Like TC formation (not shown), STC formation in the North Atlantic basin occurs most frequently in September and October (Fig. 3.3). However, Fig. 3.3 also indicates that STC formation occurs relatively frequently in June. This secondary peak in the frequency of STC formation is likely due to the presence of sufficiently warm ocean

waters in the North Atlantic basin (Fig. 3.2a) and sufficiently cold upper-tropospheric air in the midlatitudes that, when injected into the subtropics, can facilitate the development of deep convection in the early summer.

A cyclone-relative composite analysis was performed on subjectively constructed clusters of STCs identified in the 1979–2010 climatology in order to document the structure, motion, and evolution of the upper-tropospheric features linked to STC formation. STCs included in the climatology were separated into five clusters representing the most common upper-tropospheric features linked to STC formation: 1) PV Streamers (Fig. 3.5a), 2) Cutoffs (Fig. 3.5b), 3) Midlatitude Troughs (Fig. 3.5c), 4) Subtropical Disturbances (Fig. 3.5d), and 5) PV Debris (Fig. 3.5e). The separation of STCs into clusters based on the upper-tropospheric features linked to their formation is unique to this study and provides insight into the preferential pathways to STC formation.

STCs forming in association with PV streamers and cutoffs have a well-defined midlatitude connection, developing near a region of relatively high upper-tropospheric PV injected into the subtropics during an upstream AWB event (summarized in Figs. 4.2a,b and Figs. 4.3a–c, respectively). STCs forming in association with PV streamers (Fig. 4.2b) consistently develop ~48 h earlier during upstream AWB events than STCs forming in association with cutoffs (Fig. 4.3c). This ~48 h difference in the time of STC formation necessitated the separation of STCs forming in association with PV streamers and cutoffs into two distinct clusters, although the processes associated with their formation are similar.

Unlike STCs forming in association with PV streamers and cutoffs, STCs forming in association with midlatitude troughs require a precursor disturbance in the upper

troposphere to precondition the region surrounding the location of STC formation for the development of deep convection (summarized in Figs. 4.4a–c). This precursor disturbance is often injected into the subtropics ~96 h prior to STC formation during a precursor AWB event in the midlatitudes (Fig. 4.4a). Like STCs forming in association with PV streamer and cutoffs, STCs forming in association with midlatitude troughs also have a well-defined midlatitude connection (Fig. 4.4c), often forming poleward of 20°N across the majority of the North Atlantic basin (Fig. 3.6).

The Subtropical Disturbance cluster is the most distinct cluster identified in the 1979–2010 North Atlantic STC climatology. Unlike STCs included in the first three clusters, STCs forming in association with a subtropical disturbance do not have a well-defined midlatitude connection—often forming on the northeastern edge of upper-tropospheric subtropical anticyclones (summarized in Figs. 4.5a–c). In addition, the progressive PV filament associated with subtropical disturbances (Figs. 4.5a–c) is smaller in meridional extent than the upper-tropospheric disturbances associated with the previous three clusters, causing the upper-tropospheric troughs associated with subtropical disturbances to be have lower amplitude than those associated with PV streamers, cutoffs, and midlatitude troughs.

Unlike STCs included in the previous four clusters, STCs forming in association with a disorganized region of relatively high upper-tropospheric PV deposited in the subtropics several days prior to STC formation (i.e., PV debris) typically form equatorward of 30°N (Fig. 3.6) on the southeastern edge of a broad subtropical anticyclone (summarized in Figs. 4.6a–c). STCs forming in association with PV debris do not have a well-defined midlatitude connection and are the most common STCs

identified in this study (Fig. 3.4). The common occurrence of STCs forming in association with PV debris indicates that a strong midlatitude connection is not required for STC formation in the North Atlantic basin.

4.3 Suggestions for Future Work

North Atlantic cyclones included in the global climatology of baroclinically influenced tropical cyclogenesis events constructed by McTaggart-Cowan et al. (2013) were used to construct the STC climatology presented in this study. Additional STC climatologies, similar to the one presented in this study, could also be constructed for the remaining ocean basins analyzed in McTaggart-Cowan et al. (2013). These additional STC climatologies would: 1) provide insight into the intraseasonal variability associated with the location and frequency of STC formation by cataloging the position and time of STC development, as well as 2) enhance our understanding of the structure, motion, and evolution of the upper-tropospheric features linked to STC formation beyond what was gleaned from the present study. The author speculates that fewer STCs will be identified in the remaining ocean basins analyzed in McTaggart-Cowan et al. (2013), in which fewer baroclinically influenced tropical cyclogenesis events occur in the presence of an upper-tropospheric disturbance (their Fig. 6). The author also speculates that the structure, motion, and evolution of the upper-tropospheric features linked to STC formation in the remaining ocean basins analyzed in McTaggart-Cowan et al. (2013) will be relatively similar to the structure, motion, and evolution of the upper-tropospheric features linked to STC formation in the North Atlantic.

Although the cyclone-relative composite analysis presented in this study is extensive, the evaluation of additional diagnostic fields could provide further insight into the structure, motion, and evolution of upper-tropospheric features linked to STC formation than was derived from the present study. For example, cyclone-relative composites of 400–200-hPa layer-averaged Q vectors could be used to evaluate the QG forcing for ascent that was discussed, but never quantified, in the present study. Cyclone-relative composites of Tropical Rainfall Measuring Mission (TRMM) data could be used to provide evidence of the presence of deep convection near the cyclone center at the time of STC formation. All diagnostic fields included in the updated cyclone-relative composite analysis should also be tested for statistical significance in order to identify the most important and most representative upper-tropospheric features linked to STC formation within each subjectively constructed cluster.

Finally, questions remain unanswered concerning the influence of upper-tropospheric features linked to STC formation on the predictability of developing STCs. The author hypothesizes that some of the pathways to STC formation identified in this study are inherently less predictable than others and additional research is needed to address this hypothesis.

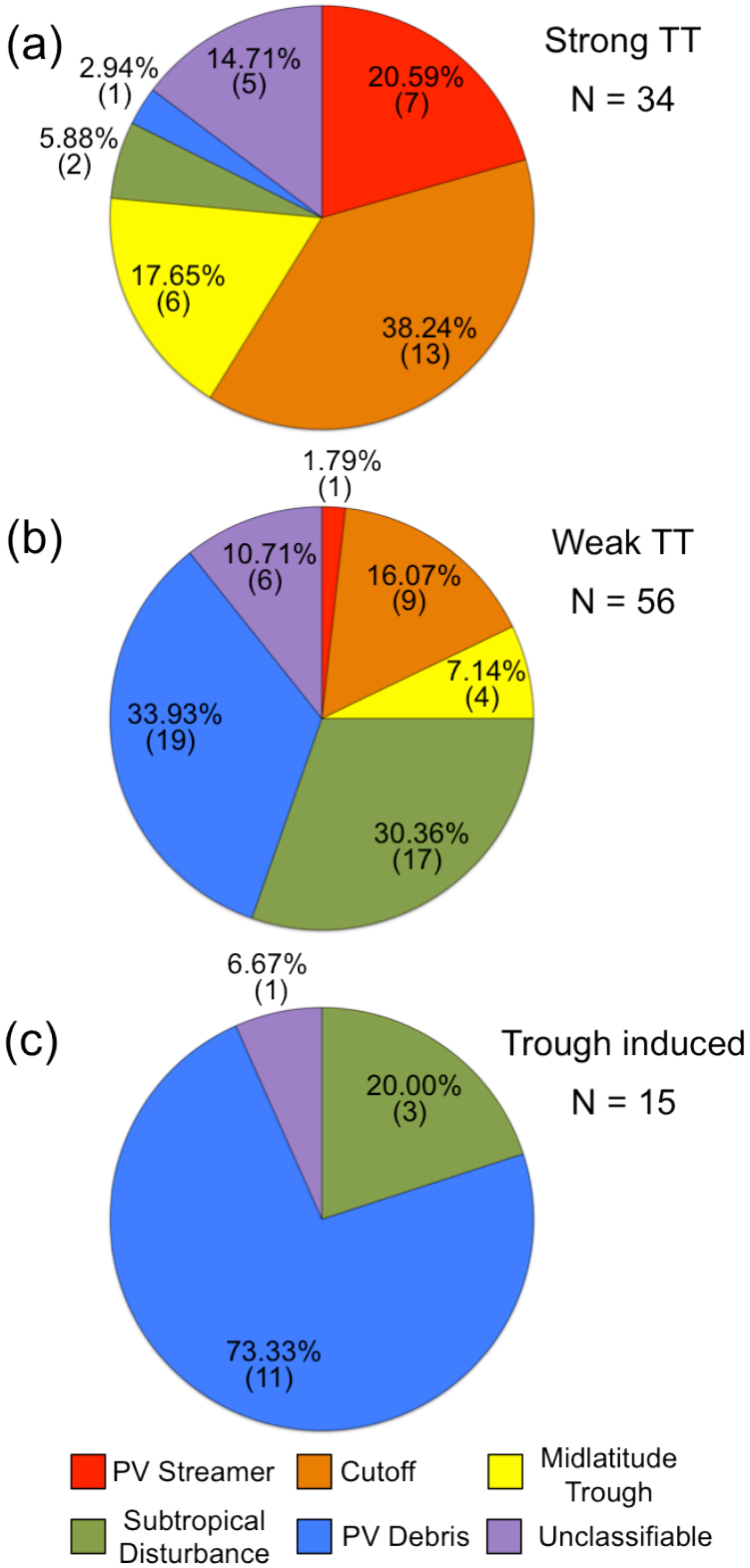

Fig. 4.1. Distribution by cluster of STCs included in the (a) Strong TT, (b) Weak TT, and (c) Trough induced development pathways identified in McTaggart-Cowan et al. (2013).

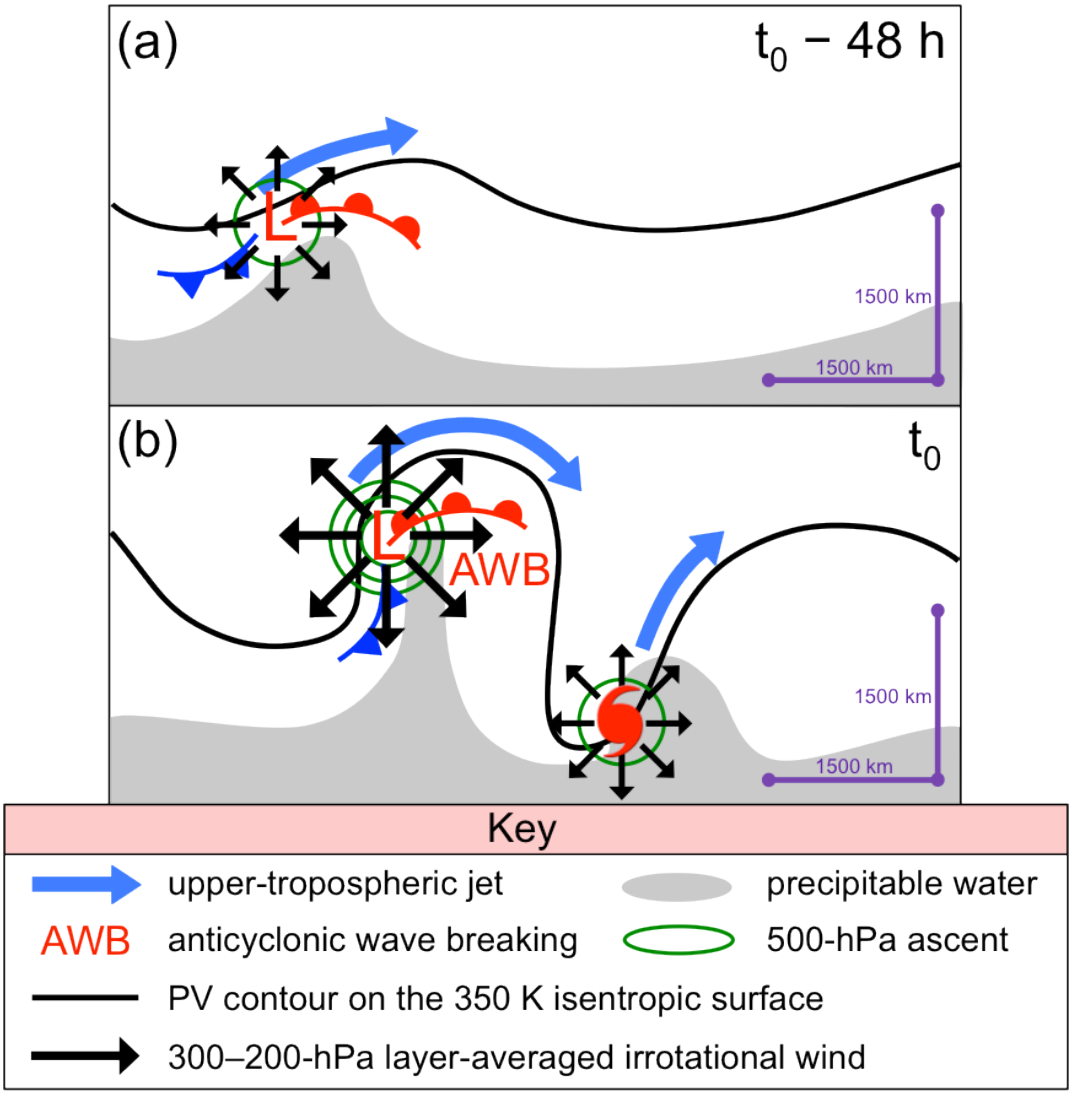

Fig. 4.2. Conceptual model of the upper-tropospheric features linked to an STC forming in association with a PV streamer at (a) t_0 – 48 h and (b) t_0. Features shown according to key; other symbols are conventional.

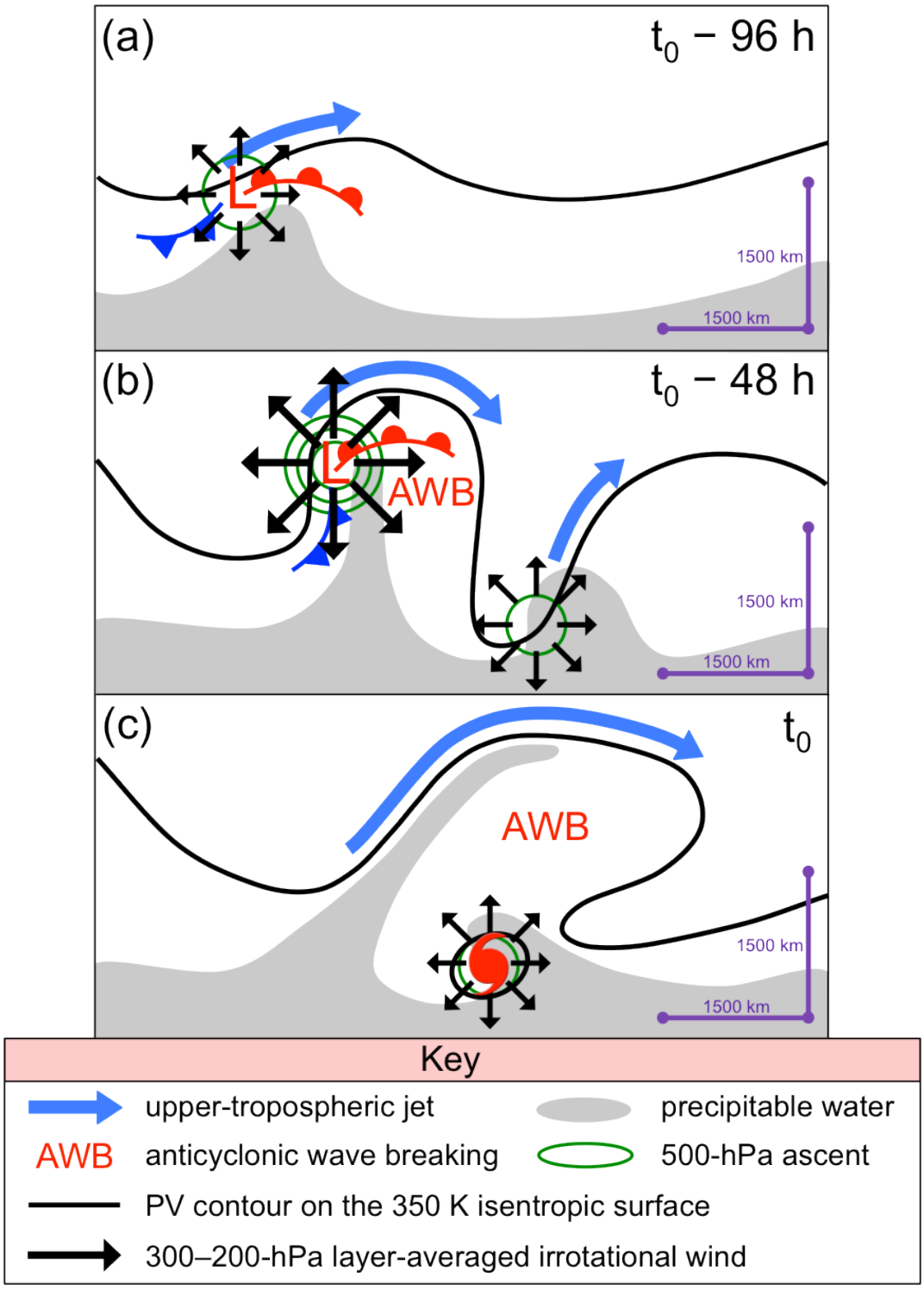

Fig. 4.3. Conceptual model of the upper-tropospheric features linked to an STC forming in association with a cutoff at (a) t_0 – 96 h, (b) t_0 – 48 h, and (c) t_0. Features shown according to key; other symbols are conventional.

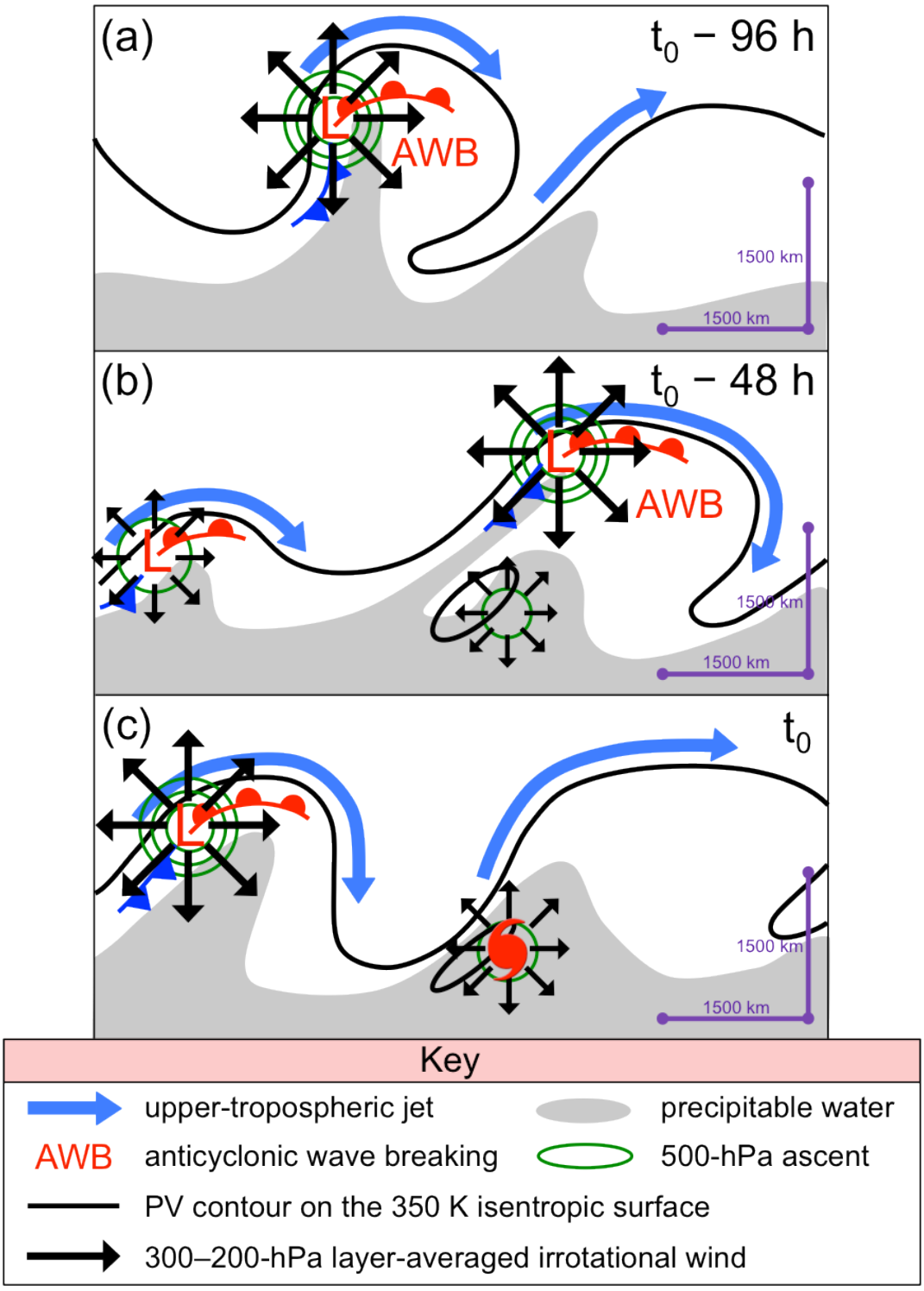

Fig. 4.4. Conceptual model of the upper-tropospheric features linked to an STC forming in association with a midlatitude trough at (a) t_0 – 96 h, (b) t_0 – 48 h, and (c) t_0. Features shown according to key; other symbols are conventional.

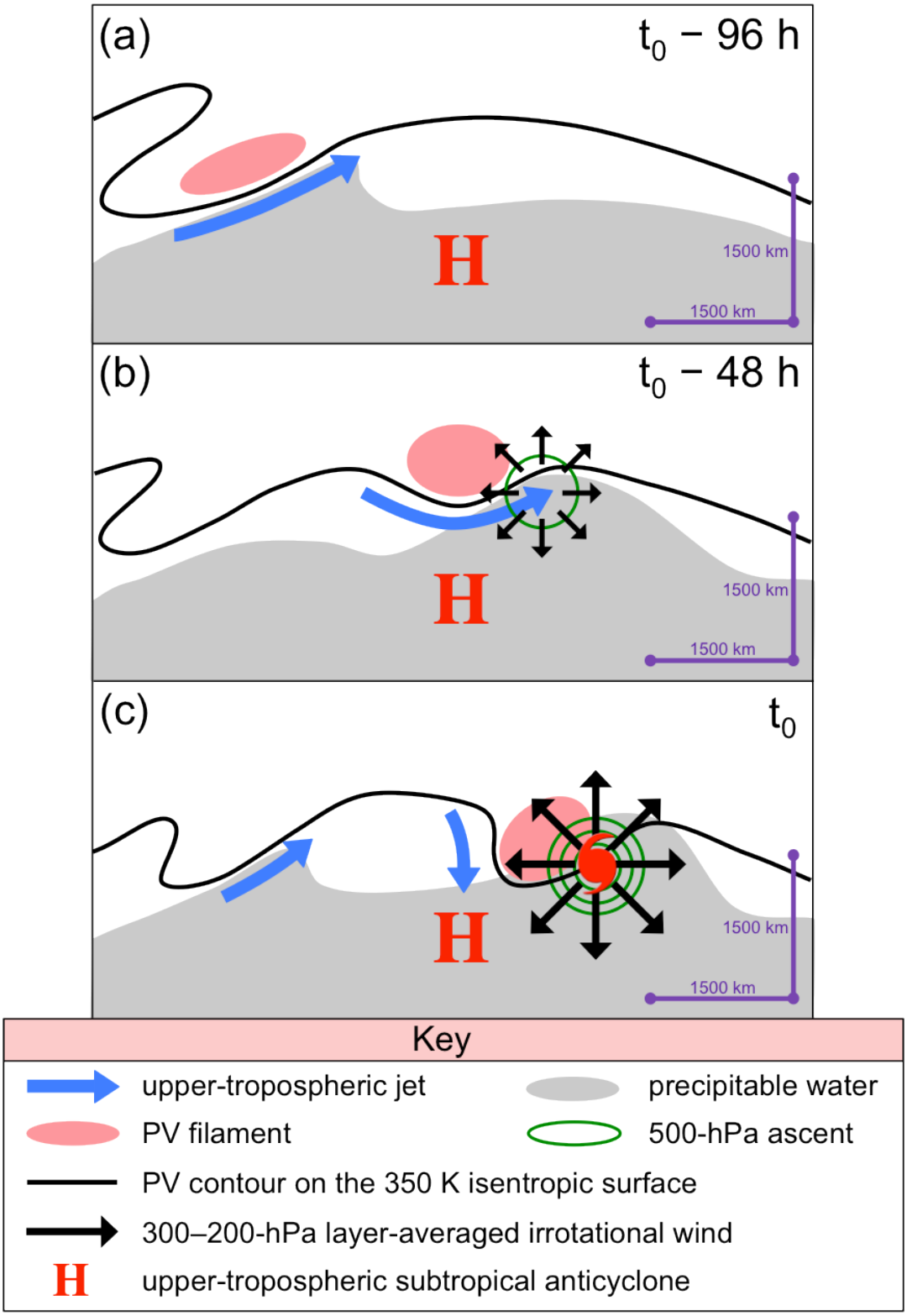

Fig. 4.5. Conceptual model of the upper-tropospheric features linked to an STC forming in association with a subtropical disturbance at (a) t_0 – 96 h, (b) t_0 – 48 h, and (c) t_0. Features shown according to key; other symbols are conventional.

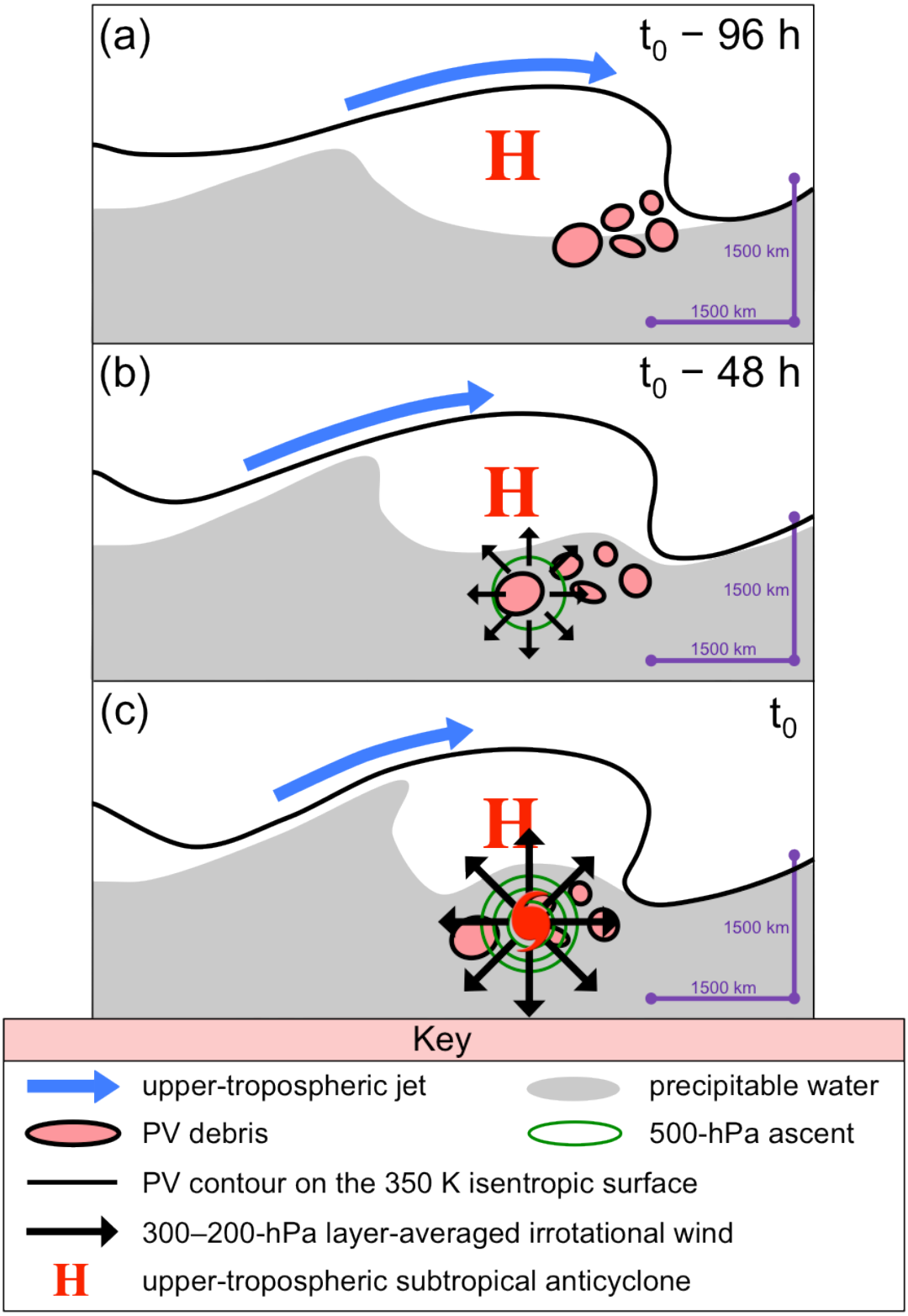

Fig. 4.6. Conceptual model of the upper-tropospheric features linked to an STC forming in association with PV debris at (a) t_0 – 96 h, (b) t_0 – 48 h, and (c) t_0. Features shown according to key; other symbols are conventional.

REFERENCES

Beven, J. L., II, 2012: Tropical cyclone report: Tropical Storm Beryl, 26–30 May 2012. National Hurricane Center Rep., 1 pp. [Available online at http://www.nhc.noaa.gov/data/tcr/AL022012_Beryl.pdf.]

——, S. R. Stewart, M. B. Lawrence, L. A. Avila, J. L. Franklin, and R. J. Pasch, 2003: Atlantic hurricane season of 2001. *Mon. Wea. Rev.*, **131,** 1454–1484.

Bosart, L. F., and J. A. Bartlo, 1991: Tropical storm formation in a baroclinic environment. *Mon. Wea. Rev.*, **191,** 1979–2013.

Bracken, W. E., and L. F. Bosart, 2000: The role of synoptic-scale flow during tropical cyclogenesis over the North Atlantic Ocean. *Mon. Wea. Rev.*, **128,** 353–376.

Davis, C. A., 2010: Simulations of subtropical cyclones in a baroclinic channel model. *J. Atmos. Sci.*, **67**, 2871–2892.

——, and L. F. Bosart, 2001: Numerical simulations of the genesis of Hurricane Diana. Part I: Control simulation. *Mon. Wea. Rev.*, **129,** 1859–1881.

——, and ——, 2003: Baroclinically induced tropical cyclogenesis. *Mon. Wea. Rev.*, **131,** 2730–2747.

——, and ——, 2004: The TT problem. *Bull. Amer. Meteor. Soc.*, **85,** 1657–1662.

DeMaria, M., J. A. Knaff, and B. H. Connell, 2001: A tropical cyclone genesis parameter for the tropical Atlantic. *Wea. Forecasting*, **16,** 219–233.

Emanuel, K. A., 1986: An air-sea interaction theory for tropical cyclones. Part I: Steady-state maintenance. *J. Atmos. Sci.*, **43,** 585–605.

——, 1995: On thermally direct circulations in moist atmospheres. *J. Atmos. Sci.*, **52,** 1529–1534.

Evans, J. L., and M. P. Guishard, 2009: Atlantic subtropical storms. Part I: Diagnostic criteria and composite analysis. *Mon. Wea. Rev.*, **137,** 2065–2080.

Franklin, J. L., L. A. Avila, J. L. Beven II, M. B. Lawrence, R. J. Pasch, and S. R. Stewart, 2001: Atlantic hurricane season of 2000. *Mon. Wea. Rev.*, **129,** 3037–3056.

Gray, W. M., 1968: Global view of the origin of tropical disturbances and storms. *Mon. Wea. Rev.*, **96,** 669–700.

Guishard, M. P., J. L. Evans, and R. E. Hart, 2009: Atlantic subtropical storms. Part II: Climatology. *J. Climate*, **22,** 3574–3594.

Hart, R. E., 2003: A cyclone phase space derived from thermal wind and thermal asymmetry. *Mon. Wea. Rev.*, **131,** 585–616.

Hulme, A. L., and J. E. Martin, 2009a: Synoptic and frontal scale influences on tropical transition events in the Atlantic basin. Part I: A six case survey. *Mon. Wea. Rev.*, **137,** 3626–3650.

——, and ——, 2009b: Synoptic- and frontal-scale influences on tropical transition events in the Atlantic basin. Part II: Tropical transition of Hurricane Karen. *Mon. Wea. Rev.*, **137,** 3626–3650.

Kalnay, E., and Coauthors, 1996: The NCEP/NCAR 40-Year Reanalysis Project, *Bull. Amer. Meteor. Soc.*, **77,** 437–471.

Knapp, K. R., M. C. Kruk, D. H. Levinson, H. J. Diamond, and C. J. Neumann, 2010: The International Best Track Archive for Climate Stewardship (IBTrACS): Unifying tropical cyclone best track data. *Bull. Amer. Meteor. Soc.*, **91,** 363–376.

McTaggart-Cowan, R., G. D. Deane, L. F. Bosart, C. A. Davis, T. J. Galarneau, 2008: Climatology of tropical cyclogenesis in the North Atlantic (1948−2004). *Mon. Wea. Rev.*, **136,** 1284–1304.

——, T. J. Galarneau, L. F. Bosart, R. W. Moore, O. Martius, 2013: A global climatology of baroclinically influenced tropical cyclogenesis. *Mon. Wea. Rev.*, **141,** 1963–1989.

Moore, P. L., and W. R. Davis, 1951: A PRESEASON HURRICANE OF SUBTROPICAL ORIGIN. *Mon. Wea. Rev.*, **79,** 189–195.

OFCM, cited 2013: National hurricane operations plan. FCM-P12-2013. [Available online at http:// www.ofcm.gov/nhop/13/pdf/FCM-P12-2013.pdf.]

Pasch, R. J., and L. A. Avila, 1992: Atlantic hurricane season of 1991. *Mon. Wea. Rev.*, **120,** 2671–2687.

Posselt, D. J., and J. E. Martin, 2004: The effect of latent heat release on the evolution of a warm occluded thermal structure. *Mon. Wea. Rev.*, **132,** 578–599.

Raymond, D.J., 1992: Nonlinear balance and potential vorticity thinking at large Rossby number. *Quart. J. Roy. Meteor. Soc.*, **118,** 987–1015.

Saha, S., and Coauthors, 2010: The NCEP Climate Forecast System Reanalysis. *Bull. Amer. Meteor. Soc.*, **91,** 1015–1057.

Simpson, R. H., 1952: EVOLUTION OF THE KONA STORM A SUBTROPICAL CYCLONE. *J. Meteor.*, **9,** 24–35.

Stoelinga, M. T., J. D. Locatelli, and P. V. Hobbs, 2002: Warm Occlusions, Cold Occlusions, and Forward-Tilting Cold Fronts. *Bull. Amer. Meteor. Soc*., **83,** 709–721.

Uppala, S. M., and Coauthors, 2005: The ERA-40 Re-Analysis. *Quart. J. Roy. Meteor. Soc.*, **131,** 2961–3012.